

REDOX MEDIATORS AND ELECTROLYTES FOR HIGH-PERFORMANCE Li-O₂ BATTERIES

by Anastasiia Tkacheva

Thesis submitted in fulfilment of the requirements
for the degree of

Doctor of Philosophy

under the supervision of
Assoc. Prof. Andrew M. McDonagh

University of Technology Sydney
Faculty of Science

February 2021

Certificate of Original Authorship

I, Anastasiia Tkacheva, declare that this thesis is submitted in fulfilment of the requirements for the award of Doctor of Philosophy, in the School of Mathematical and Physical Sciences, Faculty of Science at the University of Technology Sydney.

This thesis is wholly my own work unless otherwise referenced or acknowledged. In addition, I certify that all information sources and literature used are indicated in the thesis.

This document has not been submitted for qualifications at any other academic institution.

This research is supported by the Australian Government Research Training Program.

Signature:	Production Note:
	Signature removed prior to publication.

Date: 12/2/2021

Acknowledgements

I am sincerely grateful to all who made it possible to complete this thesis. Firstly, I would like to thank my dear husband for bringing me to Australia, so that I could start working on this exciting interdisciplinary project, for all his support and for looking after our baby instead of resting on the weekends when I could peacefully write the dissertation. Being a scientist too, he gave me a lot of useful advice. Also, I want to thank my mother for expressing interest in my PhD project and encouraging me to continue it.

I am incredibly thankful to my supervisor Assoc. Prof. Andrew M. McDonagh. He miraculously helped me find the right decision every time I got stuck and spent an enormous amount of time practising presentations with me, discussing my current work, revising my thesis and papers. It was a great pleasure to work on this project under his guidance!

In addition, I want to thank my co-supervisors: Dr Bing Sun, who advised me about Electrochemistry and helped to edit my manuscripts, and Prof. Guoxiu Wang, who together with his wife Dr Jane (Yueping) Yao made me a part of CCET group of researchers, allowing me to participate in many events and use the CCET equipment, which made a significant contribution to my professional growth. I am grateful to those who helped me in the laboratory: Dr Alexander Angeloski, Yurii Bodachivskyi, Dr Ronald Shimmon, Dr Jane (Yueping) Yao, Dr Jinqiang Zhang, Dr Dong Zhou, Kang Yan, Mahmoud El Safadi, all our friendly team of organic chemists. I also feel thankful to the subject coordinators who allowed me to deepen my knowledge in Chemistry and improve my English skills while doing the PhD: Dr Scott Chadwick, Dr Brian Reedy, Assoc. Prof. Alison Ung.

Finally, I want to thank Shri Mataji Nirmala Devi for founding the Sahaja Yoga Meditation, which helped me stay peaceful and be myself during these busy times.

Table of Contents

Certificate of Original Authorship	ii
Acknowledgements.....	iii
List of Figures.....	4
List of Tables	10
List of Schemes	11
List of Abbreviations	12
Publications Arising from This Work	17
Abstract.....	18
Overview	20
Chapter 1: Redox Mediators and Electrolytes in Li-O₂ Batteries	24
1.1. General Theoretical Considerations for Batteries	24
1.1.1. Voltaic Cells.....	24
1.1.2. Primary and Secondary Batteries	25
1.1.3. Theoretical Voltage, Capacity, and Energy	26
1.1.4. Discharge, Charge, Cycle Life, Coulombic Efficiency, State of Charge, Definitions Related to Voltage.....	28
1.2. Redox Mediators and Electrolytes in Aprotic Li-O ₂ Batteries.....	29
1.2.1. Operating Principles and Composition of Li-O ₂ Batteries.....	30
1.2.2. Shortcomings of Li-O ₂ Batteries.....	48
1.2.3. Redox Mediators	54
1.3. Conclusion	62
1.4. Research Approach and Methods.....	62
Chapter 2: Experimental Section	68
2.1. General	68
2.2. Synthesis of TEMPO-ionic Liquids (TEMPOImILs)	69
2.3. Synthesis of Substituted 2-Phenyl-nitronyl Nitroxides (RPTIOs).....	80
2.4. Electrochemical Characterisation.....	82
2.4.1. General	82

2.4.2. Preparation of Carbon-Based Cathodes	84
2.5. Description and Justification of Characterisation Techniques	85
2.5.1. Thermal Analysis	85
2.5.2. Cyclic Voltammetry	86
2.5.3. Electrochemical Impedance Spectroscopy.....	88
2.5.4. UV-visible Spectroelectrochemistry	90
2.5.5. Galvanostatic Cycling	91
2.5.6. Scanning Electron Microscopy	93
2.5.7. X-ray Diffraction.....	94
Chapter 3: TEMPO-ionic Liquids as Redox Mediators and Solvents for Li-O₂ Batteries	96
3.1. Introduction	96
3.2. Synthesis of TEMPOImILs.....	99
3.3. General Characterisation of TEMPOImILs	100
3.4. Ionic Conductivity of TEMPOImILs	101
3.5. Cyclic Voltammetry of TEMPOImILs	103
3.5.1. The Effect of Ferrocene on TEMPOImILs	104
3.5.2. Cyclic Voltammetry Studies with LiTFSI	106
3.5.3. Cyclic Voltammetry Studies with TBATFSI.....	113
3.6. Galvanostatic Cycling of the Li-O ₂ Batteries with TEMPOImILs	114
3.7. Summary	119
Chapter 4: Nitronyl-nitroxide-based Redox Mediators for Li-O₂ Batteries	122
4.1. Introduction	122
4.2. Synthesis of RPTIOs	126
4.3. Cyclic Voltammetry Studies with LiTFSI	127
4.4. Cyclic Voltammetry Studies with TBATFSI.....	131
4.5. Spectroelectrochemistry of PTIO.....	132

4.6. Reactions in Li-O ₂ Batteries upon the Addition of the Redox Mediators	134
4.7. Performance of Li-O ₂ Batteries with RPTIOs	138
4.8. Summary	142
Chapter 5: Conclusions	144
Appendix	147
A.1. TGA and DSC Data for TEMPOImILs.....	147
A.2. An Investigation of Methylated Ferrocenes as RMs for Li-O ₂ Batteries.....	152
A.2.1. Introduction	152
A.2.2. Results and Discussion.....	152
A.2.3. Summary	154
References	156

List of Figures

Figure 1. Schematic diagram of aprotic Li-O ₂ battery. ⁹	30
Figure 2. Discharge/charge profiles of Li-O ₂ batteries with IL/DMSO electrolyte at a capacity of 1000 mAh g ⁻¹ (left) and 500 mAh g ⁻¹ (right). ⁵⁸	36
Figure 3. Schematic diagram of a hybrid Li-O ₂ battery with a protected anode. ⁴⁹	37
Figure 4. Charge-discharge curves of Li-O ₂ batteries based on (a) P(VdF-HFP)/TEGDME GPE (b) liquid TEGDME electrolyte obtained at a fixed capacity of 500 mAh g ⁻¹ . ⁹²	42
Figure 5. Cycle life of Li-O ₂ batteries with PMMA based GPE. ⁸⁶	43
Figure 6. Electrochemical performance of Li-O ₂ battery with PAN-based GPE and LiNO ₃ at a fixed capacity of 400 mAh g ⁻¹ (a) charge-discharge profiles; (b) cycling stability. ⁸⁹	44
Figure 7. Preparation and appearance of ETPTA-based GPE with and without 1% w/w of glass microfillers. ⁹⁸	45
Figure 8. Electrochemical performance of Li-O ₂ battery with LAGP-PMS hybrid electrolyte at 50 °C at a fixed capacity of 1000 mAh g ⁻¹ (a) power output capability at different current densities (b), (c) charge-discharge curves and cyclability at a current density of 200 mAh g ⁻¹ . ⁸⁷	46
Figure 9. Gravimetric specific energies of various rechargeable batteries with gasoline. ²⁷	49
Figure 10. Scanning electron microscope image showing dendrites in a Li secondary battery. ¹⁰⁶	50
Figure 11. (a) The mechanism of OER with RM; (b) Charge-discharge profiles of Li-O ₂ battery with or without RM. ¹⁰	55

Figure 12. The mechanism of DBBQ facilitating ORR. ¹³⁵	57
Figure 13. Structure of TEMPOImILs.	64
Figure 14. Structure of RPTIOs.	65
Figure 15. Potential sweep in cyclic voltammetry.	86
Figure 16. A typical cyclic voltammogram.	87
Figure 17. Example of a Nyquist plot.	89
Figure 18. a) Full discharge curves; ¹⁵⁶ b) discharge/charge curves with a capacity restricted to 1000 mAh g ⁻¹ . ⁸⁸	92
Figure 19. Cycling profile of a battery. ¹⁵⁸	93
Figure 20. Structure of TEMPOImILs studied in this work.	98
Figure 21. TGA curves of TEMPOImILs in N ₂ atmosphere.	100
Figure 22. TGA and DSC data for TEMPOImIL 5e .	101
Figure 23. Temperature vs. ionic conductivity plots for pure TEMPOImILs 5a–e .	102
Figure 24. Temperature vs. ionic conductivity plots for pure TEMPOImILs 6a–e .	103
Figure 25. Temperature vs. ionic conductivity plots for pure TEMPOImILs 5a, c tested up to 80 °C.	103
Figure 26. Cyclic voltammetry plots for 10 mmol TEMPOImILs 5a, b, e in 0.1 M LiTFSI/DMA with and without added ferrocene.	105
Figure 27. Cyclic voltammograms of TEMPOImILs 5a, e, 6a, e (10mM) in LiTFSI/TEGDME under an oxygen atmosphere, 1 st cycle.	107
Figure 28. Cyclic voltammogram of TEMPOImIL 5a demonstrating the effect on the OER, 10 cycles.	108

Figure 29. Cyclic voltammograms demonstrating the effect on the OER of TEMPOImILs 6a (a), 5e (b), 6e (c), 10 cycles.....	109
Figure 30. Cyclic voltammogram of TEMPOImIL 5b (10mM) in LiTFSI/MeCN under an argon atmosphere.	112
Figure 31. Cyclic voltammograms of TEMPOImILs 5a , e , 6a , e (10mM) in TBATFSI/TEGDME, 20 cycles.....	113
Figure 32. Cyclic voltammogram of TEMPOImIL 5a (10mM) in TBATFSI/TEGDME, 100 cycles.....	114
Figure 33. Cycle life of Li-O ₂ batteries with TEMPOImILs/LiTFSI and TEGDME/LiTFSI operated at a fixed capacity of 0.13 mAh cm ⁻² in the voltage range of 2.0–4.2 V at 73 °C.	115
Figure 34. Galvanostatic discharge/charge profiles of Li-O ₂ batteries with TEGDME/LiTFSI and TEMPOImIL 5b /LiTFSI at 73 °C.	117
Figure 35. Full charge and discharge profiles of Li-O ₂ batteries with TEGDME/LiTFSI and TEMPOImIL 5d /LiTFSI at 73 °C.....	118
Figure 36. The structure of PTIO.....	123
Figure 37. Photographs of the crushed crystals of RPTIO compounds: (a) NMe ₂ PTIO, (b) MeOPTIO, (c) PTIO, (d) NO ₂ PTIO.	127
Figure 38. Cyclic voltammograms of RPTIOs (10 mM), LiTFSI (0.1 M) in TEGDME under an argon atmosphere.	128
Figure 39. Cyclic voltammograms of RPTIOs (10 mM) in LiTFSI/TEGDME under an argon atmosphere in different potential ranges.....	130

Figure 40. Cyclic voltammograms with and without RPTIOs (10 mM) in LiTFSI/TEGDME under an O ₂ and Ar atmosphere. “No RM” refers to 0.1 M LiTFSI in TEGDME.....	131
Figure 41. Cyclic voltammograms of PTIO (10 mM) in TBATFSI/TEGDME under an oxygen atmosphere: (a) full scan range, (b) enlarged region at higher positive potentials.	132
Figure 42. UV-Visible spectral changes during stepwise electrochemical oxidation of PTIO solution in TBAPF ₆ /MeCN. The potential was recorded vs. Ag/Ag ⁺ reference electrode.....	133
Figure 43. UV-Visible spectral changes during stepwise electrochemical reduction of PTIO solution in TBAPF ₆ /MeCN. The potential was recorded vs. Ag/Ag ⁺ reference electrode.....	134
Figure 44. Full discharge curves of the batteries with RPTIOs (10 mM) in LiTFSI/DEGDME and pure LiTFSI/DEGDME electrolyte in argon (a) and oxygen (b).	135
Figure 45. SEM images of CB cathodes: (a) pristine, (b) discharged containing PTIO, (c) discharged without PTIO, (d) charged containing PTIO, (e) charged without PTIO..	136
Figure 46. SEM images of discharged (top) and charged (bottom) CB cathodes with RPTIOs: a), d) MeOPTIO; b), e) NMe ₂ PTIO; c), f) NO ₂ PTIO.....	136
Figure 47. XRD patterns of pristine, discharged and charged CB cathodes with and without PTIO. Note: discharged cathodes remained attached to the stainless steel current collectors, peaks assigned to stainless steel are indicated in the diffraction patterns by **.....	137

Figure 48. XRD patterns of pristine, discharged and charged CB cathodes with and without RPTIOs.	138
Figure 49. Galvanostatic discharge/charge curves of RPTIOs (10 mM) in LiTFSI/DEGDME (1 st cycle).....	139
Figure 50. Galvanostatic cycling profiles of batteries (RPTIO (10 mM) in LiTFSI/DEGDME): (a) NMe ₂ PTIO, (b) MeOPTIO, (c) PTIO, (d) NO ₂ PTIO, and (e) pure LiTFSI/DEGDME electrolyte.....	140
Figure 51. Galvanostatic cycling profiles of the batteries with 10 mM MeOPTIO in LiTFSI/DEGDME and pure LiTFSI/DEGDME electrolyte at fixed capacities of 0.25 mAh cm ⁻² (a) and 0.5 mAh cm ⁻² (b).....	141
Figure A1. TGA and DSC data for TEMPOImIL with n = 4, R = H.	147
Figure A2. TGA and DSC data for TEMPOImIL with n = 4, R = Me.	148
Figure A3. TGA and DSC data for TEMPOImIL with n = 5, R = H.	148
Figure A4. TGA and DSC data for TEMPOImIL with n = 5, R = Me.	149
Figure A5. TGA and DSC data for TEMPOImIL with n = 6, R = H.	149
Figure A6. TGA and DSC data for TEMPOImIL with n = 6, R = Me.	150
Figure A7. TGA and DSC data for TEMPOImIL with n = 7, R = H.	150
Figure A8. TGA and DSC data for TEMPOImIL with n = 7, R = Me.	151
Figure A9. TGA and DSC data for TEMPOImIL with n = 8, R = Me.	151
Figure A10. Full discharge/charge curves of the Li-O ₂ batteries with pure LiTFSI/DEGDME electrolyte (“no OMeFc”) and 0.01 M OMeFc in LiTFSI/DEGDME electrolyte.....	153

Figure A11. Full discharge/charge curves of the Li-O₂ batteries with pure LiTFSI/DEGDME electrolyte (“no DMeFc”), 0.01 M DMeFc in LiTFSI/DEGDME electrolyte, and a mixture of both. 154

List of Tables

Table 1. Chemical structures and redox potentials of the redox mediators tested in Li-O ₂ batteries.	58
Table 2. Abbreviations and description of the structures of RPTIOs	65
Table 3. Potentials of TEMPOImILs with and without added ferrocene.....	106
Table 4. Shifts in cathodic peak potentials (E_{pc}) of TEMPOImILs after the 1 st cycle.....	110
Table 5. Redox potentials for the oxidation of RPTIOs.....	128

List of Schemes

Scheme 1. Synthesis of TEMPOImILs.....	99
Scheme 2. Redox processes in nitroxide radicals.....	106
Scheme 3. Protonation of hydroxylamine anion.	110
Scheme 4. Redox processes in nitronyl nitroxide radicals.	123
Scheme 5. Resonance structures in nitronyl nitroxide radicals.	124
Scheme 6. Synthesis of RPTIO compounds.	126

List of Abbreviations

<i>Abbreviation</i>	<i>Explanation</i>
% w/w	percentage by mass
$^1\text{O}_2$	singlet oxygen
<i>AC</i>	alternating current
<i>Ah</i>	ampere-hour
<i>CB</i>	carbon black
<i>CNT</i>	carbon nanotubes (cathode material)
<i>CP</i>	carbon paper
<i>CV</i>	cyclic voltammetry
<i>DBBQ</i>	2,5-di- <i>tert</i> -butyl-1,4-benzoquinone
<i>DEGDME</i>	diethylene glycol dimethyl ether, diglyme
<i>DFT</i>	density functional theory
<i>DMA</i>	<i>N,N</i> -dimethylacetamide
<i>DME</i>	ethylene glycol dimethyl ether, glyme, dimethoxyethane
<i>DMeFc</i>	decamethylferrocene
<i>DMF</i>	dimethylformamide
<i>DMTFA</i>	<i>N,N</i> -dimethyltrifluoroacetamide
<i>DMSO</i>	dimethyl sulfoxide
<i>DOL</i>	1,3-dioxolane

<i>DSC</i>	differential scanning calorimetry
<i>E</i>	discharge voltage
$E^0_{(cell)}$	standard cell potential
<i>EIS</i>	electrochemical impedance spectroscopy
<i>EMS</i>	ethylmethanesulfonate
$E^{0'}$	formal redox potential
E_{pa}	anodic peak potential
E_{pc}	cathodic peak potential
<i>ETPTA</i>	ethoxylated trimethylolpropane triacrylate
<i>Fc</i>	ferrocene
<i>GPE</i>	gel polymer electrolyte
<i>HMD</i>	2,2,4,4,5,5-hexamethyl-1,3-dioxolane
<i>I</i>	current
<i>IL</i>	ionic liquid
<i>i-PrOH</i>	isopropyl alcohol
<i>IR</i>	infrared
<i>LiRCO₂</i>	lithium alkyl carbonates (R = alkyl)
<i>LiTFSI</i>	lithium bis(trifluoromethanesulfonyl)imide
<i>MeCN</i>	acetonitrile
<i>MeO</i>	methoxy

<i>Nafion</i>	a sulfonated tetrafluoroethylene based fluoropolymer-copolymer
<i>NMe₂</i>	dimethylamino
<i>NMR</i>	nuclear magnetic resonance
<i>NN</i>	nitronyl nitroxide
<i>O₂⁻, O₂^{•-}</i>	superoxide anion, superoxide anion radical
<i>OCV (E_{OC})</i>	open-circuit voltage
<i>OER</i>	oxygen evolution reaction
<i>OMeFc</i>	octamethylferrocene
<i>ORR</i>	oxygen reduction reaction
<i>P(VdF-HFP)</i>	poly(vinylidene fluoride-co-hexafluoropropylene)
<i>PAN</i>	polyacrylonitrile
<i>Pc</i>	phthalocyanine
<i>PEO</i>	poly(ethylene oxide)
<i>PTIO</i>	2-phenyl-4,4,5,5,-tetramethylimidazoline-1-oxyl 3-oxide
<i>PMMA</i>	poly(methyl methacrylate)
<i>PMS</i>	poly(methyl methacrylate-styrene)
<i>PTFE</i>	poly(tetrafluoroethylene)
<i>PVA</i>	poly(vinylalcohol)
<i>Q_{nom}</i>	nominal capacity

Q_{theor}	theoretical capacity
$RPTIOs$	substituted 2-phenyl-4,4,5,5,-tetramethylimidazoline-1-oxyl 3-oxides
rGO	reduced graphene oxide (cathode material)
RH	relative humidity
RM	redox mediator
$S\ cm^{-1}$	siemens per centimeter
SEI	solid electrolyte interface
SEM	scanning electron microscopy
SHE	standard hydrogen electrode
SPE	solid polymer electrolyte
$TBAPF_6$	tetrabutylammonium hexafluorophosphate
$TBATFSI$	tetrabutylammonium bis(trifluoromethanesulfonyl)imide
t_D	discharge time
$TEGDME$	tetraethylene glycol dimethyl ether, tetraglyme
$TEMPO$	(2,2,6,6-tetramethylpiperidin-1-yl)oxyl
$TEMPOImILs$	TEMPO-substituted ionic liquids
$TEMPO-OH$	4-hydroxy-TEMPO
$TFSI^-$	bis(trifluoromethanesulfonyl)imide
TGA	thermogravimetric analysis

U	actual specific energy
U_{theor}	theoretical energy
$UV-visible$	ultraviolet-visible
V	volt
Wh	watt-hour
XRD	X-ray diffraction

Publications Arising from This Work

1. J. Zhang, B. Sun, Y. Zhao, A. Tkacheva, Z. Liu, K. Yan, X. Guo, A. M. McDonagh, D. Shanmukaraj, C. Wang, T. Rojo, M. Armand, Z. Peng, G. Wang, A versatile functionalised ionic liquid to boost the solution-mediated performances of lithium-oxygen batteries. *Nature Communications* **2019**, *10*, 602.
2. D. Zhou, A. Tkacheva, X. Tang, B. Sun, D. Shanmukaraj, P. Li, F. Zhang, M. Armand, G. Wang, Stable Conversion Chemistry-Based Lithium Metal Batteries Enabled by Hierarchical Multifunctional Polymer Electrolytes with Near-Single Ion Conduction. *Angewandte Chemie International Edition* **2019**, *58* (18), 6001-6006.
3. Zhou, D.; Shanmukaraj, D.; Tkacheva, A.; Armand, M.; Wang, G., Polymer Electrolytes for Lithium-Based Batteries: Advances and Prospects. *Chem* **2019**, *5*, 1-27.
4. Tkacheva, A.; Zhang, J.; Sun, B.; Zhou, D.; Wang, G.; McDonagh, A. M., TEMPO-Ionic Liquids as Redox Mediators and Solvents for Li-O₂ Batteries. *The Journal of Physical Chemistry C* **2020**, *124* (9), 5087-5092.
5. A. Tkacheva, B. Sun, J. Zhang, G. Wang, A. M. McDonagh, Nitronyl-nitroxide-based redox mediators for Li-O₂ batteries, *The Journal of Physical Chemistry C* **2021**, <https://doi.org/10.1021/acs.jpcc.0c08466>.

Abstract

The predicted theoretical energy density of a Li-O₂ battery is close to that of gasoline, which makes it one of the most promising forms of energy storage. To allow Li-O₂ batteries to achieve their full potential, multiple issues need to be overcome. One issue is the large charge and discharge overpotentials caused by sluggish kinetics of the reactions within the battery and the solid, insulating nature of the discharge product Li₂O₂. Applying soluble electrocatalysts (redox mediators or RMs) that aid the formation and decomposition of the Li₂O₂ can help to reduce the overpotentials. Other challenges associated with the Li-O₂ battery include instability, leakages, flammability and volatility of commonly used aprotic electrolytes. In this thesis, two series of compounds are investigated as solutions to these issues: (2,2,6,6-tetramethylpiperidin-1-yl)oxyl (TEMPO) substituted imidazolium ionic liquids (TEMPOImILs) with different lengths of alkyl linkage between the TEMPO and imidazole moieties and with either H or CH₃ on the 2-position of the imidazole ring, and phenyl nitronyl nitroxides (RPTIOs) with varied substituents on the benzene ring. The compounds were characterized using NMR and FTIR together with elemental analysis, TGA, DSC and EIS for TEMPOImILs. Redox processes were studied using cyclic voltammetry and, for RPTIOs, UV-visible spectroelectrochemistry. The effect of the RMs on the battery performance was tested by assembling and cycling Li-O₂ batteries. For RPTIOs, cathodes were analysed after cycling of the batteries using SEM and XRD, and battery tests in argon were conducted to determine if there was a contribution to the capacity from redox shuttling of the RM. It was found that TEMPOImILs can serve both as charging RMs and safer electrolyte solvents for Li-O₂ batteries, while RPTIOs not only catalyse the charge process but also provide some improvement of the discharge performance. The length of alkyl chain in TEMPOImILs did not have any noticeable effect on the battery performance, whereas TEMPOImILs with 1-methylimidazolium cations provided substantially longer cycle life than those with 1,2-dimethylimidazolium cations. The charge potentials of the batteries with RPTIOs with the electron-donating groups were the lowest, showing that altering the structures of nitronyl-nitroxide-based RMs can

directly affect battery performance. Overall, the use of the RMs in combination with other measures discussed in the thesis can lead to high-performance Li-O₂ batteries.

Overview

There is currently an active search for alternatives to non-renewable energy resources. Alternative energy sources include sunlight, nuclear reactions, wind, and tide power. In some cases, the energy generated by these types of plants must be stored. Batteries are a common and important form of energy storage. Energy storage devices are also used in transportable electronics for civilian and military purposes, uninterrupted power supplies, battery storage power stations, power tools, and electric vehicles.¹⁻² The latter are particularly interesting as an alternative to conventional vehicles.³

Most of the existing electric vehicles utilise lithium-ion (Li-ion) or nickel-metal hydride battery packs with the former prevailing during the last few years due to a higher specific energy.⁴⁻⁵ However, the theoretical specific energy for Li-ion batteries does not exceed 600 Wh·kg⁻¹, which makes it difficult to compete with the internal combustion engine.⁶⁻⁷

Lithium-oxygen (Li-O₂) secondary batteries have attracted considerable attention because their theoretical specific energy is the highest of all known cathode and anode materials and is close to that of gasoline.^{6,8} In practice, there are many issues affecting the performance of Li-O₂ batteries. An important problem is the accumulation of the discharge product, Li₂O₂, that blocks the cathode surface leading to a high charge overpotential and poor cycle life.⁹⁻¹¹ To address this issue, soluble electrocatalysts (redox mediators) have been proposed that have a better contact area than traditionally used heterogeneous catalysts.⁹⁻¹⁰

Other drawbacks include the formation of Li metal dendrites, flammability, volatility and instability of all known liquid electrolytes in the presence of reactive oxygen species.^{9,12-13} New electrolytes targeting these issues need to be considered.

It was hypothesised here that new redox mediators that reduce the charge overpotential and improve the cyclability of Li-O₂ batteries could be synthesised. In addition, electrolytes could be chosen such that they suppress the dendritic Li growth and provide safer batteries. Overall, the project aimed to develop high-performance Li-O₂ batteries. Thus, the specific project aims are:

- To synthesise compounds with properties suitable for the use as redox mediators and/or electrolytes in Li-O₂ batteries.
- To fabricate and characterise Li-O₂ batteries that integrate the proposed redox mediators and/or electrolytes.
- To analyse the effect of implementing the new redox mediators and/or electrolytes on the charge and discharge overpotentials, charge and discharge capacity and cycle life of Li-O₂ batteries.

To satisfy these aims, two series of compounds have been proposed: (i) TEMPO-functionalised imidazolium ionic liquids and (ii) substituted phenyl nitronyl nitroxides. While the latter were used solely as redox mediators, the former compounds combined the properties of redox mediators and electrolyte solvents.

The thesis is organised as follows: Chapter 1 provides a brief overview of theory of batteries with some important definitions and analyses the information available in the literature about Li-O₂ batteries, *i.e.*, operating principles, drawbacks emphasising the need for new redox mediators and electrolytes, redox mediators and electrolytes applied to date. Chapter 2 contains a detailed explanation of the research approach and methods used in this

project, including synthetic methods and characterisation techniques, and presents experimental data. Chapter 3 focuses on the synthesis and general characterisation of TEMPO-functionalised imidazolium ionic liquids, followed by the analysis of electrochemical results. Chapter 4 presents and discusses the results obtained for experiments using substituted phenyl nitronyl nitroxides as RMs. Chapter 5 summarises the essential findings and suggests directions for future research. Appendices include figures containing TGA and DSC data for TEMPOImILs and a study investigating the potential of octa- and deca-methylferrocenes to be used as RMs for Li-O₂ batteries.

Chapter 1: Redox Mediators and Electrolytes in Li-O₂ Batteries

Chapter 1: Redox Mediators and Electrolytes in Li-O₂ Batteries

1.1. General Theoretical Considerations for Batteries

This section provides a general overview of some fundamental concepts related to battery operation.

Batteries convert stored chemical energy into electrical energy by electrochemical oxidation/reduction reactions.⁹ A *battery* consists of one or more voltaic cells electrically connected in an appropriate series or parallel arrangement depending on the desired output voltage and capacity. Apart from voltaic cells, batteries usually include casing material, terminals, markings, and sometimes additional components such as monitors, controls, fuses, and diodes.¹⁴ These other components are not discussed further here.

1.1.1. Voltaic Cells

A *voltaic cell* is composed of two half-cells. Each *half-cell* contains an electrode immersed in a conducting material and is separated from the other half-cell by a porous membrane or connected by a salt bridge through which ions of the conducting material can pass. Current will flow when the two electrodes are connected, and the voltaic cell will produce electricity.¹⁵

In each half-cell, a chemical oxidation or reduction reaction occurs. The electrode at which electron affinity is stronger, other conditions being equal, will undergo a reduction reaction, while the one that has a comparably lower electron affinity will be oxidised. According to this, it is possible to predict the direction of the current.¹⁵

According to the convention widely adopted for voltaic cells, the electrode at which oxidation happens spontaneously (during discharge of a cell) is a “negative” pole or *anode*, and the one at which reduction happens spontaneously is a “positive” pole or *cathode*.¹⁴

The anode, cathode and a conducting material need to be selected correctly to assembly a functional voltaic cell. Ideally, these components should not react with each other. Non-toxic and relatively cheap materials are also attractive for practical purposes. For the electrodes, materials with a high theoretical capacity, appropriate working voltage, good conductivity and high stability should be considered. Efficient reducing agents with a high negative standard electrode potential are good candidates for anode materials, and strong oxidants with high positive potential may be appropriate as cathode materials (this will provide higher theoretical voltage of the cell). The conducting material must have suitable ionic conductivity, but at the same time should be electronically insulating, otherwise internal short-circuiting will occur. The properties of the conducting material should not dramatically change with temperature. Conducting materials include aqueous solutions of electrolytes, fused salts, non-aqueous liquid and solid electrolytes.¹⁴

1.1.2. Primary and Secondary Batteries

Depending on the ability to be recharged, batteries can be primary (non-rechargeable) and secondary (rechargeable).

Primary batteries generally have a good shelf life and high energy density at low to moderate discharge rates. They can be used only once and need to be discarded after the anode has been exhausted. Primary batteries are applied in portable electronics, photography, toys, lighting, and military devices.¹⁴⁻¹⁵

In *secondary batteries*, dissolved electrode material can be re-formed. Secondary batteries can substitute primary batteries in some devices and can be more economical. Furthermore, secondary batteries can store energy from primary energy sources and deliver the energy to a load on demand.¹⁴

1.1.3. Theoretical Voltage, Capacity, and Energy

The *theoretical voltage* of a voltaic cell is also called the electromotive force or standard cell potential ($E^0_{(cell)}$) and is measured in volts (V). It is an algebraic sum of the two electrode potentials (Eq. 1).

$$E^0_{(cell)} = E^0_{(cathode)} - E^0_{(anode)} \quad (1)$$

Electrode potential is the difference in the electrical potential at the surface of separation between the electrode and the conducting material. If it is an oxidation reaction, for example, a metal yielding ions into the solution of a corresponding salt, then the metal will become negatively charged to the solution; therefore, the potential difference between the metal and the solution will have a negative sign.¹⁵

Standard electrode potentials E^0 of the half-cells are often reported against the standard (or normal) hydrogen electrode (SHE or NHE) which has a potential chosen to be 0 V. The SHE is composed of a platinum electrode immersed in a solution of hydrochloric acid with hydrogen gas bubbled through it.¹⁶ For Li-based batteries, the reference electrode typically used is Li redox couple (Li/Li^+) which has a potential of -3.05 V vs. SHE at 25°C in an aqueous solution.¹⁰

The *theoretical capacity* of a cell is the total amount of charge that may be obtained from the active materials and is measured in ampere-hours (Q_{theor} , Ah), which is

proportional to coulombs. In other words, the capacity is the amount of time a battery can supply a certain current until the cut-off voltage is reached.¹⁷ In practice, it is calculated by integrating the discharge current, I , over the discharge time, t_D (Eq. 2).² This equation allows the calculation of a *nominal capacity* Q_{nom} (capacity obtained under specific conditions).

$$Q_{nom} = \int_0^{t_D} I(t)dt = I \times t_D \text{ (for a constant current } I) \quad (2)$$

Gravimetric specific capacity is a capacity per kilogram of active material (Ah kg^{-1}). For an individual compound, it equals 26.8Ah mol^{-1} or 96487 C mol^{-1} divided by the molecular weight of the compound and multiplied by a number of electrons transferred in the reaction. To calculate the theoretical gravimetric specific capacity of a cell, one should add reciprocals of the capacities of reactants in the overall chemical reaction and inverse the obtained value.¹⁴

The *theoretical energy* (U_{theor}) of a cell is a product of the theoretical voltage and capacity and is measured in Watt hours (Wh, Eq. 3), which is proportional to joules.

$$U_{theor}(\text{Wh}) = E^0_{(cell)} (V) \times Q_{theor} (\text{Ah}) \quad (3)$$

Theoretical *gravimetric specific energy* (Wh kg^{-1}) is the energy per kilogram of active material or a product of the theoretical voltage and gravimetric specific capacity.¹⁴ In practice, predicted energy of the battery is only partially achieved due to many reasons.¹⁴

Actual specific energy U of a cell can be calculated from charge/discharge (galvanostatic cycling) curves by integrating the discharge voltage (E , V) curve over the course of discharge and multiplying it by half of the applied constant current I (Eq. 4).²

$$U = \frac{1}{2} I \int_0^{t_D} E(t) dt \quad (4)$$

1.1.4. Discharge, Charge, Cycle Life, Coulombic Efficiency, State of Charge, Definitions Related to Voltage

In rechargeable batteries, the reaction at the electrodes can proceed in either forward or reverse directions.

The *discharge* is a process of conversion of the chemical energy of the battery into electric energy. During discharge, the reactions in a voltaic cell happen spontaneously and, consequently, the current flows from the anode to the cathode. A battery cell is completely discharged when the anode material had been consumed.¹⁴

Charge or recharge (also referred to as electrolysis) is a process of conversion of the electric energy from the external current into chemical energy within the battery. During the charge, an external current applied in the opposite direction reverses the reactions and leads to the re-forming of the anode and the cathode electrolyte.¹⁴

The *cycle life* (lifetime, life span, cyclability) is the number of complete discharge-charge cycles under specified conditions a cell can experience before it fails to meet specific performance criteria, *e.g.*, a certain capacity or voltage value.¹⁴

Coulombic efficiency is a ratio between the amount of charge obtained from the battery during discharge to the amount of charge supplied during charging.²

Overpotential is the difference between practically and thermodynamically determined potentials of the redox process.¹⁴

The *cut-off voltage* is the voltage at which a battery cell is considered fully discharged and further discharging will cause harm.

The *open-circuit voltage* (OCV) of a cell is the voltage measured at zero current.²

1.2. Redox Mediators and Electrolytes in Aprotic Li-O₂ Batteries

There has been significant development in the field of Li-O₂ batteries in the last decade as they are considered the most promising power sources for electric vehicles.^{9,18} Many authors refer to Li-O₂ batteries as “lithium-air batteries”, but in most cases not air but pure oxygen gas is used as the cathode material to avoid side reactions occurring in the presence of CO₂ and H₂O.¹⁹⁻²¹

The development of aqueous Li-O₂ batteries started in the 1970s and they were susceptible to corrosion that decreased the capacity of the battery.²¹⁻²⁴ The prototype of the non-aqueous Li-O₂ cell with molten salt electrolyte was reported by Semkow and Sammels in 1987.²⁵ In 1996, Abraham and Jiang presented the first Li-O₂ battery with polymer-based aprotic electrolyte. The lifetime of this battery was short partially because the oxygen from the air penetrated through the electrolyte and reacted with the Li anode causing its degradation.²⁵⁻²⁶ Later, numerous studies were conducted to improve the rechargeability of Li-O₂ batteries.

This section surveys the published information about the development of Li-O₂ batteries, their operating principles and mechanisms, main challenges affecting performance, known solutions to these challenges, types of electrolytes applied to date, and the incorporation of redox mediators. This information is crucial to assemble a high-performance Li-O₂ battery.

1.2.1. Operating Principles and Composition of Li-O₂ Batteries

Currently, there are three main types of rechargeable Li-O₂ batteries: with aprotic, hybrid aqueous/aprotic, and solid-state electrolytes.^{9,24} Liquid electrolytes are composed of a salt (ion-conducting agent) and the electrolyte solvent in which it is dissolved.

1.2.1.1. Aprotic Li-O₂ Batteries

In aprotic Li-O₂ batteries, an aprotic electrolyte separates the Li metal anode and cathode from each other (Fig. 1).

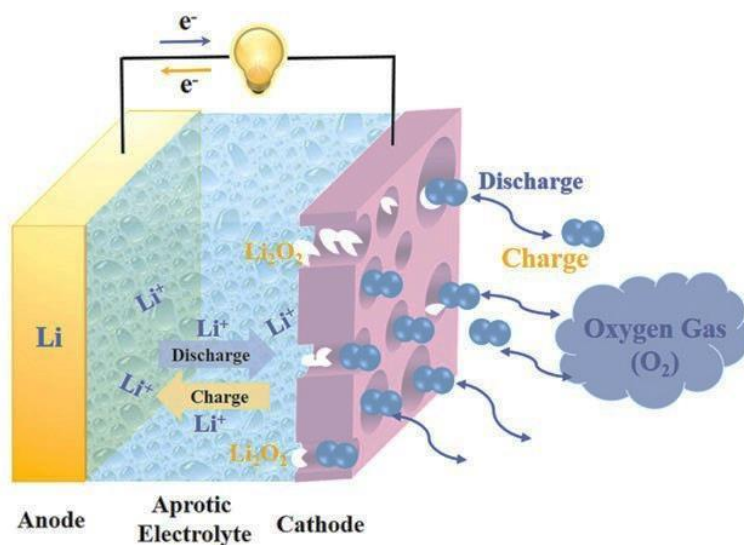
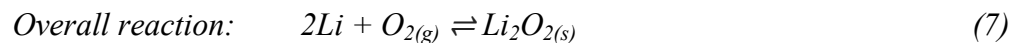
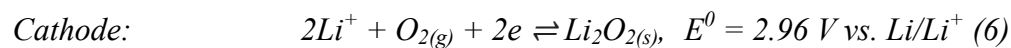
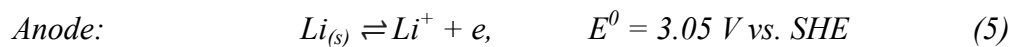


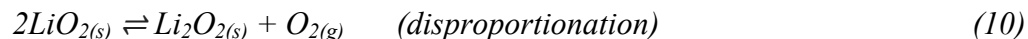
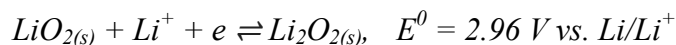
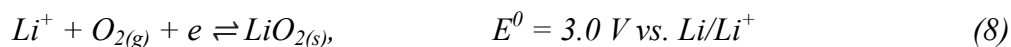
Figure 1. Schematic diagram of aprotic Li-O₂ battery.⁹

The reactions at the electrodes follow Equations 5 and 6. Upon discharge, Li anode forms Li ions, and the electrons flow from the anode to the cathode surface where oxygen reduction reaction (ORR) occurs. During charging, a reversible reaction proceeds at the cathode where lithium peroxide (Li₂O₂) is decomposed yielding O₂ and Li ions (oxygen evolution reaction, OER).⁹



Apart from Li_2O_2 , other compounds have been reported to form during battery operation. These compounds are discussed in detail below.

Firstly, it was found that lithium superoxide (LiO_2) forms during discharge as an intermediate product (Eq. 8), though there are controversial opinions regarding the mechanism of its conversion to Li_2O_2 (Eq. 8, 9).^{9,18,27-28}



LiO_2 would be a desirable discharge product because of its higher solubility in aprotic solvents compared to Li_2O_2 . Recently, some authors claimed that they achieved a one-electron discharge process in Li- O_2 batteries leading to a formation of only LiO_2 (Eq. 8).²⁹⁻
³⁰ However, these results have been refuted by Papp and co-workers who showed that Raman shifts that were previously assigned to LiO_2 are indeed related to the decomposition of poly(vinylidene fluoride) binder commonly used in the preparation of the carbon cathode.³¹

Secondly, it was suggested that Li_2O might also form as a discharge product in Li- O_2 batteries according to the Equation 11:^{19,32}



However, while having a higher specific energy and energy density, Li₂O forms more slowly than Li₂O₂, and its formation can only be observed at a cut-off voltage lower than 2 V.^{19,32}

In addition, there are some contaminants that can be formed in aprotic Li-O₂ batteries: LiOH, Li₂CO₃, LiRCO₂ (where R = alkyl or H), and Li₃N. Pathways for the formation of these compounds have been extensively studied:

1. Decomposition of the solvents by O₂ and reactive oxygen species (O₂⁻, O₂²⁻, Li₂O₂, LiO₂/LiO₂⁻);^{9,11,18-19,32-35}
2. Reaction of Li/Li₂O₂/Li⁺ with H₂O, N₂, CO₂ from the air;^{9,11,21,36-37}
3. Oxidation of carbon-based cathode in the presence of Li₂O₂ or LiO₂.^{9,19,21,38-39}

There have been several investigations into the effect of the addition of water to aprotic Li-O₂ batteries.⁴⁰⁻⁴⁷ The addition of small amounts of water to aprotic electrolyte or the use of oxygen gas with increased humidity led to a higher discharge capacity and lower initial charging potential. Initially many of the researchers related this phenomenon to a conversion of Li₂O₂ into LiOH that can be decomposed at lower voltages,⁴¹⁻⁴⁵ while others proposed that it is the “solubilisation” of LiO₂ intermediate that changes the growth pattern of Li₂O₂ discharge product leading to increased capacity (Section 1.2.2.4).^{40,46} A review by Dai et al. favours the second hypothesis about the increased solubility of LiO₂.⁴⁷ In some cases, the cycle life of a cell was affected because of the solvent decomposition at increased potentials in humid media, especially for ether-based solvents.

Aprotic electrolyte solvents applied in Li-O₂ batteries to date include: alkyl carbonates; ether-based solvents – ethylene glycol dimethyl ether (glyme, dimethoxyethane, DME),

diethylene glycol dimethyl ether (diglyme, DEGDME), tetraethylene glycol dimethyl ether (tetraglyme, TEGDME), 1,3-dioxolane (DOL), 2,2,4,4,5,5-hexamethyl-1,3-dioxolane; amides – dimethylformamide (DMF), *N,N*-dimethylacetamide (DMA), *N,N*-dimethyl-trifluoroacetamide (DMFTA); dimethyl sulfoxide (DMSO), ethylmethanesulfonate (EMS), acetonitrile (MeCN), sulfones, and ionic liquids.^{9,24-25,48}

There are several reviews and papers about the electrolyte salts added to Li-O₂ battery solvents.^{9,49-52} Stable lithium bis(trifluoromethanesulfonyl)imide (LiTFSI) salt is widely used nowadays, and it was found to form a protective layer on Li metal based on LiF.⁵³

Ionic liquids (ILs) have been extensively studied as electrolyte solvents for Li-O₂ batteries as they have near-zero vapour pressure, high stability and very low flammability.^{9,19-21,24-25,32,35}

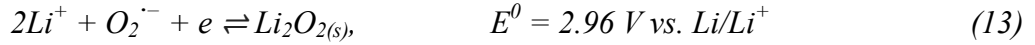
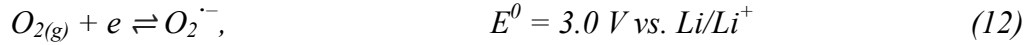
In 2012, the use of imidazolium ionic liquids as electrolytes for Li-O₂ batteries was first reported.⁵⁴ The authors used one pyrrol- and two imidazole-based ionic liquids and increased the operating temperature up to 150 °C. The authors claimed that in some cases the reduction of the discharge product Li₂O₂ into Li₂O was observed, but they did not present any conclusive evidence for this process.

Initially, low rate capability was a serious drawback of IL batteries, as it drastically lowered their suitability for use in electric vehicles. In 2016, a battery was reported consisting of a composite LiFePO₄ anode, electrolytic manganese dioxide and ruthenium supported on Super P (carbon black) as a cathode, and 1-methyl-3-propylimidazolium bis(trifluoromethylsulfonyl)imide with dissolved LiTFSI as an electrolyte.⁴¹ This battery exhibited a low charge overpotential of only 0.36 V and at a relative humidity (RH) of

$\geq 51\%$ had a lithium hydroxide hydrate ($\text{LiOH} \cdot \text{H}_2\text{O}$) instead of Li_2O_2 as the main discharge product, according to XRD results. The authors proposed a new mechanism for ORR in Li-O_2 batteries (the main reactions are shown in Eqs. 12–17 below) where with increasing RH the reaction route changes from Route 1 to Route 2 (see below).

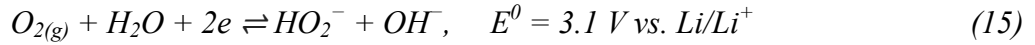
Route 1. Low humidity.

Cathode:



Route 2. High humidity.

Cathode:



According to Route 1, at low RH, the first reaction step is the formation of oxygen anion radicals $\text{O}_2^{\cdot-}$ (Eq. 12), which then react with Li ions to produce Li_2O_2 (Eq. 13). However, in this case, Li_2O_2 may further react with water to yield some amount of LiOH (Eq. 14). At $\text{RH} \geq 51\%$, initially, the formation of hydrogen peroxide and hydroxide anions (HO_2^- and OH^-) occurs (Route 2, Eq. 15). This step is the same as in the proposed mechanism for the formation of Li_2O_2 in aqueous electrolytes saturated with LiOH (Eq 20 in Section 1.2.1.2).

Equations 16, 17 show how the LiOH discharge product is formed, which can further react with H₂O to produce LiOH·H₂O observed at high RH.

The battery demonstrated a high rate capability and excellent cyclic stability at RH of 51% as it ran for 218 cycles and 95 cycles at high current densities of 500 and 1000 mA g⁻¹, respectively, and a capacity of 1000 mAh g⁻¹.

Another study focussing on the rate capability of IL-based batteries was published by Zhang and Wen in 2017.⁵⁵ The ether-functionalised ammonium ionic liquid (*N,N*-diethyl-*N*-methyl-*N*-(2-methoxyethyl) ammonium bis(trifluoromethylsulfonyl)) was added to single-walled carbon nanotubes to compose a cross-linked network gel cathode. The ionic liquid was used solely as an electrolyte solvent and Li foil as an anode. The battery was tested in pure oxygen. The battery exhibited a high rate capability at 80 °C as it could deliver a capacity of 1000 mAh g⁻¹ for 25 cycles at a current density of 5.0 mA cm⁻². It was discovered using XRD that with increasing current density, the discharge product changed from Li₂O₂ to LiOH. The performance of an imidazolium ionic liquid at high temperature was similar to that of its ammonium analogue, although the OCV was unstable.

Solvate ionic liquids (SILs) are concentrated mixtures of organic solvents and lithium salts that behave like ionic liquids due to the formation of a chelate complex between the solvent molecules and salt ions. Recently, the stability of a glyme SIL was evaluated as an electrolyte in Li-O₂ batteries that contained an equimolar mixture of glyme and LiTFSI in comparison with a conventional LiTFSI/glyme electrolyte (a mixture of LiTFSI with an excess of glyme).⁵⁶ The SIL exhibited higher stability in the oxygen atmosphere.

Mixtures of ionic liquids with aprotic electrolytes or with gel polymer electrolytes (GPEs) are actively studied nowadays.^{24,57} For instance, Asadi et al. reported a battery with a mixture of imidazolium ionic liquid:DMSO (1:3) as an electrolyte solvent, lithium carbonate-protected Li metal anode and a molybdenum disulfide-based cathode.⁵⁸ The battery performed 100 cycles and 700 cycles at a capacity of 1000 and 500 mAh g⁻¹, respectively, under a current density of 500 mA g⁻¹ in an air-like atmosphere.

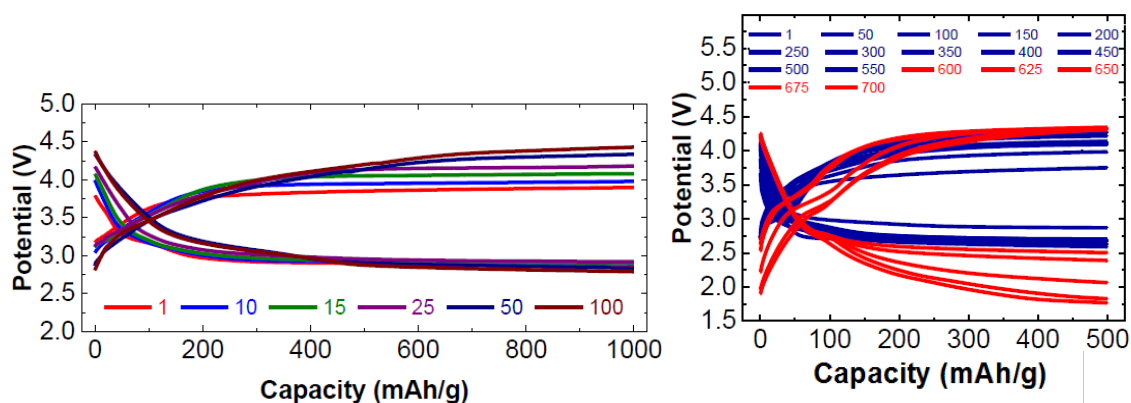


Figure 2. Discharge/charge profiles of Li-O₂ batteries with IL/DMSO electrolyte at a capacity of 1000 mAh g⁻¹ (left) and 500 mAh g⁻¹ (right).⁵⁸

1.2.1.2. Hybrid Aqueous/Aprotic Li-O₂ Batteries

Another type of rechargeable Li-O₂ battery uses hybrid aqueous/aprotic electrolytes and follows the mechanism of aqueous Li-O₂ batteries. The aqueous electrolyte generally consists of a Li salt, acid or LiOH dissolved in water. Rechargeable Li-O₂ batteries with aqueous electrolyte require a protective layer for the Li anode to avoid the reactions between Li and the electrolyte.⁵⁹ In addition, a buffer layer should be used as a separator to eliminate the reaction between the protective layer and Li anode. These considerations lead

to a three-layer construction of hybrid aqueous/aprotic Li-O₂ batteries depicted in Figure 2.⁶⁰

As a protective layer, LISICON-type (Li analogues of NASICON – Sodium (Na) Super Ionic CONductor, Na_{1+x}Zr₂Si_xP_{3-x}O₁₂, 0 < x < 3) and garnet-type Li-ion conducting materials are commonly used, with the most favourable LTAP glass ceramic protective layer (Li_{1+x+y}Ti_{2-x}Al_xP_{3-y}Si_yO₁₂) that does not permit H₂O and O₂ molecules.⁵⁹⁻⁶⁴ As a buffer layer, solid-state Li-ion conductors, polymer electrolytes, or organic solvents can be applied.⁵⁹

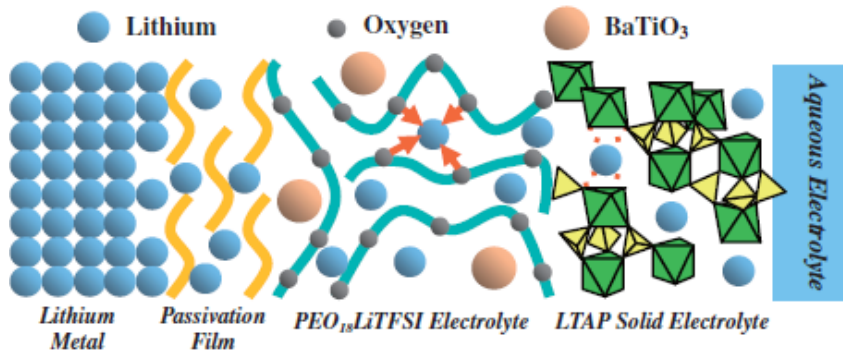
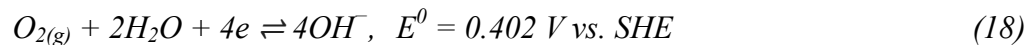


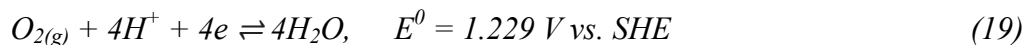
Figure 3. Schematic diagram of a hybrid Li-O₂ battery with a protected anode.⁴⁹

In hybrid aqueous/aprotic and aqueous batteries, the anode reaction is the same as in the aprotic batteries (Eq. 5), while the reactions at the cathode slightly vary depending on the pH of the aqueous electrolyte. Oxygen is reduced at the cathode yielding hydroxide ions in a basic solution or water in an acidic solution. The main discharge product is LiOH, which has been detected by XRD (Eqs. 18–20).^{59,62,65}

Cathode (basic solution):



Cathode (acidic solution):

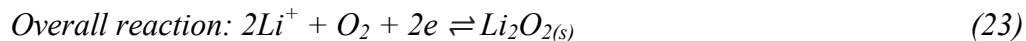
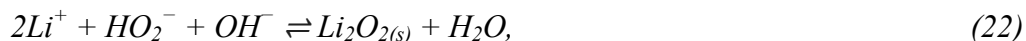
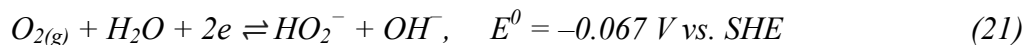


Overall reaction for both acidic and basic solutions:



Another proposed mechanism⁵⁹ for aqueous Li-O₂ batteries involves two-electron transfer reactions at the cathode with the formation of species that can react with Li ions to form Li₂O₂ (Eqs. 21–23). In this case, hydrolysis of Li₂O₂ is prevented by the use of an electrolyte saturated with LiOH (basic solutions).

Cathode (basic solution):



According to this mechanism, in basic solutions, the discharge product is Li₂O₂, the same as in aprotic Li-O₂ batteries. However, only one example of this mechanism has been reported⁶⁶ in a hybrid aqueous/aprotic Li-O₂ battery. A similar mechanism has also been discussed in the context of aprotic Li-O₂ batteries if small amounts of water are added to the aprotic electrolyte.⁶⁷

A drawback of hybrid Li-O₂ batteries is that the electrolyte is consumed during the operation of a battery and LiOH starts precipitating due to oversaturation. The precipitation of LiOH substantially decreases capacity; however, several solutions to this problem have been proposed.¹⁸ For example, by the addition of a RuO₂ oxygen evolution electrode to the

standard hybrid aqueous/aprotic Li-O₂ battery with carbon black oxygen reduction air electrode, it became possible to achieve a practical specific energy of 810 Wh kg⁻¹ at 1.5 V and the capacity of the air electrode of 2000 mAh g⁻¹_{cathode}. However, the battery cycle life did not exceed seven cycles in the air atmosphere due to the formation of Li₂CO₃.⁶⁸

1.2.1.3. Solid- and Quasi-solid-state Li-O₂ Batteries*

To address the issues of electrolyte degradation in Li-O₂ batteries, along with flammability and volatility,¹²⁻¹³ solid electrolytes were applied and have been described in several reviews.^{13,24,70-72} Solid electrolytes can be made using organic (polymers) as well as inorganic compounds (ceramics). The first solid-state batteries were tested by Kumar *et al*²⁶ and included both glass-ceramic and polymer-ceramic materials. Later, solid-state batteries with purely inorganic solid electrolytes were developed.⁷² In these batteries, the formation of Li₂O₂, LiOH and Li₂CO₃ was observed, and it was suggested that the overall mechanism is similar to that in the aqueous batteries.^{21,72-73} The main drawbacks of the batteries with inorganic solid electrolytes are brittleness and high resistance on the interface between cathode/anode materials and the electrolyte; while batteries with solid polymer electrolytes (SPEs) are more flexible, but generally suffer from low ionic conductivity.¹³

To date, three polymeric materials have been reported for use in solid-state Li-O₂ batteries: poly(ethylene oxide) (PEO),⁷⁴⁻⁷⁶ Nafion (a sulfonated tetrafluoroethylene based fluoropolymer-copolymer),⁷⁷ and poly(vinylalcohol) (PVA).⁷⁸ Among these, there are only two reports about the cycle life of the batteries. Thus, Cheng and Scott reported that a battery with the electrolyte based on lithiated Nafion could survive in ambient air for about

* This section is based on a chapter describing SPEs in Li-O₂ batteries written by Anastasiia Tkacheva in a recent review⁶⁹

20 cycles with the initial capacity of $300 \text{ mAh g}_{(\text{solids})}^{-1}$.⁷⁷ Ein-Eli *et al.* presented the cycling performance of the battery with PEO-based SPE studied at 80°C . The battery operated for 40 cycles at a capacity limit of $210 \text{ mAh g}_{(\text{CNT})}^{-1}$, which is the highest reported for solid-state polymer Li-O₂ batteries to date.⁷⁹

The poor cycle life of batteries with SPEs is in some cases caused by the instability of the polymers in the Li-O₂ battery system. Recently, the interaction of various polymers with KO₂ or Li₂O₂ was investigated.^{13,80} PEO appeared to be relatively stable, though other studies indicated that PEO is susceptible to auto-oxidation during the operation of Li-O₂ batteries.^{76,80-81} The stability of PVA in Li-O₂ battery has not yet been studied. It would be useful to further investigate all-solid-state Li-O₂ batteries with the polymers that have proved to be relatively stable, such as poly(methyl methacrylate) (PMMA), poly(tetrafluoroethylene) (PTFE) and Nafion.⁸⁰ Currently, these polymers are widely applied in GPE-based Li-O₂ batteries, along with the compounds such as ethoxylated trimethylolpropane triacrylate (ETPTA).

Other factors causing unsatisfactory performance in Li-O₂ batteries with SPEs include low ionic conductivity and high interfacial resistance between Li₂O₂, possible by-products (LiOH, Li₂CO₃, lithium alkyl carbonates), carbon-based cathodes, and SPE.^{13,82} The addition of plasticisers (non-volatile organic solvents or low molecular weight polymers) improves the ionic conductivity though partially sacrificing the rigidity required to suppress the formation of Li dendrites.^{24,49,83} On the other hand, mixing a polymer with ceramic nanofillers is assumed to reduce interfacial resistance and increase the ionic conductivity while maintaining the appropriate mechanical properties.^{13,75,84-86} However, even with the addition of nanosized fillers such as SiO₂ or sulfonated ZrO₂ to PEO-based SPE the ionic

conductivity did not exceed $10^{-4} \text{ S cm}^{-1}$.^{74,76} There are some examples of lowering interfacial resistance by using the same polymer or ionic liquid as a binder during preparation of the cathode^{55,87-88} and by adding solid electrocatalysts,^{13,77,82} yet this approach did not lead to significant improvements in case of SPEs.²⁷ Hence, switching to GPEs was essential to achieve the acceptable ionic conductivity ($\geq 10^{-3} \text{ S cm}^{-1}$).⁸⁹

GPEs are obtained by swelling SPEs with plasticisers to a certain extent. They are referred to as quasi-solid-state Li-O₂ batteries. In terms of mechanical properties and safety, GPEs are similar to solid electrolytes, while their ionic conductivity and interfacial resistance are close to those of liquid electrolytes.^{13,49,85-86} The methods for the preparation of GPEs are described elsewhere.²⁵

There are several reports regarding the application in Li-O₂ batteries of GPEs based on the polymers where stability in the presence of reactive oxygen species remains doubtful, such as PAN,⁸⁹⁻⁹¹ poly(vinylidene fluoride-co-hexafluoropropylene) (P(VdF-HFP))^{13,57,92-94}, and PEO⁹⁵. However, the employment of electrocatalysts can improve stability by lowering charge voltages.^{82,93} In some cases, stable cycling performance was achieved without any additives. For instance, a battery based on P(VdF-HFP) electrolyte plasticised with TEGDME exhibited longer cycle life compared to conventional TEGDME-based electrolyte (Fig. 4).⁹²

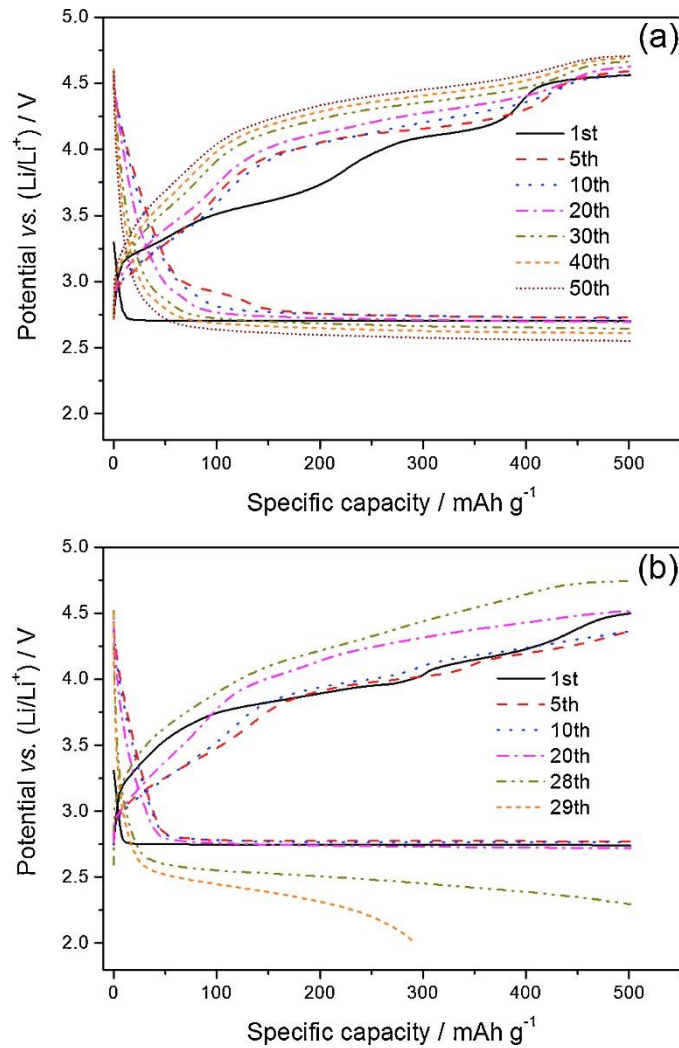


Figure 4. Charge-discharge curves of Li-O₂ batteries based on (a) P(VdF-HFP)/TEGDME GPE (b) liquid TEGDME electrolyte obtained at a fixed capacity of 500 mAh g⁻¹ ⁹².

The addition of ceramic fillers to GPEs has led to improvements in capacity and cycle life of Li-O₂ batteries.^{13,82} For example, a Li-O₂ battery with PMMA-based GPE containing polystyrene and nanofumed SiO₂ stably cycled more than 100 times in ambient air with a capacity restricted to 500 mAh g⁻¹ (Fig. 5). The ionic conductivity, however, was slightly lower than optimum (2.5·10⁻⁴ S cm⁻¹).⁸⁶

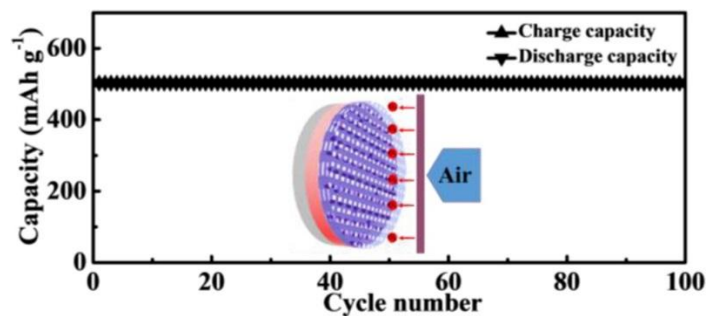


Figure 5. Cycle life of Li-O₂ batteries with PMMA based GPE.⁸⁶

Soluble electrocatalysts (redox mediators, RMs) that act as electron carriers improved the kinetics of Li₂O₂ formation and decomposition, leading to lower discharge and especially charge overpotentials and increased cycle life of Li-O₂ batteries.^{10,82,93,96} Recently, Anju and Sampath demonstrated a battery with PAN-based GPE plasticised with DMA with the addition of LiNO₃ as an RM which achieved more than 120 cycles at a capacity limited to 400 mAh g⁻¹ (Fig. 6). In this study, titanium carbonitride (TiC_{0.7}N_{0.3}) was used both as a cathode material and a solid electrocatalyst.⁸⁹

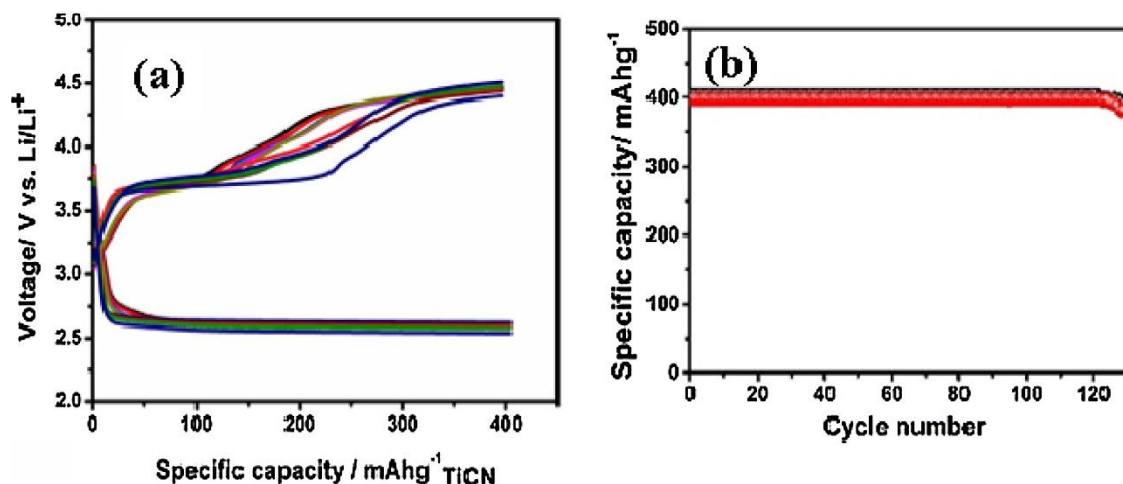


Figure 6. Electrochemical performance of Li-O₂ battery with PAN-based GPE and LiNO₃ at a fixed capacity of 400 mAh g⁻¹ (a) charge-discharge profiles; (b) cycling stability.⁸⁹

The addition of 0.05 M LiI to P(VdF-HFP)-ETPTA-based GPE led to the efficient Li-O₂ battery which survived in the air with a relative humidity of 15% for about 400 cycles with a fixed capacity of 1000 mAh g_{GO}⁻¹. The discharge voltage of this battery was higher than 2.3 V throughout the operation.⁹³

Hybrid inorganic/organic electrolytes somewhat alleviate the main drawbacks of both pure inorganic compounds (brittleness) and polymers (low ionic conductivity) and have demonstrated outstanding performances in Li-O₂ batteries.^{13,85,97} Recently, El-Zahab *et al.* incorporated one-dimensional glass micro-sized fillers into GPE based on ETPTA plasticised with TEGDME (Fig. 7).⁹⁸ Compared to pure GPE, the battery with 1% w/w of glass microfillers exhibited much higher ionic conductivity and Li ion transference number, which resulted in prolonged cycling performance.

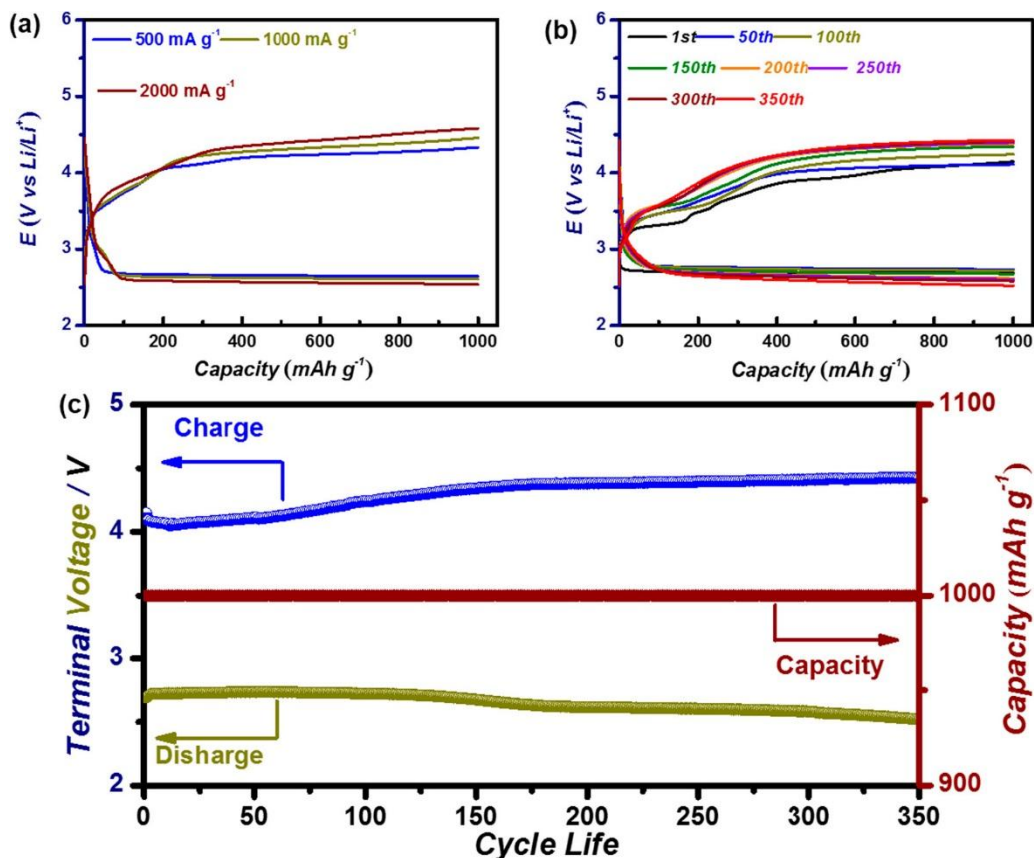


Figure 8. Electrochemical performance of Li-O₂ battery with LAGP-PMS hybrid electrolyte at 50 °C at a fixed capacity of 1000 mAh g⁻¹ (a) power output capability at different current densities (b), (c) charge-discharge curves and cyclability at a current density of 200 mA h g⁻¹.⁸⁷

Li-O₂ batteries with polymer electrolytes have achieved specific energy densities of 1350–2700 Wh kg⁻¹_(cathode active material)^{87,93,95,100} for many cycles, which is higher than reported for Li-ion batteries.^{95,101} Compared to liquid electrolytes, polymer-based Li-O₂ batteries generally exhibit greater cycle life and coulombic efficiency, though lower charge and discharge capacity.⁹²⁻⁹³

Molten salts as electrolytes for Li-O₂ batteries have been proposed³⁸ where the main discharge product in a molten LiNO₃–KNO₃ eutectic system was Li₂O₂ that was sparingly

soluble in the electrolyte. The increased solubility of Li_2O_2 led to a better rate capability and low overpotentials of only 50 mV. Nevertheless, during cycling, carbon electrode passivation by Li_2CO_3 occurred that reduced the cycle life. The formation of Li_2CO_3 was attributed to the reaction between the intermediate discharge product LiO_2 and the carbon cathode.³⁸

The properties of polymerised ionic liquids have been investigated for their prospective use in Li secondary batteries.^{29,102} To date, there is one report about their application in Li- O_2 batteries, whereby poly(diallyldimethylammonium bis(trifluoromethanesulfonyl)imide) was used as an electrolyte and helped to achieve an energy density as high as $1,214 \text{ Wh kg}^{-1}_{\text{cell}}$, though cycle life of this battery was short.¹⁰³

In summary, Li- O_2 batteries require electrolytes of a special composition to overcome the interconnected problems arising during their operation. Stability in the presence of oxygen and reactive oxygen species, high ionic conductivity ($\geq 10^{-3} \text{ S cm}^{-1}$), and low interfacial resistance are key factors of successful performance. Furthermore, the electrolyte should hinder O_2 and H_2O diffusion, which causes deterioration of Li metal anode and premature cell death. The use of highly hydrophobic polymers and ionic liquids is a promising solution to H_2O crossover. Currently, all-solid-state electrolytes do not meet most of the above requirements, which results in reduced performance. The use of GPEs with the addition of redox mediators or ceramic electrolytes helps to achieve longer cycle life and even allow the fabrication of Li- O_2 batteries with prospective use in flexible electronic devices. For the future application of Li- O_2 batteries in EVs, Li ion transference number and interfacial resistance at the 3-phase interface should be further improved.

1.2.2. Shortcomings of Li-O₂ Batteries

Li-O₂ batteries have an extremely high theoretical gravimetric specific energy of ~3500 Wh kg⁻¹ on the basis of Li₂O₂ mass^{9-10,18,35,37,59,72} or about 11430 Wh kg⁻¹ on the basis of only Li metal mass.^{6,21,33} This value is close to that of gasoline (Fig. 9). It exceeds the theoretical gravimetric specific energy calculated for Li-ion (387 Wh kg⁻¹) and Li-S batteries (2567 Wh kg⁻¹).³⁵ The practical specific energy of gasoline (approximately 1700 Wh kg⁻¹) is expected to be achievable for Li-O₂ batteries.²⁷ The reasons for such high theoretical specific energy value are:

1. High theoretical capacity due to a light weight of the active materials (Li metal and oxygen gas) and two-electron electrochemical process compared to one-electron process for Li-ion batteries
2. High theoretical voltage due to the highest negative voltage of Li among all the metals.

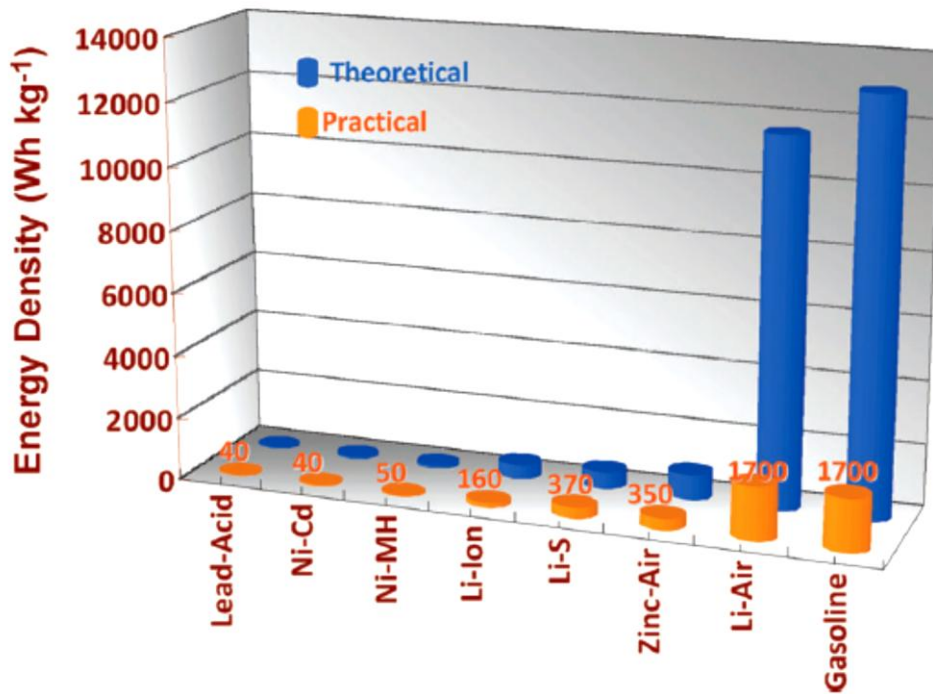


Figure 9. Gravimetric specific energies of various rechargeable batteries with gasoline.²⁷

For aqueous Li-O₂ batteries, the theoretical specific energy calculated on the basis of LiOH mass is slightly lower; 2450 Wh kg⁻¹.⁶⁰ Considering that in aqueous Li-O₂ batteries the electrolyte is gradually consumed, Kraytsberg and Ein-Eli have recalculated the theoretical specific energy to be 1300 Wh kg⁻¹ for alkaline electrolytes and 1400 Wh kg⁻¹ for acidic electrolytes. If the insolubility of the discharge product Li₂O₂ and its precipitation on the cathode is taken into account, then for aprotic Li-O₂ batteries the value becomes 2790 Wh kg⁻¹.¹⁰⁴

It is difficult to assess the maximum practical specific energy values achieved in Li-O₂ batteries to date as authors seldom reveal the exact method they use for the calculation. Comparison of specific energies for the batteries from different papers is therefore unreliable.¹⁰⁵ Apart from the value of specific energy, other aspects need to be considered such as cycle life, rate capability, energy efficiency, safety, cost, and environmental impacts.² Currently, several main issues affect the performance of Li-O₂ batteries.

1.2.2.1. Dendrite Formation

The formation of Li metal dendrites (Fig. 10) reduces the coulombic efficiency of the battery and can ultimately lead to short-circuiting between the anode and cathode.^{9,27,29}

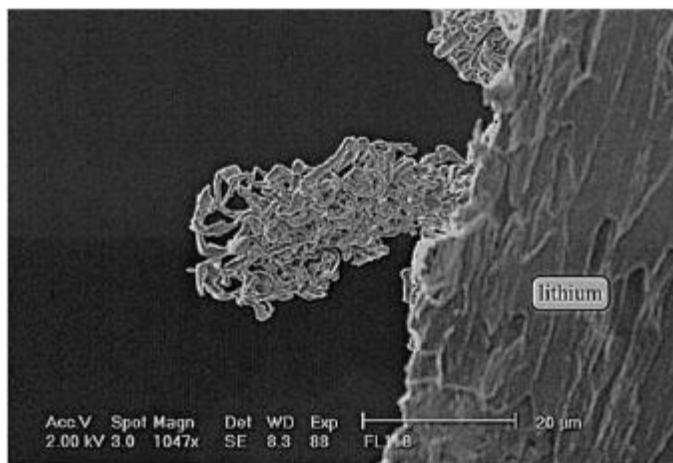


Figure 10. Scanning electron microscope image showing dendrites in a Li secondary battery.¹⁰⁶

The propagation of Li metal dendrites can be retarded by using mechanical or chemical protection methods, which were summarised in several recent reviews and papers.¹⁰⁷⁻¹¹⁰ Chemical methods aim to build an effective solid electrolyte interface (SEI) – a protective layer on the surface of Li metal anode that prevents its interaction with the electrolyte. This layer is obtained during the reaction of Li metal with an additive. A stable SEI can form with the use of electrolytes and solvents such as LiNO_3/DMA ¹¹¹, α -fluorinated amines (e.g., DMFTA)¹¹², additives like lithium 2-bromoethanesulfonate,¹² Cs or Rb ions,¹¹³ LiF, LiTFSI, LiNO_3 , vinylene carbonates and sultones¹¹⁴, 2,2,2-trichloroethylchloroformate¹¹⁵, boric acid¹¹⁶.

Mechanical protection includes the use of protective membranes or coatings, Li metal hosts¹¹⁰, solid/gel electrolytes.²⁷ Another approach is to replace a Li metal anode with composite materials.^{9,59,117} Anodes with the composition LiFePO_4 , $\text{Li}_4\text{Ti}_5\text{O}_{12}$ were successfully applied in Li- O_2 batteries, however, in these cases the specific energy was

significantly lower. Li-metal alloys such as $\text{Li}_x\text{Si-C}$, $\text{Li}_x\text{Sn-C}$, and $\text{Li}_x\text{Al-C}$ that have an anode potential closer to that of Li metal were also investigated.¹¹⁷

1.2.2.2. Electrolyte Decomposition

There are many reports describing electrolytes for Li-O_2 batteries. Aprotic electrolytes gradually react with oxygen and Li species to form LiOH , Li_2CO_3 , LiRCO_2 leading to clogging of the cathode surface and premature death of the cell.¹² In the case of carbonate-based solvents, Li_2CO_3 and LiRCO_2 were found to be formed instead of Li_2O_2 during discharge, which indicates severe decomposition of the electrolyte.⁹ Ether-based solvents are more stable and produce Li_2O_2 as the main discharge product, but they still degrade over time. The performance of ether-based solvents strongly depends on the Li salt added to the electrolyte. DMSO and amide-based solvents were found to react with bare Li metal, though they are relatively stable in the presence of reactive oxygen species.²⁴

The abstraction of hydrogen attached to a carbon atom in an α -position to an electron-withdrawing atom (*e.g.*, nitrogen or oxygen) by reactive oxygen species leads to degradation of many commonly used solvents in Li-O_2 batteries. To solve this problem, a new liquid electrolyte – fully methylated cyclic ether (2,2,4,4,5,5-hexamethyl-1,3-dioxolane, HMD) – was introduced in Li-O_2 batteries.⁴⁸ The methylation of all carbon atoms prevents the abstraction of α -H providing a highly stable electrolyte. The cycle life of a Li-O_2 battery with HMD and boric acid used to protect Li metal anode was 157 cycles, which is four times higher than for DOL or DME solvents.

1.2.2.3. Li_2CO_3 and LiOH formation

The accumulation of LiOH and Li_2CO_3 introduces high charge overpotentials due to higher voltages needed to decompose these compounds.³⁶ According to DFT calculations, the voltage required for the decomposition of Li_2CO_3 and LiOH is 4.38–4.61 V and 4.67–5.02 V vs. Li/Li^+ , respectively, which are higher than that for Li_2O_2 .³⁶ The values for the formation of Li_2CO_3 and LiOH derived from the Nernst equation are 3.82 V^{36,118-119} and 3.35 V^{9,36} vs. Li/Li^+ . The use of iridium decorated boron carbide ($\text{Ir}/\text{B}_4\text{C}$) composite cathode facilitated complete decomposition of Li_2CO_3 ,¹¹⁹ assigned to the catalytic activity of iridium and boron carbide and the high oxygen adsorbability on the iridium surface.

1.2.2.4. Li_2O_2 Morphologies

The effect of the discharge product morphology on the performance of $\text{Li}-\text{O}_2$ batteries has attracted significant attention. The morphology of the discharge product can be greatly affected by the donor number of the solvent, which is a quantitative measure of the solvent's Lewis basicity, i.e., its ability to donate an electron pair to a Lewis acid, in other words, solvate Lewis acids and cations. Low donor number solvents such as DME, TEGDME, CH_3CN favour the surface route formation of Li_2O_2 leading to a film-like discharge product that requires lower charge voltage to be decomposed.¹²⁰⁻¹²¹ On the contrary, high donor number solvents (DMA, DMSO, H_2O) facilitate the solution route leading to a toroid-like discharge product that has a higher capacity. Lyu *et. al* elucidated the effect of the O_2 adsorbability on the cathode surface on the Li_2O_2 growth mechanism.¹²⁰ The authors claimed that the ability of the cathode to adsorb O_2 is a crucial factor determining the growth model of Li_2O_2 . Employing the solution route formation of Li_2O_2 coupled with the use of redox mediators may be a strategy to reduce the overpotential. The

addition of small amounts of water or potassium ions¹²² was found to promote solution route formation of Li_2O_2 . On the other hand, Kwon and co-workers proposed that the surface route mechanism can ultimately lead to better performance due to a limited transfer of the discharge product into solution, where it can precipitate on the non-conducting elements of a cell.⁵⁶

1.2.2.5. Li_2O_2 Precipitation on the Cathode and its Sluggish Kinetics

Clogging of the carbon-based cathode by Li_2O_2 and sluggish kinetics of the OER introduce a high charge overpotential in Li-O₂ batteries (up to 1–1.5 V compared to 0.3 V for the discharge).⁹ The contrast between the charge and discharge overpotential values can be explained by different reaction mechanisms of ORR and OER. ORR is likely to proceed through an intermediate LiO_2 (Eqs. 8–10), while during OER, insoluble, electronically insulating Li_2O_2 needs to be directly decomposed into oxygen and Li ions.¹²³

Initially, to reduce the charge and discharge overpotentials, heterogeneous catalysts were applied. Carbon-based materials were found to have an evident catalytic activity for ORR.^{9,20,32,123} Ru nanoparticles supported on reduced graphene oxide exhibited a significant effect on lowering the charge overpotential and improving battery cycle life by decreasing the Li_2O_2 particle size.⁹ Perovskite-based catalysts (*e.g.*, $\text{La}_{0.65}\text{Sr}_{0.35}\text{MnO}_3$) were also found to reduce Li_2O_2 particle size, thus, decreasing the charge overpotential.¹¹ However, as stated above, a smaller particle size of Li_2O_2 leads to a decreased capacity. Interestingly, by employing RuO_2 hollow spheres as the carbon-free cathode material or

carbon nanotubes coated with RuO_2 , it became possible to reduce both charge and discharge overpotentials while maintaining a high discharge capacity.⁹

Despite these results, in many reviews it was noted that heterogeneous catalysts might not have a long-term effect on the OER due to their low mobility; moreover, noble metal catalysts were often found to accelerate the electrolyte decomposition.^{9-10,32,123} As a possible solution to this problem, soluble electrocatalysts or “redox mediators” (RMs) were proposed that have a larger contact area with solid Li_2O_2 .

1.2.3. Redox Mediators

Redox mediators (RMs) are soluble electrocatalysts that have been applied in various Li-O_2 batteries since 2011 to reduce the charge and/or discharge overpotentials.¹⁰

The charging redox mediator acts as an electron transfer carrier between the cathode surface and insulating Li_2O_2 . Specifically, a suitable redox mediator couple, denoted as RM^+/RM , dissolved in an aprotic electrolyte makes a solution-phase catalyst for the charge process. The catalytic mechanism of the redox couple RM^+/RM includes two steps (Fig. 11a). During the charging process, RM is oxidised to RM^+ on the cathode surface. Then, RM^+ diffuses to the surface of Li_2O_2 and immediately oxidises the Li_2O_2 to O_2 , resulting in the regeneration of RM. Therefore, the charging voltage can be reduced to the redox potential of RM^+/RM , leading to an improvement in the energy efficiency of the battery. Figure 11b shows the charge-discharge profiles of Li-O_2 battery with and without RM.

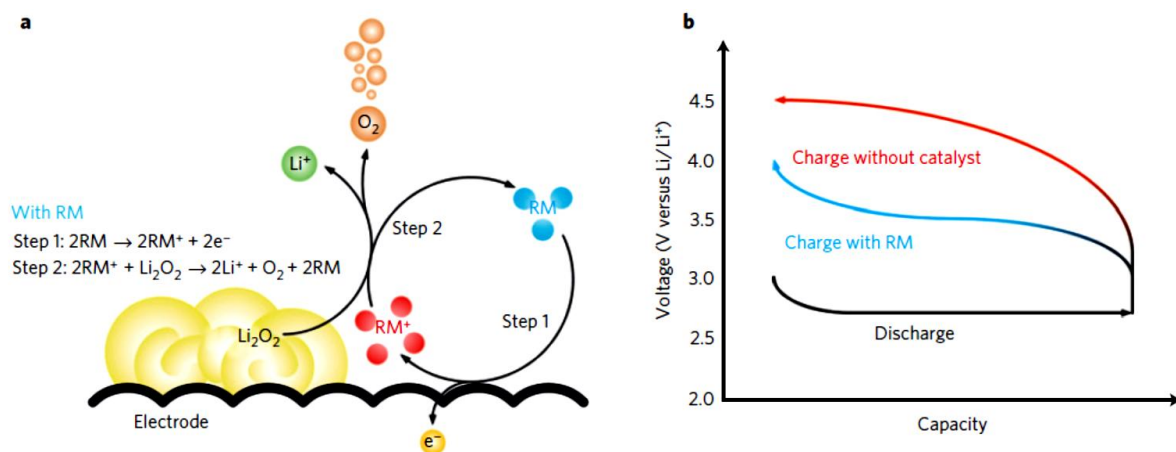


Figure 11. (a) The mechanism of OER with RM; (b) Charge-discharge profiles of $\text{Li}-\text{O}_2$ battery with or without RM.¹⁰

It is known that parasitic reactions between carbon cathode and reactive oxygen species, along with electrolyte decomposition processes, occur at high voltages. Consequently, the reduction of charge overpotential can substantially decrease the number of side reactions that proceed on charging in $\text{Li}-\text{O}_2$ batteries.¹²⁴ Some RMs, on the contrary, undergo parasitic reactions with the electrolyte, Li metal anode or oxygen-containing species.¹⁰ The protection of Li metal described in Section 1.2.2.1 can minimise side effects of the use of redox mediators.¹²⁵

There are several criteria for a compound to be considered as a redox mediator for the charge process in $\text{Li}-\text{O}_2$ batteries:^{9-10,124}

Redox potential slightly higher than 2.96 V versus Li/Li^+ : To oxidise Li_2O_2 without substantially lowering the energy efficiency, the formal oxidation potential of the RM (E'_{ox}), the potential at given conditions, Eq. 24) should be between 3 and 4 V vs. Li/Li^+ (Eq. 6), or its ionisation potential in low donor number solvents should be approximately 6

eV.¹⁰ In Table 1, structures and redox potentials vs. Li/Li⁺ of various RMs that were tested in Li-O₂ batteries are presented. The RMs known to date can be divided into organic, inorganic and organometallic. The performance of most of these RMs was summarised in a recent review.¹²⁶ In organic RMs, the formation of RM⁺ occurs through the removal of an electron from sulphur or nitrogen atoms, while in organometallic compounds RM⁺ generally forms by oxidation of the metal centre. The redox action of inorganic RMs is based on the oxidation of the anions. The lowest redox potential is attributed to lithium iodide LiI (2.95–3.55 V vs. Li/Li⁺) and *tris*[4-(diethylamino)phenyl]amine (3.1 V vs. Li/Li⁺). However, both of them were found to react with Li metal.¹²⁶⁻¹²⁷



Singly occupied molecular orbital (SOMO) energies of the RM⁺ should be higher than the highest occupied molecular orbital (HOMO) energy of the electrolyte to prevent electrolyte oxidation: For example, Li-O₂ batteries with tetrathiafulvalene¹²⁸ and cobalt *bis*(terpyridine)¹²⁹ added as RMs exhibited CO₂ evolution and low oxygen recovery, that implies the existence of a side reaction either with the carbon cathode or with the electrolyte. Cu/Fe phthalocyanine (Pc) was found to react with the electrolyte and to catalyse irreversible disproportionation of Li₂O₂ into Li₂O.¹³⁰

High stability in the presence of reactive oxygen species, and high solubility in the electrolyte. For example, cobalt(II) phthalocyanine (CoPc) has a limited solubility in organic solvents that affects its performance. To improve the solubility, Pc moiety can be slightly modified. This approach was applied by Matsuda and co-workers.¹³¹

RMs for the discharge process facilitate the formation of Li_2O_2 . In most cases, a RM reduces into RM^- at the cathode surface and oxidises oxygen molecules into superoxide anion radicals $\text{O}_2^{\cdot-}$, which then react with Li ions to form Li_2O_2 .¹³²⁻¹³⁴ Some exceptions are quinone-based RMs, e.g., 2,5-di-tert-butyl-1,4-benzoquinone (DBBQ), which forms LiDBBQ upon interaction with Li ions and reacts with oxygen to yield LiDBBQO_2 , which then converts to Li_2O_2 and DBBQ (Fig. 12).¹³⁵

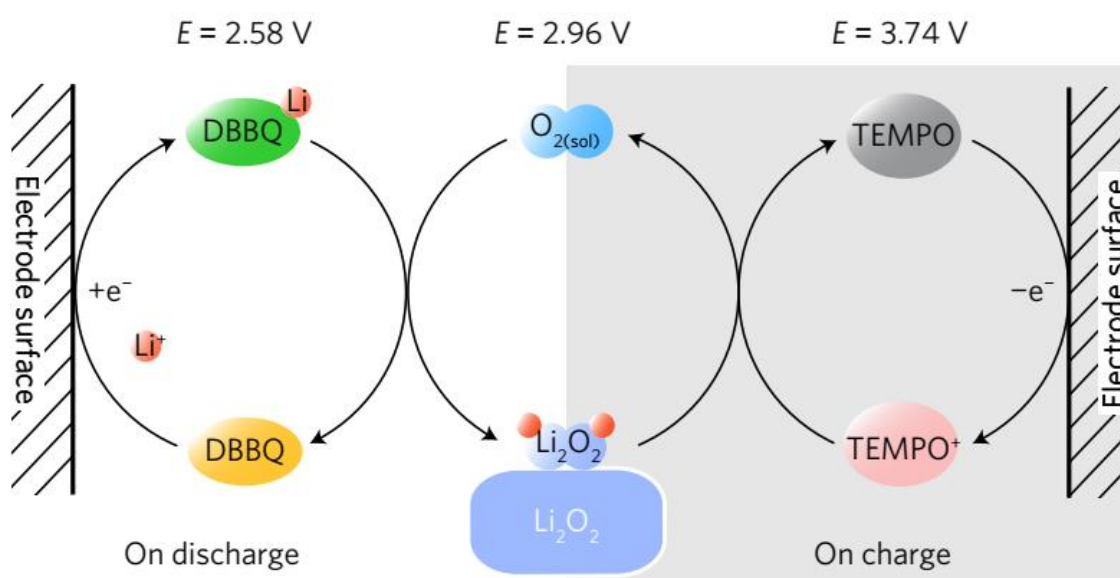
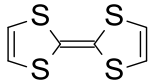
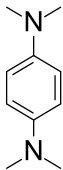
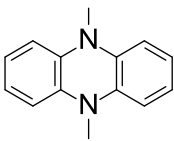
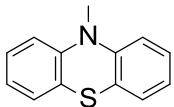
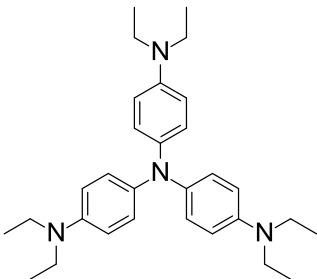
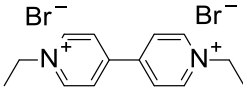
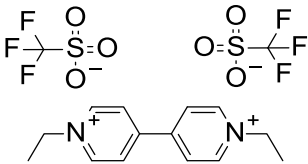


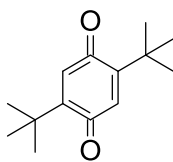
Figure 12. The mechanism of DBBQ facilitating ORR.¹³⁵

The potential for a redox couple RM/RM^- ($E_{\text{red}}^{\circ'}$), consequently, should be slightly lower than 2.96 V.

Table 1. Chemical structures and redox potentials of the redox mediators tested in Li-O₂ batteries.

Name	Structural or general formula	Redox Potential (V vs. Li/Li ⁺)	Reference
Tetrathiafulvalene (TTF)		3.6* 3.43**	10 126
<i>N,N,N',N'</i> -tetramethyl- <i>p</i> -phenylenediamine (TMPD)		3.3*	10
5,10-Dimethyl-phenazine (DMPZ)		3.29* 3.4	10 126
<i>N</i> -Methylpheno-thiazine (MPT)		3.67*	125,126
<i>Tris</i> [4-(diethyl-amino)-phenyl]amine (TDPA)		3.1* 3.4	136 126
Ethyl viologen dibromide (EV)		2.65* (discharging RM)	137
Ethyl viologen di-(trifluoromethanesulfonate)		≈2.4 in ionic liquids (discharging RM)	133,138

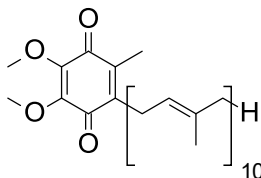
2,5-Di-*tert*-butyl-1,4-benzoquinone (DBBQ)



2.58****
(discharging RM)

135

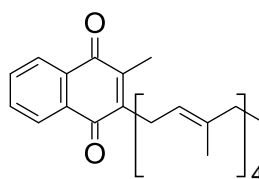
Coenzyme Q10
(ubiquinone-10)



2.63*

139

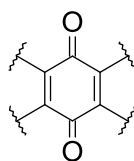
Vitamin K2
(menaquinone 4)



2.54****

140

Other quinone derivatives
(1,4-naphthoquinone,
anthraquinone, 2-methyl-
1,4-naphthoquinone, 2-
methoxy-1,4-
naphthoquinone,
benzoquinone, tetramethyl-
1,4-benzoquinone, methoxy-
benzoquinone)



≈2.35–2.8
(discharging RMs)

141

Stable nitroxide radicals
(TEMPO, 4-methoxy-
TEMPO, AZADO, 1-
methyl-AZADO, TMAO,
2,2,5-trimethyl-4-
phenyl-3-azahexane-3-
nitroxide, *tert*-amyl-*tert*-
butyl nitroxide, TEMPO-
functionalized
imidazolium IL, PTIO)

General formula of the
redox active centre:



3.6–3.9***

142

3.74**** for
TEMPO

143

2.1 and 3.7 for
PTIO** (dual RM)

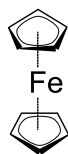
132

3.0 and 3.75 for
TEMPO-

144

imidazolium IL***
(dual RM)

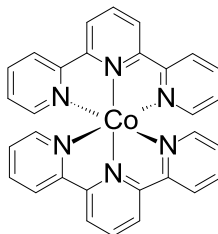
Ferrocene (Fc)



3.6

10

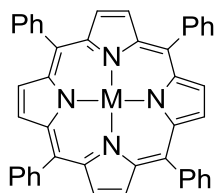
Cobalt (II)
bis(terpyridine)
(Co(Terp)₂)



3.38***

129

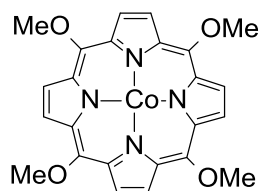
Metal tetraphenyl-
porphyrins
(M-TPP, M = Co(II), Zn,
Mn(II), Cu(II) or Fe(II))



3.0–4.5***
 $E^0_{\text{Co}} < E^0_{\text{Zn}} <$
 $E^0_{\text{Mn}} < E^0_{\text{Cu}} <$
 E^0_{Fe}

145

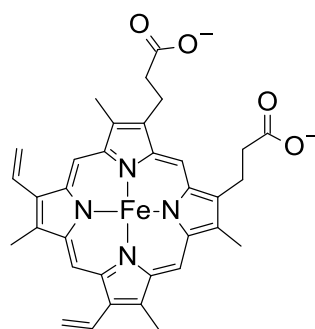
Cobalt (II)
tetramethoxy-porphyrin
(Co-OMe-TTP)



~3.8***

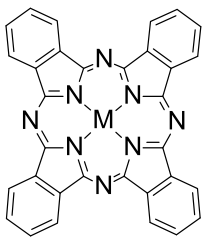
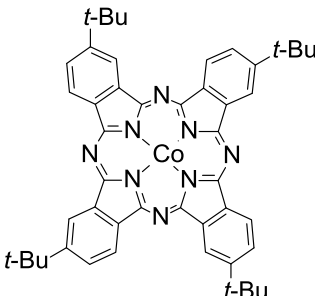
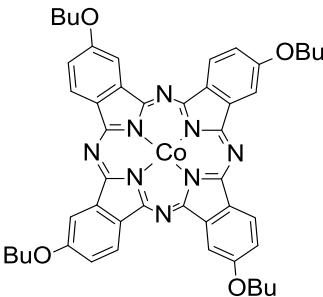
145

Heme (substituted iron
(II) porphirin)



4.2*

126

Metal phthalocyanines (MPc, M = Co(II) ¹³¹ , Fe(II), Cu(II)/Fe(II) ¹³⁰)		M = Fe (II), 2.5 and 3.65** (dual RM)	126,134
Cobalt (II) 2,9,16,23- tetra- <i>tert</i> -butyl- 29 <i>H</i> ,31 <i>H</i> -phthalocyanine (tb-CoPc ¹³¹ or Co- <i>tert</i> - butyl-Pc ¹⁴⁵)		~3.7* ~3.7***	131 145
Cobalt (II) tetrabutoxy- phthalocyanine (Co- butoxy-Pc)		~3.55***	145
Lithium iodide	LiI	2.95–3.55,* 3.0*, 3.0****, 3.25*	10 126
Caesium iodide	CsI	Not reported	146
Indium(III) iodide	InI ₃	Not reported	127
Lithium bromide	LiBr	3.5*** 4.0***	129 124
Lithium nitrate	LiNO ₃	3.6–3.8***	129,147

* in TEGDME. ** in DMSO. *** in DEGDME. **** in DME.

1.3. Conclusion

A significant difficulty in assembling a high-performance Li-O₂ battery is that all of the factors affecting the battery performance, such as electrolyte decomposition, Li₂O₂ insulating nature, Li dendrite formation, reactivity of carbon cathode, and high charge overpotential, are interconnected, and their relationships towards each other are not yet fully understood. Any perturbations to the existing system can simultaneously affect multiple factors, and all the changes should be carefully considered. Even the use of redox mediators and new solvents can bring both improvement and detriment if other factors are not elucidated.

The work presented in this thesis builds upon the current knowledge and addresses new redox mediators that may improve both the charge overpotential and cyclability characteristics of Li-O₂ batteries, as well as explores safe, stable alternatives to the common aprotic electrolytes.

1.4. Research Approach and Methods

For this project, a comparative research approach was chosen where systematically varied series of compounds with slightly different structures were investigated. This method not only contributes to the fundamental knowledge in chemistry and electrochemistry by elucidating the influence of the minor changes in the structure on the battery performance but also ensures the high clarity of the obtained data through easy identification of unusual results.

This study required a function-oriented design of the compounds as they had to satisfy several essential criteria for the RMs or electrolytes in Li-O₂ batteries (Sections 1.2.3 and

1.2.1.3). Before commencing the synthesis, it was necessary to carefully consider what changes in the structures might lead to a better battery performance compared to the original RMs and electrolytes, even though unambiguous prediction of such properties is impossible.

Initially, this project investigated new redox mediators to efficiently oxidise the discharge product (solid-state lithium peroxide particles, Li_2O_2) during the charging process. The Li-O₂ battery generally comprises three basic components: a Li anode, a membrane soaked in electrolyte for Li ion diffusion and prevention of the oxygen from crossing, and a porous cathode loaded with catalyst materials. The recharge of Li-O₂ batteries depends on oxidising solid Li_2O_2 , which is formed within the porous cathode during the discharge process. However, Li_2O_2 is electronically insulating, which induces the poor electrochemical kinetics on charging and leads to high-voltage hysteresis. On charging, the voltage of the cell increases by as high as 1–1.5 V, indicating a severe polarisation for the oxidation of Li_2O_2 . High voltages also provoke electrolyte decomposition and parasitic reactions involving carbon-based cathode. A soluble RM can significantly promote the oxidation of Li_2O_2 , thus, lowering the charge overpotential and reducing the formation of side products. RM acts according to the mechanism described in Section 1.2.3.

Another aim of this project was to find better alternatives to currently applied electrolytes. In practice, instability, flammability and volatility of the electrolytes are serious drawbacks that prevent the application of Li-O₂ batteries in vehicle propulsion systems. In this respect, ionic liquids have many advantages compared to commonly used aprotic solvents (Section 1.2.1.1).

In the first series of compounds, TEMPO-substituted ionic liquids (TEMPOImILs, Fig. 13), we combined the properties of redox mediators and highly efficient solvents, which was achieved using the standard synthetic methodology described in detail in Section 2.2.

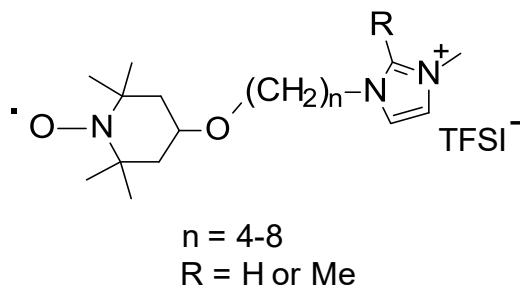


Figure 13. Structure of TEMPOImILs.

The function of the RM is performed by a nitroxide radical (2,2,6,6-tetramethylpiperidin-1-yl)oxyl (TEMPO) that has been tested previously (Table 1, Section 1.2.3). The TEMPO-OH moiety is attached to imidazolium cation with bis(trifluoromethanesulfonyl)imide (TFSI⁻) counter ion through the alkyl chain. The effect of varying alkyl chain length on the ionic conductivity of the TEMPOImILs and the performance of the batteries with pure TEMPOImIL/LiTFSI electrolytes was analysed.

The second series of the RMs (RPTIOs, Fig. 14, Table 2) is based on 2-phenyl-4,4,5,5-tetramethylimidazoline-1-oxyl 3-oxide (PTIO), which has also been studied earlier (Table 1, Section 1.2.3). It is claimed that this RM can improve both charge and discharge overpotentials. The synthesis of the RMs was performed using published methods (Section 2.3). The RPTIOs contained substituents with different electron affinities on the 4-position of the benzene ring (Fig. 14, Table 2). The redox potentials of the RPTIOs and the performance of the batteries with catalytic amounts of these RMs were investigated.

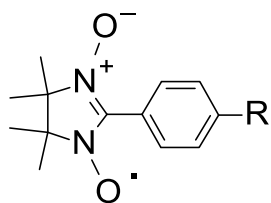


Figure 14. Structure of RPTIOs.

Table 2. Abbreviations and description of the structures of RPTIOs

Short name	R
PTIO	H
NMe ₂ PTIO	NMe ₂
OMePTIO	OMe
NO ₂ PTIO	NO ₂

To characterise the obtained compounds, various NMR techniques, IR spectroscopy and elemental analysis were applied. The water content and decomposition temperature of pure TEMPOImIL electrolyte solvents were tested using TGA and DSC. Ionic conductivity of TEMPOImILs was evaluated using AC impedance spectroscopy. Cyclic voltammetry of TEMPOImILs and RPTIOs was performed to measure the redox potentials and stability in an oxygen atmosphere. UV-visible spectroelectrochemistry of PTIO was applied to determine the reversibility of redox processes.

Prototype lithium-oxygen battery cells were fabricated using Li metal anodes, glass fibre separators and different types of carbon-based cathodes. While RPTIOs were added in low concentrations into an aprotic electrolyte, TEMPOImILs were used solely as electrolyte solvents. Heating battery cells to 73 °C in the oven was applied to increase the ionic conductivity of TEMPOImILs. The specific capacity and cycle life of the batteries were

determined by galvanostatic charge/discharge cycling. SEM and XRD analysis of pristine, discharged and charged cathodes of the batteries with RPTIOs were performed to prove the identity of the discharge product. Batteries with RPTIOs were also tested in an argon atmosphere to ensure that the capacity is provided by the formation and decomposition of the Li_2O_2 (Eq. 7), rather than redox shuttling of the RMs. A detailed description and justification of the applied methods can be found in Chapter 2 (Section 2.5).

Chapter 2: Experimental Section

Chapter 2: Experimental Section

2.1. General

4-Hydroxy-2,2,6,6-tetramethylpiperidin-1-oxyl (4-hydroxy-TEMPO, 97%), 1-methylimidazole (99%), 1,2-dimethylimidazole (97%), 4-dibromobutane (99%), tetra-*n*-butylammonium bromide ($\geq 99\%$), 1,5-dibromopentane (97%), 1,6-dibromohexane (96%), 1,8-dibromooctane (98%), phenylhydrazine (97%), 2,3-dimethyl-2,3-dinitrobutane (98%), tetrahydrofuran ($\geq 99.9\%$), benzaldehyde ($\geq 99\%$), 4-(dimethylamino)benzaldehyde ($\geq 99\%$), 4-methoxybenzaldehyde, cadmium sulfate, sodium periodate ($\geq 99.8\%$), TBATFSI ($\geq 99.0\%$), TEGDME (for cyclic voltammetry, 99%), DEGDME (99.5%), acetonitrile (99.8%) and LiTFSI for cyclic voltammetry and synthesis (96%) were purchased from Sigma-Aldrich. Ammonium chloride ($\geq 99.5\%$) was purchased from Univar. 4-Nitrobenzaldehyde ($\geq 98.0\%$) was purchased from Merck. Zinc dust with particle size < 10 μm ($\geq 98\%$, Sigma Aldrich) was kindly provided by Assoc. Prof. Shanlin Fu. 1,7-dibromoheptane (95+%) was purchased from Oakwood Chemicals. TEGDME (98+%) and LiTFSI (99.8+%) for the battery tests were purchased from DoDoChem. All solvents used in synthetic procedures were analytical grade. LiTFSI, TEGDME, DEGDME and phenylhydrazine were stored in the glove box. TEGDME and DEGDME were dried with 3 Å molecular sieves (Sigma-Aldrich) for at least one week before use. All other chemicals were used as received.

All procedures were conducted in the fumehood or glove box. Special precautions were taken while using cadmium sulphate, which is a known carcinogen and mutagen.

NMR spectra were recorded using an Agilent Technologies NMR spectrometer operating at a frequency of 500.3 MHz for ^1H and 125.7 MHz for ^{13}C experiments with DMSO- d_6 as a solvent. Elemental analysis was performed by the Campbell Microanalytical Laboratory, Department of Chemistry, University of Otago, New Zealand. FTIR spectra were acquired using Thermo Scientific Nicolet 6700 FTIR spectrometer. Photographs of crystals of RPTIOs crushed between two microscope slides were obtained using an AmScope 18MP USB3.0 Digital Camera attached to ZEISS Stemi 305 stereo microscope.

TGA and DSC curves were obtained simultaneously using a Thermal Advantage SDT-Q600 thermal analyser. Experiments were conducted in the temperature range of 25-700 °C at a heating rate of 10 °C min $^{-1}$ under a nitrogen gas flow of 150 mL min $^{-1}$. Samples were placed in alumina crucibles.

2.2. Synthesis of TEMPO-ionic Liquids (TEMPOImILs)

TEMPOImILs were synthesised using modified literature methods (Scheme 1).¹⁴⁸⁻¹⁴⁹ ^1H and ^{13}C NMR spectra were obtained after adding phenylhydrazine directly into the NMR tubes. Spectra, therefore, contain signals corresponding to the reduction product of the nitroxide radical.¹⁵⁰ The assignment of the NMR signals was supported by gHSQC and DEPT NMR experiments using the TEMPOImILs.

4-(2,2,6,6-tetramethyl-1-oxyl-4-piperidoxyl)butyl bromide (TEMPOLC $_4$ Br, 2a). To a solution of 4-hydroxy-2,2,6,6-tetramethylpiperidin-1-oxyl (0.500 g, 0.0029 mol) in toluene (5 mL) was added potassium hydroxide (0.65 g, 0.0116 mol) and tetra-*n*-butylammonium bromide (0.093 g, 0.3 mmol). After stirring for 5 minutes, 1,4-dibromobutane (0.53 g, 0.0116 mmol) was added, and the mixture was vigorously stirred at room temperature for

24 h. The solvent was then removed on a rotary evaporator, and the mixture was purified using silica column chromatography (2 x 15 cm) eluting with a hexane:dichloromethane mixture using a gradient from 100:0 to 0:100 (by volume). The product was dried under high vacuum to yield 0.34 g (51%) of 4-(2,2,6,6-tetramethyl-1-oxyl-4-piperidoxyl)butyl bromide as a red viscous oil.

TEMPOLC_nBr with n = 5–8 (**2b–e**) were obtained as red viscous oils using the same method with the following yields: **2b** – 50%, **2c** – 56%, **2d** – 75%, **2e** – 54%.

TEMPOLC₄Br (**2a**). ¹H NMR (DMSO-*d*₆, 500 MHz): δ 1.03 (s, 6H, CH₃), 1.07 (s, 6H, CH₃), 1.19-1.26 (m, 2H, C(3)_{Pip}-H and C(5)_{Pip}-H), 1.54-1.61 (m, 2H, -OCH₂CH₂-), 1.80-1.87 (m, 4H, C(3)_{Pip}-H and C(5)_{Pip}-H, -CH₂CH₂Br), 3.39 (t, 2H, *J* = 6.5 Hz, -OCH₂-), 3.49-3.55 (m, 1H, H(4)_{Pip}), 3.54 (t, 2H, *J* = 6.5 Hz, -CH₂Br).

TEMPOLC₅Br (**2b**). ¹H NMR (DMSO-*d*₆, 500 MHz): δ 1.04 (s, 6H, CH₃), 1.08 (s, 6H, CH₃), 1.21-1.28 (m, 2H, H(3)_{Pip} and H(5)_{Pip}), 1.38-1.52 (m, 4H, -OCH₂(CH₂)₂-), 1.76-1.86 (m, 4H, H(3)_{Pip} and H(5)_{Pip}, -CH₂CH₂Br), 3.37 (t, 2H, *J* = 6.5 Hz, -OCH₂-), 3.39-3.45 (m, 1H, H(4)_{Pip}), 3.52 (m, 2H, -CH₂Br).

TEMPOLC₆Br (**2c**). ¹H NMR (DMSO-*d*₆, 500 MHz): δ 1.04 (s, 6H, CH₃), 1.07 (s, 6H, CH₃), 1.19-1.26 (m, 2H, H(3)_{Pip} and H(5)_{Pip}), 1.26-1.50 (m, 6H, -OCH₂(CH₂)₃-), 1.76-1.87 (m, 4H, H(3)_{Pip} and H(5)_{Pip}, -CH₂CH₂Br), 3.36 (t, 2H, *J* = 6.5 Hz, -OCH₂-), 3.39-3.45 (m, 1H, H(4)_{Pip}), 3.51 (t, 2H, *J* = 6.5 Hz, -CH₂Br).

TEMPOLC₇Br (**2d**). ¹H NMR (DMSO-*d*₆, 500 MHz): δ 1.05 (s, 6H, CH₃), 1.09 (s, 6H, CH₃), 1.19-1.46 (m, 10H, H(3)_{Pip} and H(5)_{Pip}, -OCH₂(CH₂)₄-), 1.76-1.86 (m, 4H, H(3)_{Pip}

and H(5)_{Pip}, -CH₂CH₂Br), 3.37 (t, 2H, *J* = 6.9 Hz, -OCH₂-), 3.37-3.43 (m, 1H, H(4)_{Pip}), 3.51 (t, 2H, *J* = 6.9 Hz, -CH₂Br).

TEMPOLC₈Br (**2e**). ¹H NMR (DMSO-*d*₆, 500 MHz): δ 1.03 (s, 6H, CH₃), 1.06 (s, 6H, CH₃), 1.19-1.49 (m, 12H, H(3)_{Pip} and H(5)_{Pip}, -OCH₂(CH₂)₅-), 1.75-1.86 (m, 4H, H(3)_{Pip} and H(5)_{Pip}, -CH₂CH₂Br), 3.35 (t, 2H, *J* = 6.5 Hz, -OCH₂-), 3.46-3.52 (m, 1H, H(4)_{Pip}), 3.52 (t, 2H, *J* = 6.5 Hz, -CH₂Br).

1-methyl-3-(4-(2,2,6,6-tetramethyl-1-oxyl-4-piperidoxyl)-butyl)imidazolium bromide (TEMPOLC₄Im^{Me}Br, **3a**). To a solution of 1-methylimidazole (0.0673 g, 0.82 mmol) in acetonitrile (1 mL) a solution of 4-(2,2,6,6-tetramethyl-1-oxyl-4-piperidoxyl)butyl bromide (TEMPOLC₄Br, **2a**, 0.210 g, 0.68 mmol) in acetonitrile (1 mL) was added. The mixture was stirred at 60 °C for 6 hours. After removing the solvent on a rotary evaporator, the residue was purified by trituration (x3) with sonication in diethyl ether and dried under high vacuum overnight to give 0.170 g (80%) of red viscous oil.

TEMPOLC_{*n*}Im^{Me}Br with *n* = 5–8 (**3b–e**) and 1,2-dimethyl-3-(4-(2,2,6,6-tetramethyl-1-oxyl-4-piperidoxyl)-alkyl)imidazolium bromides (TEMPOLC_{*n*}Im^(Me)₂Br, **4a–e**) were obtained similarly. Compounds **3b–e** were isolated as red viscous oils with the yields: **3b** – 42%, **3c** – 79%, **3d** – 75%, **3e** – 88%. Compounds **4a–e** were filtered after trituration to give red powders with the following yields: **4a** – 72%, **4b** – 80%, **4c** – 86%, **4d** – 68%, **4e** – 45%. ¹H NMR shifts for compound **3a** matched the literature data.¹⁵¹

TEMPOLC₄Im^{Me}Br (**3a**). ¹H NMR (DMSO-*d*₆, 500 MHz): δ 1.03 (s, 6H, CH₃), 1.06 (s, 6H, CH₃), 1.18-1.26 (m, 2H, H(3)_{Pip} and H(5)_{Pip}), 1.39-1.47 (m, 2H, -OCH₂CH₂-), 1.78-1.86 (m, 4H, H(3)_{Pip} and H(5)_{Pip}, -CH₂CH₂N<), 3.39 (t, 2H, *J* = 6.5 Hz, -OCH₂-), 3.47-3.54

(m, 1H, H(4)_{Pip}), 3.85 (s, 3H, (CH₃)_{Im}), 4.18 (t, 2H, $J = 7.0$ Hz, -CH₂N<), 7.74 (s, 1H, H(4)_{Im} or H(5)_{Im}), 7.77 (s, H(4)_{Im} or H(5)_{Im}), 9.15 (s, 1H, H(2)_{Im}).

TEMPOLC₅Im^{Me}Br (**3b**). ¹H NMR (DMSO-*d*₆, 500 MHz): δ 1.03 (s, 6H, CH₃), 1.06 (s, 6H, CH₃), 1.18-1.30 (m, 4H, H(3)_{Pip} and H(5)_{Pip}, -CH₂CH₂CH₂N<), 1.45-1.52 (m, 2H, -OCH₂CH₂-), 1.75-1.85 (m, 4H, H(3)_{Pip} and H(5)_{Pip}, -CH₂CH₂N<), 3.36 (t, 2H, $J = 6.4$ Hz, -OCH₂-), 3.46-3.53 (m, 1H, H(4)_{Pip}), 3.85 (s, 3H, (CH₃)_{Im}), 4.16 (t, 2H, $J = 7.1$ Hz, -CH₂N<), 7.72 (s, 1H, H(4)_{Im} or H(5)_{Im}), 7.78 (s, H(4)_{Im} or H(5)_{Im}), 9.15 (s, 1H, H(2)_{Im}).

TEMPOLC₆Im^{Me}Br (**3c**). ¹H NMR (DMSO-*d*₆, 500 MHz): δ 1.04 (s, 6H, CH₃), 1.07 (s, 6H, CH₃), 1.19-1.35 (m, 6H, H(3)_{Pip} and H(5)_{Pip}, -(CH₂)₂CH₂CH₂N<), 1.41-1.49 (m, 2H, -OCH₂CH₂-), 1.71-1.86 (m, 4H, H(3)_{Pip} and H(5)_{Pip}, -CH₂CH₂N<), 3.36 (t, 2H, $J = 6.4$ Hz, -OCH₂-), 3.46-3.53 (m, 1H, H(4)_{Pip}), 3.85 (s, 3H, (CH₃)_{Im}), 4.16 (t, 2H, $J = 7.1$ Hz, -CH₂N<), 7.70-7.72 (m, 1H, C(4)_{Im}-H or C(5)_{Im}-H), 7.76-7.78 (m, C(4)_{Im}-H or C(5)_{Im}-H), 9.15 (s, 1H, H(2)_{Im}).

TEMPOLC₇Im^{Me}Br (**3d**). ¹H NMR (DMSO-*d*₆, 500 MHz): δ 1.03 (s, 6H, CH₃), 1.06 (s, 6H, CH₃), 1.18-1.32 (m, 8H, H(3)_{Pip} and H(5)_{Pip}, -(CH₂)₃CH₂CH₂N<), 1.39-1.47 (m, 2H, -OCH₂CH₂-), 1.71-1.85 (m, 4H, H(3)_{Pip} and H(5)_{Pip}, -CH₂CH₂N<), 3.35 (t, 2H, $J = 6.6$ Hz, -OCH₂-), 3.45-3.52 (m, 1H, H(4)_{Pip}), 3.85 (s, 3H, (CH₃)_{Im}), 4.16 (t, 2H, $J = 7.2$ Hz, -CH₂N<), 7.71-7.73 (m, 1H, H(4)_{Im} or H(5)_{Im}), 7.78-7.80 (m, H(4)_{Im} or H(5)_{Im}), 9.21 (s, 1H, H(2)_{Im}).

TEMPOLC₈Im^{Me}Br (**3e**). ¹H NMR (DMSO-*d*₆, 500 MHz): δ 1.04 (s, 6H, CH₃), 1.07 (s, 6H, CH₃), 1.19-1.30 (m, 10H, H(3)_{Pip} and H(5)_{Pip}, -(CH₂)₄CH₂CH₂N<), 1.41-1.48 (m, 2H, -OCH₂CH₂-), 1.73-1.86 (m, 4H, H(3)_{Pip} and H(5)_{Pip}, -CH₂CH₂N<), 3.35 (t, 2H, $J = 6.8$ Hz, -

OCH₂-), 3.46-3.53 (m, 1H, H(4)_{Pip}), 3.84 (s, 3H, (CH₃)_{Im}), 4.14 (t, 2H, *J* = 7.6 Hz, -CH₂N<), 7.70 (s, 1H, H(4)_{Im} or H(5)_{Im}), 7.77 (s H(4)_{Im} or H(5)_{Im}), 9.15 (s, 1H, H(2)_{Im}).

TEMPOLC₄Im^(Me)₂Br (**4a**). ¹H NMR (DMSO-*d*₆, 500 MHz): δ 1.04 (s, 6H, CH₃), 1.07 (s, 6H, CH₃), 1.19-1.26 (m, 2H, H(3)_{Pip} and H(5)_{Pip}), 1.42-1.50 (m, 2H, -OCH₂CH₂-), 1.69-1.78 (m, 2H, -CH₂CH₂N<), 1.81-1.87 (m, 2H, H(3)_{Pip} and H(5)_{Pip}), 2.58 (s, 3H, C(2)_{Im}CH₃), 3.40 (t, 2H, *J* = 6.3 Hz, -OCH₂-), 3.48-3.55 (m, 1H, H(4)_{Pip}), 3.75 (s, 3H, N(1)_{Im}CH₃), 4.13 (t, 2H, *J* = 7.4 Hz, -CH₂N<), 7.62-7.65 (m, 1H, H(4)_{Im} or H(5)_{Im}), 7.65-7.67 (m, 1H, H(4)_{Im} or H(5)_{Im}).

TEMPOLC₅Im^(Me)₂Br (**4b**). ¹H NMR (DMSO-*d*₆, 500 MHz): δ 1.04 (s, 6H, CH₃), 1.07 (s, 6H, CH₃), 1.19-1.34 (m, 4H, H(3)_{Pip} and H(5)_{Pip}, -CH₂CH₂CH₂N<), 1.46-1.52 (m, 2H, -OCH₂CH₂-), 1.68-1.76 (m, 2H, -CH₂CH₂N<), 1.79-1.86 (m, 2H, H(3)_{Pip} and H(5)_{Pip}), 2.58 (s, 3H, C(2)_{Im}CH₃), 3.36 (t, 2H, *J* = 6.5 Hz, -OCH₂-), 3.45-3.54 (m, 1H, H(4)_{Pip}), 3.75 (s, 3H, N(1)_{Im}CH₃), 4.10 (t, 2H, *J* = 7.3 Hz, -CH₂N<), 7.62-7.65 (m, 1H, H(4)_{Im} or H(5)_{Im}), 7.65-7.67 (m, 1H, H(4)_{Im} or H(5)_{Im}).

TEMPOLC₆Im^(Me)₂Br (**4c**). ¹H NMR (DMSO-*d*₆, 500 MHz): δ 1.05 (s, 6H, CH₃), 1.09 (s, 6H, CH₃), 1.22-1.37 (m, 6H, H(3)_{Pip} and H(5)_{Pip}, -(CH₂)₂CH₂CH₂N<), 1.44-1.52 (m, 2H, -OCH₂CH₂-), 1.65-1.73 (m, 2H, -CH₂CH₂N<), 1.81-1.87 (m, 2H, H(3)_{Pip} and H(5)_{Pip}), 2.55 (s, 3H, C(2)_{Im}CH₃), 3.37 (t, 2H, *J* = 6.4 Hz, -OCH₂-), 3.47-3.56 (m, 1H, H(4)_{Pip}), 3.72 (s, 3H, N(1)_{Im}CH₃), 4.06 (t, 2H, *J* = 7.4 Hz, -CH₂N<), 7.62-7.65 (m, 1H, H(4)_{Im} or H(5)_{Im}), 7.65-7.67 (m, 1H, H(4)_{Im} or H(5)_{Im}).

TEMPOLC₇Im^(Me)₂Br (**4d**). ¹H NMR (DMSO-*d*₆, 500 MHz): δ 1.03 (s, 6H, CH₃), 1.07 (s, 6H, CH₃), 1.19-1.34 (m, 8H, H(3)_{Pip} and H(5)_{Pip}, -(CH₂)₃CH₂CH₂N<), 1.40-1.48 (m, 2H,

-OCH₂CH₂-), 1.65-1.73 (m, 2H, -CH₂CH₂N<), 1.80-1.86 (m, 2H, H(3)_{Pip} and H(5)_{Pip}), 2.57 (s, 3H, C(2)_{Im}CH₃), 3.35 (t, 2H, *J* = 6.6 Hz, -OCH₂-), 3.45-3.53 (m, 1H, H(4)_{Pip}), 3.74 (s, 3H, N(1)_{Im}CH₃), 4.09 (t, 2H, *J* = 7.3 Hz, -CH₂N<), 7.61-7.64 (m, 1H, H(4)_{Im} or H(5)_{Im}), 7.64-7.67 (m, 1H, H(4)_{Im} or H(5)_{Im}).

TEMPOLC₈Im^(Me)₂Br (**4e**). ¹H NMR (DMSO-*d*₆, 500 MHz): δ 1.04 (s, 6H, CH₃), 1.08 (s, 6H, CH₃), 1.19-1.33 (m, 10H, H(3)_{Pip} and H(5)_{Pip}, -(CH₂)₄CH₂CH₂N<), 1.41-1.49 (m, 2H, -OCH₂CH₂-), 1.65-1.73 (m, 2H, -CH₂CH₂N<), 1.81-1.87 (m, 2H, H(3)_{Pip} and H(5)_{Pip}), 2.54-2.59 (m, 3H, C(2)_{Im}CH₃), 3.36 (t, 2H, *J* = 6.5 Hz, -OCH₂-), 3.46-3.54 (m, 1H, H(4)_{Pip}), 3.72-3.76 (m, 3H, N(1)_{Im}CH₃), 4.08 (t, 2H, *J* = 7.6 Hz, -CH₂N<), 7.60-7.67 (m, 2H, H(4)_{Im} and H(5)_{Im}).

1-Methyl-3-(4-(2,2,6,6-tetramethyl-1-oxyl-4-piperidoxyl)-butyl)imidazolium bis(trifluoromethane)sulfonimide (TEMPOLC₄Im^{Me}TFSI, **5a**). To a solution of TEMPOLC₄Im^{Me}Br (**3a**, 0.690 g, 1.77 mmol) in water (2.5 mL) at 70 °C, was added a solution of LiTFSI (0.508 g, 1.77 mmol) in water (2.5 mL) at 70 °C. The oil that immediately formed was extracted with dichloromethane (3 x 1 mL). The combined organic fractions were washed with water (3 x 5 mL). A silver(I) nitrate test indicated the absence of bromide ions in the final solution. The solution was concentrated using a rotary evaporator and purified by column chromatography on silica (2 x 15cm) eluting with chloroform followed by ethyl acetate:methanol using a gradient from 10:0 to 10:1 (by volume). Compound **5a** was dried at 90–100 °C under high vacuum with stirring for 2 hours to give a red viscous oil (0.808 g, 79%). It was stored in a glove box under an inert atmosphere.

TEMPOLC_nIm^{Me}TFSI with n = 5–8 (**5b–e**) and 1,2-dimethyl-3-(4-(2,2,6,6-tetramethyl-1-oxy-4-piperidoxyl)-alkyl)imidazolium bis(trifluoromethane)sulfonimides (TEMPOLC_nIm^(Me)₂TFSI, **6a–e**) were synthesised likewise to give red viscous oils, yields: **5b** – 91%, **5c** – 97%, **5d** – 93%, **5e** – 79%; **6b** – 93%, **6c** – 95%, **6d** – 90%, **6e** – 93%. Compound **6a** was isolated in the form of red powder (91%). ¹H NMR signals for compound **6b** matched the literature data.¹⁴⁴

TEMPOLC₄Im^{Me}TFSI (**5a**). ¹H NMR (DMSO-*d*₆, 500 MHz): δ 1.06 (s, 6H, CH₃), 1.09 (s, 6H, CH₃), 1.21-1.29 (m, 2H, H(3)_{Pip} and H(5)_{Pip}), 1.41-1.49 (m, 2H, -OCH₂CH₂-), 1.78-1.88 (m, 4H, H(3)_{Pip} and H(5)_{Pip}, -CH₂CH₂N<), 3.40 (t, 2H, *J* = 6.3 Hz, -OCH₂-), 3.49-3.56 (m, 1H, H(4)_{Pip}), 3.83 (s, 3H, (CH₃)_{Im}), 4.15 (t, 2H, *J* = 7.1 Hz, -CH₂N<), 7.66 (s, 1H, H(4)_{Im} or H(5)_{Im}), 7.72 (s, H(4)_{Im} or H(5)_{Im}), 9.05 (s, 1H, H(2)_{Im}). ¹³C NMR (DMSO-*d*₆, 126 MHz): δ 20.7 ((CH₃)_{Pip}), 26.4 (-CH₂CH₂N<), 26.9 (-OCH₂CH₂-), 32.6 ((CH₃)_{Pip}), 35.9 ((CH₃)_{Im}), 44.8 (C(3)_{Pip}, C(5)_{Pip}), 48.9 (-CH₂N<), 58.1 (C(2)_{Pip}, C(6)_{Pip}), 66.6 (-OCH₂-), 70.2 (C(4)_{Pip}), 119.7 (q, CF₃, *J* = 322 Hz), 122.4, 123.8 (C(4)_{Im}, C(5)_{Im}), 136.7 (C(2)_{Im}). Anal. Calcd for C₁₉H₃₁F₆N₄O₆S₂: C 38.71, H 5.30, N 9.50. Found: C 38.42, H 5.29, N 9.48.

TEMPOLC₅Im^{Me}TFSI (**5b**). ¹H NMR (DMSO-*d*₆, 500 MHz): δ 1.03 (s, 6H, CH₃), 1.06 (s, 6H, CH₃), 1.18-1.30 (m, 4H, H(3)_{Pip} and H(5)_{Pip}, -CH₂CH₂CH₂N<), 1.45-1.52 (m, 2H, -OCH₂CH₂-), 1.75-1.85 (m, 4H, H(3)_{Pip} and H(5)_{Pip}, -CH₂CH₂N<), 3.36 (t, 2H, *J* = 6.5 Hz, -OCH₂-), 3.46-3.53 (m, 1H, H(4)_{Pip}), 3.84 (s, 3H, (CH₃)_{Im}), 4.15 (t, 2H, *J* = 7.0 Hz, -CH₂N<), 7.69 (s, 1H, H(4)_{Im} or H(5)_{Im}), 7.75 (s, H(4)_{Im} or H(5)_{Im}), 9.09 (s, 1H, H(2)_{Im}). ¹³C NMR (DMSO-*d*₆, 126 MHz): δ 20.8 ((CH₃)_{Pip}), 22.6 (-CH₂(CH₂)₂N<), 29.2 (-CH₂CH₂N<), 29.5 (-OCH₂CH₂-), 32.6 ((CH₃)_{Pip}), 35.9 ((CH₃)_{Im}), 44.9 (C(3)_{Pip}, C(5)_{Pip}), 49.0 (-CH₂N<),

58.2 (C(2)_{Pip}, C(6)_{Pip}), 67.1 (-OCH₂-), 70.3 (C(4)_{Pip}), 119.8 (q, CF₃, $J = 322$ Hz), 122.4, 123.7 (C(4)_{Im}, C(5)_{Im}), 136.6 (C(2)_{Im}). Anal. Calcd for C₂₀H₃₃F₆N₄O₆S₂·0.5H₂O: C 39.21, H 5.59, N 9.15. Found: C 39.03, H 5.48, N 9.27.

TEMPOLC₆Im^{Me}TFSI (**5c**). ¹H NMR (DMSO-*d*₆, 500 MHz): δ 1.05 (s, 6H, CH₃), 1.09 (s, 6H, CH₃), 1.20-1.36 (m, 6H, H(3)_{Pip} and H(5)_{Pip}, -(CH₂)₂CH₂CH₂N<), 1.43-1.51 (m, 2H, -OCH₂CH₂-), 1.73-1.87 (m, 4H, H(3)_{Pip} and H(5)_{Pip}, -CH₂CH₂N<), 3.36 (t, 2H, $J = 6.6$ Hz, -OCH₂-), 3.46-3.53 (m, 1H, H(4)_{Pip}), 3.83 (s, 3H, (CH₃)_{Im}), 4.12 (t, 2H, $J = 7.1$ Hz, -CH₂N<), 7.67 (s, 1H, H(4)_{Im} or H(5)_{Im}), 7.73 (s, H(4)_{Im} or H(5)_{Im}), 9.07 (s, 1H, H(2)_{Im}). ¹³C NMR (DMSO-*d*₆, 126 MHz): δ 20.8 ((CH₃)_{Pip}), 25.4, 25.6 (-(CH₂)₂(CH₂)₂N<), 29.6 (-CH₂CH₂N<), 29.7 (-OCH₂CH₂-), 32.6 ((CH₃)_{Pip}), 35.9 ((CH₃)_{Im}), 44.9 (C(3)_{Pip}, C(5)_{Pip}), 49.0 (-CH₂N<), 58.2 (C(2)_{Pip}, C(6)_{Pip}), 67.3 (-OCH₂-), 70.2 (C(4)_{Pip}), 119.8 (q, CF₃, $J = 321$ Hz), 122.4, 123.7 (C(4)_{Im}, C(5)_{Im}), 136.6 (C(2)_{Im}). Anal. Calcd for C₂₁H₃₅F₆N₄O₆S₂·H₂O: C 39.68, H 5.87, N 8.81. Found: C 39.45, H 5.55, N 8.97.

TEMPOLC₇Im^{Me}TFSI (**5d**). ¹H NMR (DMSO-*d*₆, 500 MHz): δ 1.04 (s, 6H, CH₃), 1.08 (s, 6H, CH₃), 1.18-1.34 (m, 8H, H(3)_{Pip} and H(5)_{Pip}, -(CH₂)₃CH₂CH₂N<), 1.41-1.49 (m, 2H, -OCH₂CH₂-), 1.71-1.87 (m, 4H, H(3)_{Pip} and H(5)_{Pip}, -CH₂CH₂N<), 3.36 (t, 2H, $J = 6.6$ Hz, -OCH₂-), 3.46-3.53 (m, 1H, H(4)_{Pip}), 3.84 (s, 3H, (CH₃)_{Im}), 4.16 (t, 2H, $J = 7.0$ Hz, -CH₂N<), 7.67 (s, 1H, H(4)_{Im} or H(5)_{Im}), 7.74 (s, H(4)_{Im} or H(5)_{Im}), 9.07 (s, 1H, H(2)_{Im}). ¹³C NMR (DMSO-*d*₆, 126 MHz): δ 20.8 ((CH₃)_{Pip}), 25.7, 25.8, 28.5 (-CH₂(CH₂)₂N<, -O(CH₂)₂CH₂-, -CH₂(CH₂)₃N<), 29.6 (-CH₂CH₂N<), 29.8 (-OCH₂CH₂-), 32.6 ((CH₃)_{Pip}), 35.9 ((CH₃)_{Im}), 44.9 (C(3)_{Pip}, C(5)_{Pip}), 49.0 (-CH₂N<), 58.1 (C(2)_{Pip}, C(6)_{Pip}), 67.4 (-OCH₂-), 70.2 (C(4)_{Pip}), 119.8 (q, CF₃, $J = 322$ Hz), 122.4, 123.7 (C(4)_{Im}, C(5)_{Im}), 136.6 (C(2)_{Im}). Anal. Calcd for C₂₂H₃₇F₆N₄O₆S₂: C 41.83, H 5.90, N 8.87. Found: C 41.79, H 5.92, N 8.63.

TEMPOLC₈Im^{Me}TFSI (**5e**). ¹H NMR (DMSO-*d*₆, 500 MHz): δ 1.03 (s, 6H, CH₃), 1.06 (s, 6H, CH₃), 1.18-1.32 (m, 10H, H(3)_{Pip} and H(5)_{Pip}, -(CH₂)₄CH₂CH₂N<), 1.40-1.48 (m, 2H, -OCH₂CH₂-), 1.73-1.85 (m, 4H, H(3)_{Pip} and H(5)_{Pip}, -CH₂CH₂N<), , 3.35 (t, 2H, *J* = 6.5 Hz, -OCH₂-), 3.45-3.54 (m, 1H, H(4)_{Pip}), 3.84 (s, 3H, (CH₃)_{Im}), 4.14 (t, 2H, *J* = 7.0 Hz, -CH₂N<), 7.69 (s, 1H, H(4)_{Im} or H(5)_{Im}), 7.75 (s, H(4)_{Im} or H(5)_{Im}), 9.09 (s, 1H, H(2)_{Im}). ¹³C NMR (DMSO-*d*₆, 126 MHz): δ 20.8 ((CH₃)_{Pip}), 25.7, 25.9 (-(CH₂)₂(CH₂)₄N<), 28.6, 28.9 (-CH₂(CH₂)₂N<, -O(CH₂)₂CH₂-), 29.6 (-CH₂CH₂N<), 29.9 (-OCH₂CH₂-), 32.5 ((CH₃)_{Pip}), 35.9 ((CH₃)_{Im}), 44.9 (C(3)_{Pip}, C(5)_{Pip}), 49.0 (-CH₂N<), 58.1 (C(2)_{Pip}, C(6)_{Pip}), 67.38 (-OCH₂-), 70.1 (C(4)_{Pip}), 119.7 (q, CF₃, *J* = 322 Hz), 122.4, 123.8 (C(4)_{Im}, C(5)_{Im}), 136.6 (C(2)_{Im}). Anal. Calcd for C₂₃H₃₉F₆N₄O₆S₂: C 42.78, H 6.09, N 8.68. Found: C 42.63, H 5.99, N 8.74.

TEMPOLC₄Im^(Me)₂TFSI (**6a**). ¹H NMR (DMSO-*d*₆, 500 MHz): δ 1.05 (s, 6H, CH₃), 1.08 (s, 6H, CH₃), 1.20-1.28 (m, 2H, H(3)_{Pip} and H(5)_{Pip}), 1.43-1.51 (m, 2H, -OCH₂CH₂-), 1.71-1.78 (m, 2H, -CH₂CH₂N<), 1.82-1.88 (m, 2H, H(3)_{Pip} and H(5)_{Pip}), 2.55 (s, 3H, C(2)_{Im}CH₃), 3.41 (t, 2H, *J* = 6.2 Hz, -OCH₂-), 3.49-3.56 (m, 1H, H(4)_{Pip}), 3.73 (s, 3H, N(1)_{Im}CH₃), 4.11 (t, 2H, *J* = 7.2 Hz, -CH₂N<), 7.57-7.60 (m, 1H, H(4)_{Im} or H(5)_{Im}), 7.60-7.63 (m, 1H, H(4)_{Im} or H(5)_{Im}). ¹³C NMR (DMSO-*d*₆, 126 MHz): δ 9.2 (C(2)_{Im}CH₃), 20.7 ((CH₃)_{Pip}), 26.4 (-CH₂CH₂N<), 26.7 (-OCH₂CH₂-), 32.7 ((CH₃)_{Pip}), 34.8 (N(1)_{Im}CH₃), 44.9 (C(3)_{Pip}, C(5)_{Pip}), 47.6 (-CH₂N<), 58.2 (C(2)_{Pip}, C(6)_{Pip}), 66.8 (-OCH₂-), 70.3 (C(4)_{Pip}), 119.8 (q, CF₃, *J* = 322 Hz), 121.0, 122.5 (C(4)_{Im}, C(5)_{Im}), 144.2 (C(2)_{Im}). Anal. Calcd for C₂₀H₃₃F₆N₄O₆S₂·H₂O: C 38.64, H 5.67, N 9.01. Found: C 38.39, H 5.55, N 8.78.

TEMPOLC₅Im^(Me)₂TFSI (**6b**). ¹³C NMR (DMSO-*d*₆, 126 MHz): δ 9.2 (C(2)_{Im}CH₃), 20.8 ((CH₃)_{Pip}), 22.8 (-CH₂(CH₂)₂N<), 29.2 (-CH₂CH₂N<), 29.3 (-OCH₂CH₂-), 32.6 ((CH₃)_{Pip}), 34.8 (N(1)_{Im}CH₃), 44.9 (C(3)_{Pip}, C(5)_{Pip}), 47.7 (-CH₂N<), 58.2 (C(2)_{Pip}, C(6)_{Pip}), 67.2 (-OCH₂-), 70.3 (C(4)_{Pip}), 119.7 (q, CF₃, *J* = 322 Hz), 121.0, 122.4 (C(4)_{Im}, C(5)_{Im}), 144.1 (C(2)_{Im}). Anal. Calcd for C₂₁H₃₅F₆N₄O₆S₂·1.5H₂O: C 39.12, H 5.94, N 8.69. Found: C 39.42, H 5.74, N 8.26.

TEMPOLC₆Im^(Me)₂TFSI (**6c**). ¹H NMR (DMSO-*d*₆, 500 MHz): δ 1.06 (s, 6H, CH₃), 1.10 (s, 6H, CH₃), 1.22-1.37 (m, 6H, H(3)_{Pip} and H(5)_{Pip}), -(CH₂)₂CH₂CH₂N<, 1.43-1.51 (m, 2H, -OCH₂CH₂-), 1.65-1.73 (m, 2H, -CH₂CH₂N<), 1.82-1.88 (m, 2H, H(3)_{Pip} and H(5)_{Pip}), 2.55 (s, 3H, C(2)_{Im}CH₃), 3.37 (t, 2H, *J* = 6.7 Hz, -OCH₂-), 3.47-3.56 (m, 1H, H(4)_{Pip}), 3.72 (s, 3H, N(1)_{Im}CH₃), 4.06 (t, 2H, *J* = 7.1 Hz, -CH₂N<), 7.56-7.59 (m, 1H, H(4)_{Im} or H(5)_{Im}), 7.59-7.62 (m, 1H, H(4)_{Im} or H(5)_{Im}). ¹³C NMR (DMSO-*d*₆, 126 MHz): δ 9.2 (C(2)_{Im}CH₃), 20.8 ((CH₃)_{Pip}), 25.5, 25.7 (-(CH₂)₂(CH₂)₂N<), 29.3 (-CH₂CH₂N<), 29.7 (-OCH₂CH₂-), 32.6 ((CH₃)_{Pip}), 34.8 (N(1)_{Im}CH₃), 44.9 (C(3)_{Pip}, C(5)_{Pip}), 47.7 (-CH₂N<), 58.1 (C(2)_{Pip}, C(6)_{Pip}), 67.3 (-OCH₂-), 70.2 (C(4)_{Pip}), 119.8 (q, CF₃, *J* = 322 Hz), 121.0, 122.4 (C(4)_{Im}, C(5)_{Im}), 144.2 (C(2)_{Im}). Anal. Calcd for C₂₂H₃₇F₆N₄O₆S₂: C 41.83, H 5.90, N 8.87. Found: C 41.64, H 5.88, N 8.57.

TEMPOLC₇Im^(Me)₂TFSI (**6d**). ¹H NMR (DMSO-*d*₆, 500 MHz): δ 1.05 (s, 6H, CH₃), 1.08 (s, 6H, CH₃), 1.21-1.32 (m, 8H, H(3)_{Pip} and H(5)_{Pip}), -(CH₂)₃CH₂CH₂N<, 1.42-1.49 (m, 2H, -OCH₂CH₂-), 1.65-1.74 (m, 2H, -CH₂CH₂N<), 1.82-1.87 (m, 2H, H(3)_{Pip} and H(5)_{Pip}), 2.55 (s, 3H, C(2)_{Im}CH₃), 3.36 (t, 2H, *J* = 6.7 Hz, -OCH₂-), 3.47-3.56 (m, 1H, H(4)_{Pip}), 3.72 (s, 3H, N(1)_{Im}CH₃), 4.07 (t, 2H, *J* = 7.3 Hz, -CH₂N<), 7.57-7.60 (m, 1H,

H(4)_{Im} or H(5)_{Im}), 7.60-7.63 (m, 1H, H(4)_{Im} or H(5)_{Im}). ¹³C NMR (DMSO-*d*₆, 126 MHz): δ 9.2 (C(2)_{Im}CH₃), 20.8 ((CH₃)_{Pip}), 25.79, 25.81 (-CH₂(CH₂)₂N<, -O(CH₂)₂CH₂-), 28.6 (-CH₂(CH₂)₃N<), 29.3 (-CH₂CH₂N<), 29.8 (-OCH₂CH₂-), 32.6 ((CH₃)_{Pip}), 34.8 (N(1)_{Im}CH₃), 44.9 (C(3)_{Pip}, C(5)_{Pip}), 47.7 (-CH₂N<), 58.1 (C(2)_{Pip}, C(6)_{Pip}), 67.4 (-OCH₂-), 70.1 (C(4)_{Pip}), 119.8 (q, CF₃, *J* = 322 Hz), 121.0, 122.4 (C(4)_{Im}, C(5)_{Im}), 144.2 (C(2)_{Im}). Anal. Calcd for C₂₃H₃₉F₆N₄O₆S₂: C 42.78, H 6.09, N 8.68. Found: C 42.94, H 6.03, N 8.37.

TEMPOLC₈Im^(Me)₂TFSI (**6e**). ¹H NMR (DMSO-*d*₆, 500 MHz): δ 1.07 (s, 6H, CH₃), 1.11 (s, 6H, CH₃), 1.21-1.34 (m, 10H, H(3)_{Pip} and H(5)_{Pip}, -(CH₂)₄CH₂CH₂N<), 1.43-1.52 (m, 2H, -OCH₂CH₂-), 1.65-1.73 (m, 2H, -CH₂CH₂N<), 1.83-1.89 (m, 2H, H(3)_{Pip} and H(5)_{Pip}), 2.53 (s, 3H, C(2)_{Im}CH₃), 3.38 (t, 2H, *J* = 6.3 Hz, -OCH₂-), 3.48-3.56 (m, 1H, H(4)_{Pip}), 3.71 (s, 3H, N(1)_{Im}CH₃), 4.05 (t, 2H, *J* = 7.3 Hz, -CH₂N<), 7.54-7.57 (m, 1H, H(4)_{Im} or H(5)_{Im}), 7.57-7.60 (m, 1H, H(4)_{Im} or H(5)_{Im}). ¹³C NMR (DMSO-*d*₆, 126 MHz): δ 9.14 (C(2)_{Im}-CH₃), 20.81 ((CH₃)_{Pip}), 25.81, 25.93 (-CH₂)₂(CH₂)₄N<), 28.74, 28.99 (-CH₂(CH₂)₂N<, -O(CH₂)₂CH₂-), 29.36 (-CH₂CH₂N<), 29.93 (-OCH₂CH₂-), 32.57 ((CH₃)_{Pip}), 34.74 (N(1)_{Im}CH₃), 44.96 (C(3)_{Pip}, C(5)_{Pip}), 47.74 (-CH₂N<), 58.15 (C(2)_{Pip}, C(6)_{Pip}), 67.48 (-OCH₂-), 70.18 (C(4)_{Pip}), 119.79 (q, CF₃, *J* = 322 Hz), 121.08, 122.42 (C(4)_{Im}, C(5)_{Im}), 144.13 (C(2)_{Im}). Anal. Calcd for C₂₄H₄₁F₆N₄O₆S₂·1.66H₂O: C 41.80, H 6.48, N 8.12. Found: C 42.06, H 6.24, N 7.80.

2.3. Synthesis of Substituted 2-Phenyl-nitronyl Nitroxides (RPTIOs)

N,N'-dihydroxy-2,3-diamino-2,3-dimethylbutane,¹⁵² dihydroxyimidazolidine compounds¹⁵³ and nitronyl nitroxide compounds (RPTIOs)¹⁵⁴ were synthesised according to the literature procedures (Scheme 6).

N,N'-dihydroxy-2,3-diamino-2,3-dimethylbutane. NH_4Cl (1.92 g, 0.036 mol) and CdSO_4 (0.020 g, 0.096 mol) were added to a solution of 2,3-dimethyl-2,3-dinitrobutane (1.55 g, 8.8 mmol) in tetrahydrofuran/water (10:1 by volume, 66 mL) under nitrogen. The mixture was cooled to 15 °C, and then zinc powder (3.12 g, 0.048 mol) was added over a period of 30 min with vigorous stirring. The reaction mixture was stirred for 1 h at 15 °C, and the resultant precipitate was collected by filtration and washed with tetrahydrofuran (3×20 mL). The filtrate was concentrated using a rotary evaporator, 30 mL of acetone was added, and more product was collected by filtration. The solid was dried in high vacuum for 24 h. The yield of the crude *N,N'*-dihydroxy-2,3-diamino-2,3-dimethylbutane was 1.59 g (white powder). This compound is unstable in air and was used directly in the subsequent procedures.

2-phenyl-4,4,5,5-tetramethylimidazoline-3-oxide-1-oxyl (PTIO). A portion of the crude *N,N'*-dihydroxy-2,3-diamino-2,3-dimethylbutane (0.74 g) was dissolved in MeOH (30 mL), and benzaldehyde (0.23 g) was added. The progress of the reaction was monitored by TLC. The mixture was stirred for 19 h at room temperature, and then the precipitate was filtered and washed with ice-cold MeOH. The precipitate was dried in high vacuum for 24 h to yield 0.460 g of white powder. ^1H NMR signals of the obtained *N,N'*-dihydroxy-2-phenyl-4,4,5,5-tetramethylimidazolidine were equivalent to literature values.¹⁵³ *N,N'*-dihydroxy-2-phenyl-4,4,5,5-tetramethylimidazolidine (0.449 g, 1.9 mmol) was dissolved in 4 mL of

dichloromethane and 2 mL of H₂O, and NaIO₄ (0.667 g, 3.1 mmol) was added. Blue colouration occurred almost instantly, and the mixture was stirred for a further 30 min. The dichloromethane layer was removed using a pipette, and the remaining aqueous layer was extracted with dichloromethane (3 x 5 mL). Dichloromethane was removed in vacuo, and the obtained blue powder was immediately purified using silica column chromatography (1 x 10 cm, eluent – EtOAc). The compound was recrystallized from the hexane-EtOAc mixture at –20 °C. The precipitate was collected by filtration, washed with ice-cold diethyl ether, dried in high vacuum for 16 h and stored in a freezer. Blue crystals (0.188 g, 42%). FTIR (ν , cm⁻¹): 3066, 2987, 2974, 2937, 1574, 1458, 1445, 1423, 1395, 1361, 1311, 1292, 1217, 1160, 1145, 1073, 1028, 1004, 976, 933, 865, 767, 692, 622, 612, 541, 508.

All other RPTIOs were synthesised similarly. ¹H NMR signals of all *N,N'*-dihydroxy-2-(4-*R*-phenyl)-4,4,5,5-tetramethylimidazolidines matched literature data.¹⁵³ FTIR spectra of all RPTIOs were consistent with the limited literature data¹⁵⁵ and a full description of the data is included here. The percentage yields of RPTIOs were calculated based on the mass of *N,N'*-dihydroxy-2-phenyl-4,4,5,5-tetramethylimidazolidine (obtained in the last synthetic step).

2-(4-dimethylaminophenyl)-4,4,5,5-tetramethylimidazoline-3-oxide-1-oxyl (NMe₂PTIO). Greenish blue crystals, 40%. FTIR (ν , cm⁻¹): 3096, 2983, 2916, 2815, 1603, 1540, 1448, 1412, 1386, 1353, 1320, 1296, 1207, 1166, 1126, 1061, 944, 869, 831, 727, 635, 616, 571, 540.

2-(4-methoxyphenyl)-4,4,5,5-tetramethylimidazoline-3-oxide-1-oxyl (MeOPTIO). Blue crystals, 79%. FTIR (ν , cm⁻¹): 2987, 2939, 2846, 1606, 1574, 1536, 1487, 1447, 1415,

1385, 1355, 1301, 1255, 1212, 1186, 1164, 1132, 1021, 1110, 959, 942, 871, 831, 811, 788, 633, 614, 585, 524.

2-(4-nitrophenyl)-4,4,5,5-tetramethylimidazoline-3-oxide-1-oxyl (NO₂PTIO). Dark green crystals, 42%. FTIR (ν , cm⁻¹): 3101, 2994, 2950, 2864, 1601, 1519, 1448, 1420, 1391, 1356, 1309, 1213, 1164, 1149, 1129, 1104, 1011, 837, 746, 690, 639, 607, 539.

2.4. Electrochemical Characterisation

2.4.1. General

Cyclic voltammetry and electrochemical impedance spectroscopy were performed using a CHI660D electrochemical workstation. Spectroelectrochemical data were obtained using the “amperometric *it*-curve” method on the CHI660D electrochemical workstation whilst simultaneously collecting spectra using an Agilent Cary 60 UV-Visible spectrophotometer. Cyclic voltammetry was conducted in a conventional three-electrode cell. Glassy carbon (\varnothing 3 mm), platinum wire and non-aqueous Ag/Ag⁺ were used as a working, counter and a reference electrode, respectively. The glassy carbon working electrode was polished, washed and dried prior to use as well as between different measurements. For spectroelectrochemistry, the same electrodes were used except for the working electrode, which was platinum gauze. Spectroelectrochemistry was conducted in a thin layer quartz glass cell with the path length of 1 mm. The Ag/Ag⁺ reference electrode consisted of a silver wire immersed in 0.1 M LiTFSI (or 0.5 M TBATFSI) and 0.01 M AgNO₃ in TEGDME (for TEMPOImILs studies) or in CH₃CN (for RPTIOs) and conductivity to the bulk solution was maintained via a Vycor frit. For the CV tests, the Ag/Ag⁺ reference electrode was calibrated against a Li/Li⁺ reference electrode. Li/Li⁺ reference electrodes

were fabricated by wrapping Li foil ($1 \times 1 \text{ cm}^2$) around a nickel wire. For TEMPOImILs studies, the potential of Ag/Ag^+ with 0.1 M LiTFSI or 0.5 M TBATFSI in TEGDME was 3.55 V or 3.66 V vs. Li/Li^+ , respectively. For RPTIOs studies, the potential of Ag/Ag^+ with 0.1 M LiTFSI or 0.5 M TBATFSI in TEGDME was 3.41 V or 3.56 V vs. Li/Li^+ , respectively. CV tests were conducted in TEGDME with 0.5 M TBATFSI or 0.1 M LiTFSI and 10 mM of RMs at a scan rate of 100 mV s^{-1} . For spectroelectrochemistry, $3 \times 10^{-7} \text{ M}$ solutions of PTIO in CH_3CN with 0.3 M TBAPF₆ were used, while the Ag/Ag^+ reference electrode solution was 0.3 M TBAPF₆ and 0.01 M AgNO_3 dissolved in CH_3CN . The measurements were done under a N_2 and O_2 atmosphere for TEMPOImILs, and under an Ar and O_2 atmosphere for RPTIOs and spectroelectrochemical tests. The saturation of gases was achieved by bubbling dry gas for 10 min. The cells for CV tests were assembled in an argon-filled glove box with water and oxygen levels of less than 0.1 ppm.

Electrochemical impedance spectroscopy (EIS) was conducted in the frequency range 100 kHz to 1 Hz with an amplitude of AC voltage of 5 mV. The tests were performed by soaking two stainless steel blocking electrodes in the pure TEMPOImILs samples. The system was sealed in a glove box. Samples were kept at each test temperature for 30 min prior to each measurement to reach thermal equilibrium. At each test temperature, three measurements were done.

Galvanostatic discharge-charge tests were carried out on a Neware Battery Testing System. A two-electrode Swagelok-type cell with an air hole (0.785 cm^2) on the cathode side was used to test the electrochemical performances. The cells were assembled in an argon-filled glove box with water and oxygen levels of less than 0.1 ppm. Li metal (16 mm) and glass fibre (18 mm) were used as an anode and separator, respectively. For

TEMPOImILs, carbon nanotube cathodes (12 mm) were used, while for RPTIOs – carbon black (12 mm). For TEMPOImILs, 0.5 M LiTFSI was dissolved in TEMPOImIL to prepare the electrolyte. The electrolyte for RPTIOs was prepared by dissolving 0.01 M RM in 0.5 M LiTFSI/DEGDME solution. The cells with TEMPOImILs rested for 1 h at 60 °C prior to being purged with oxygen.

A field emission scanning electron microscopy (FESEM, Zeiss Supra 55 VP) was used to examine the morphology of the carbon black cathodes charged to 1 mAh cm⁻², discharged to 1 mAh cm⁻² and pristine. X-ray diffraction (XRD) studies were performed using a Bruker D8 X-ray diffractometer using Cu K α radiation. For XRD and SEM analysis, batteries were disassembled in a glove box, and the cathodes were soaked in dry DEGDME with occasional stirring for 20 min and dried for 30 minutes in the glove box chamber. Dried cathodes were then attached either to SEM sample stub using copper tape or to glass/silicon slides for XRD using parafilm and were taken out of the glove box in a sealed container just before the tests to avoid any interference from the components of the air. In some cases, to prevent the cathodes from being damaged, stainless steel current collectors with the cathodes attached to them were cut and used for the XRD and SEM studies directly.

2.4.2. Preparation of Carbon-Based Cathodes

Cathodes were prepared using a procedure similar to the one described in literature.¹⁴⁴ To prepare CNT cathodes, firstly, 2% aqueous solution of PTFE was made by diluting 60% PTFE solution with water. After sonicating this solution for 10 min, it was diluted with *i*-PrOH, and CNTs were added at a ratio CNTs:PTFE = 9:1 (by weight). The mixture was sonicated for 1 h and then vigorously stirred for 18 h. The obtained slurry was cast on

precut glass fibre separators which were washed with acetone and dried at 100 °C for 5 h before casting. The casting was done on a hotplate at 80 °C using a graduated pipette. The cathodes were further dried at 100 °C for 18 h. The loading of the cathode material was approximately 0.5 mg cm^{-2} .

Carbon Black cathodes were prepared similarly to CNT cathodes with the same carbon loading. Carbon Black:PTFE mixture was stirred for 48 h instead of 18 h.

2.5. Description and Justification of Characterisation Techniques

2.5.1. Thermal Analysis

The thermal analysis technique applied in this project combined thermogravimetric analysis (TGA) and differential scanning calorimetry (DSC). The instrument incorporates both techniques.

In the TGA experiment, a percentage of mass loss ($m/m_{\text{init}} \times 100$) of a sample is recorded as a function of temperature or time. TGA can indicate the presence of volatile impurities in a sample such as water or solvents, as well as provide a decomposition pattern of a sample. In the current project, heating was conducted under an inert atmosphere to avoid reactions with oxygen.

DSC measures the heat flow (in W g^{-1} or $\text{J s}^{-1} \text{g}^{-1}$) into/from a sample vs. temperature or time. Here, DSC data helped to identify whether the change in mass on the TGA curve is related to an endothermic or exothermic process. Exothermic processes include freezing, solidifying, condensing, combustion, hydration, decomposition and represent local maxima on the DSC curve. Endothermic peaks (local minima) could be due to evaporation, melting, dehydration.

2.5.2. Cyclic Voltammetry

In voltammetric techniques, an external potential is applied to the electrode, and the current flowing through the electrochemical cell is measured as a function of the applied potential. In cyclic voltammetry, the applied potential drops linearly with time at a certain rate until it reaches a predetermined value called the switching potential (E_λ), then it rises back to the initial value E_0 , and the cycle (or the scan) is repeated (Fig. 15).

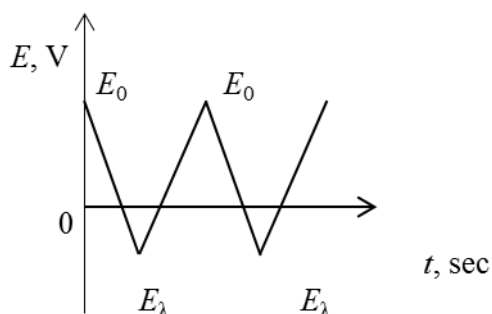


Figure 15. Potential sweep in cyclic voltammetry.

Instrumentation for cyclic voltammetry includes a potentiostat, an electrochemical cell and a computer. The electrochemical cell generally consists of a sample dissolved in a solvent, ionic electrolyte and three electrodes: a working (indicator) electrode, where the reaction occurs, a reference electrode and a counter (auxiliary) electrode. The potentiostat is used to apply a potential between the working and counter electrode and to monitor the current on the working electrode with respect to the reference electrode. The concentration of an ionic electrolyte is 10–100 times higher than that of a sample to avoid the effect of migration.

At a certain applied voltage, a reduction process at the electrode begins and the current exponentially increases until it reaches a peak value - the cathodic peak current (i_p^c , Fig. 16).

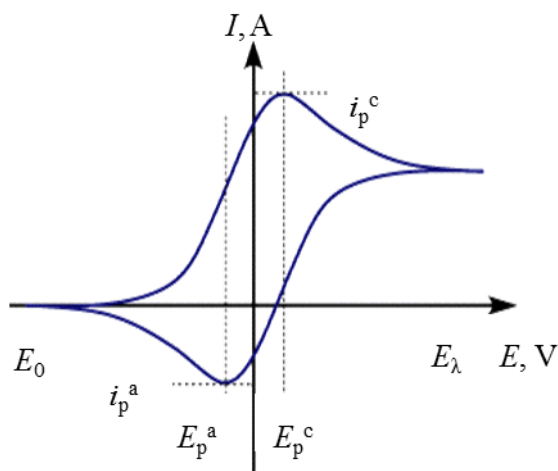


Figure 16. A typical cyclic voltammogram.

A steep rise in the current is due to the exponential dependence of the rate of electron transfer on the applied potential. After reaching i_p^c , the current decreases owing to a reduced concentration of the reactants near the surface of the electrode (in the absence of stirring).

In the reverse process, the oxidation reaction occurs at the electrode and the current drops until it reaches anodic peak current (i_p^a) value. The peak voltages E_p^a and E_p^c correspond to i_p^a and i_p^c , respectively.

In this project, cyclic voltammetry was used to determine formal oxidation potentials E_{ox}' of the RMs and stability of the compounds in an oxygen atmosphere.

If the current decreases with each subsequent scan, it indicates decomposition of the compound, as there are fewer species available to be reduced or oxidised near the working electrode.

Formal potentials were calculated according to the Equation 25:

$$E^{o'} = \frac{E_p^a + E_p^c}{2} \quad (25)$$

2.5.3. Electrochemical Impedance Spectroscopy

In electrochemical impedance spectroscopy (EIS), an AC voltage E_t of small amplitude is applied to a system and the resulting current I_t is measured (Eqs. 26–28).

$$E_t = E_0 \sin(\omega t) \quad (26)$$

$$\omega = 2\pi f \quad (27)$$

$$I_t = I_0 \sin(\omega t + \varphi) \quad (28),$$

where ω is a radial frequency (in radians/second), f is frequency measured in Hz, φ is a shift in phase.

Thus, according to Ohm's law, the impedance (the ability of a circuit to oppose the flow of electrical current) can be found by applying the Equation 29, in which it is expressed as a function of magnitude (Z_0) and a phase shift φ .

$$Z = \frac{E_t}{I_t} = \frac{E_0 \sin(\omega t)}{I_0 \sin(\omega t + \varphi)} = Z_0 \frac{\sin(\omega t)}{\sin(\omega t + \varphi)}, \quad (29)$$

By representing E_t and I_t as complex functions, one can derive a complex equation for the impedance:

$$Z(\omega) = Z' - jZ'', \quad (30)$$

where Z' and Z'' are the real and imaginary components of the impedance $Z(\omega)$, respectively, and $j = \sqrt{-1}$.

In this project, EIS measurements were conducted to calculate the ionic conductivity of TEMPOImILs at different temperatures. To depict the impedance, Nyquist plots were used, in which $-Z''$ is plotted vs. Z' (Fig. 17). A probe with two stainless steel plate blocking electrodes for the EIS experiments was kindly provided by Dr Dong Zhou. This probe eliminated the influence of charge transfer reactions. The probe was inserted into a plastic vial containing a TEMPOImIL, so that the TEMPOImIL entirely covered the platinum plates, and was sealed inside a glove box. The samples were heated to certain temperatures using a Buchi oven. Nyquist graphs for each measurement were plotted. The x-intercept on the Nyquist plot provides a value of a bulk resistance R_b , from which the ionic conductivity σ can be calculated using the Equation 31.

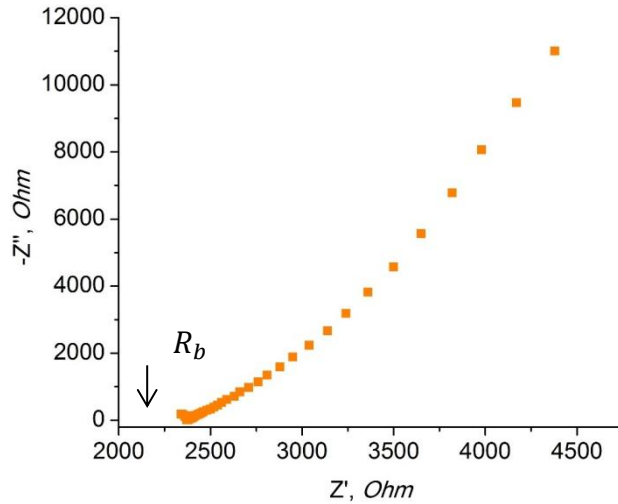


Figure 17. Example of a Nyquist plot.

$$\sigma = \frac{l}{R_b A}, \quad (31)$$

where l is a distance between the platinum electrodes and A is their area.

2.5.4. UV-visible Spectroelectrochemistry

UV-visible spectroelectrochemistry involves monitoring electrochemical processes using ultraviolet and visible absorption spectroscopy. The UV-visible absorption spectra collected at various applied potentials can give information about the mechanisms and reversibility of the electrochemical reactions.

According to Beer-Lambert Law, the absorbance A of a material is directly proportional to its concentration in solution C and the length of the light path l (Eq. 32):

$$A = \varepsilon Cl, \quad (32)$$

where ε is a molar extinction coefficient.

Molar extinction coefficients can be easily identified by obtaining a UV-visible absorption spectrum of a solution with a known C and l . The absorbance A is a maximum on the absorption curve. During spectroelectrochemical experiments performed in this project, the potential applied to a spectroelectrochemical cell was increased or decreased stepwise by 0.1 V at potentials close to the value corresponding to a redox process, and multiple UV-visible spectra were collected at each potential value until the system reached equilibrium.

During the electrochemical oxidation, compound R is converted into R^+ (Eq. 33):



Upon applying the oxidation potential, the absorption bands related to R^+ arise in the UV-visible spectra, and the spectra change until there are only R^+ species present. Overlay

of the collected absorption curves might intersect at certain wavelengths, called isosbestic points. If the UV-visible absorption curves related to the redox process in the Equation 33 have localised isosbestic points (no shifting is observed), then the conversion of R into R⁺ is likely a one-step process without intermediates. In a reversible process, during a reverse potential scan (backward scan in case of the oxidation) the absorption curves should regain their original appearance. In this project, UV-visible spectroelectrochemistry assisted in investigating the reversibility of the oxidation and reduction of PTIO (PTIO).

2.5.5. Galvanostatic Cycling

Galvanostatic cycling is used in battery testing to obtain discharge/charge, cyclability, and power/energy profiles and to extract from them such valuable characteristics as specific capacity, voltage values, specific energy, capacity retention, and capacity fading for high power applications. In the current work, charge/discharge and cyclability profiles were obtained as the required characteristics voltage values and cycle life of the batteries.

In galvanostatic techniques, a constant current is applied to an electrode, and the resulting potential is recorded as a function of time. In galvanostatic cycling, the sign of a constant applied current is reversed at each transition time. Discharge/charge profiles (galvanostatic cycling profiles, load curves) represent the dependence of voltage on the applied constant current (Fig. 18a,b). The measurements can be performed without restricting the capacity (full discharge/charge curves, Fig. 18a) to obtain the maximum values of the discharge/charge capacity a battery can reach within a certain voltage range. One can extract data about the specific capacity directly from the graph (it is the rightmost value) or using the Equation 2 (Section 1.1.3). The discharge/charge voltage values ($E_{d/c}$) on the graphs will differ from the OCV (E_{OC}) due to ohmic resistance (resistance of the

material to the flow of the current) and polarisation of the electrodes. The voltage values can be approximated using the Equation 34:

$$E_{d/c} = E_{OC} - I_{d/c}R_{app}, \quad (34)$$

where R_{app} is a total resistance and $I_{d/c}$ is a current for discharge or charge process.

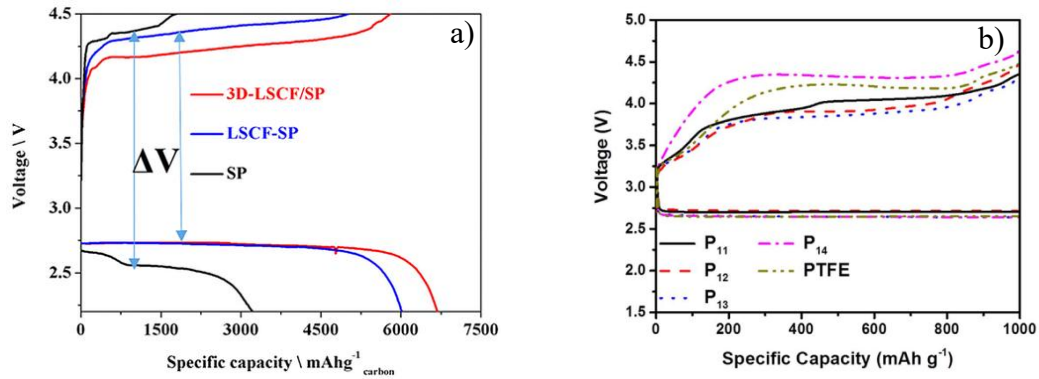


Figure 18. a) Full discharge curves;¹⁵⁶ b) discharge/charge curves with a capacity restricted to 1000 mAh g⁻¹.⁸⁸

Often the capacity values are restricted by fixing the duration of discharge and charge (Fig. 18b). Such restriction helps to obtain data about the cycle life and voltage values of the battery while reducing the contribution from side reactions (e.g., decomposition of the solvent at high voltages) by “cutting off” extra plateaus on the discharge/charge curves.

Cyclability (or cycling profile) is a different representation of discharge/charge profiles which helps to depict data about the cycle life of a battery more clearly. It might be presented as end voltage vs. the number of cycles, discharge capacity vs. the number of cycles (capacity retention), or both voltage and capacity vs. the number of cycles on the same graph (Fig. 19).

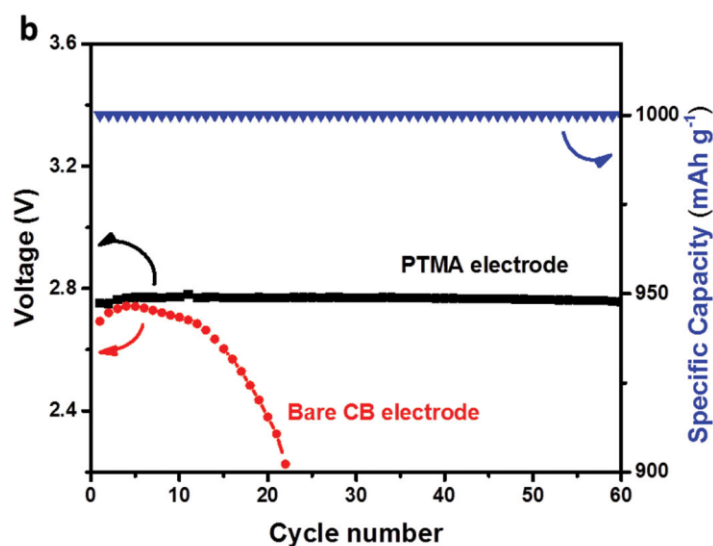


Figure 19. Cycling profile of a battery.¹⁵⁸

2.5.6. Scanning Electron Microscopy

Scanning electron microscopy (SEM) was used to obtain micro- or nanoscale images samples using a focused beam of high-energy electrons. A Zeiss Supra field emission scanning electron microscope was used equipped with a Schottky field emission gun in which the electrons are pulled by a strong electrostatic field from a heated to 1800 K tungsten single crystal coated with titanium oxide. The electron beam hits the sample to produce backscattered electrons, secondary electrons, X-rays, light or heat. The electrons that come out of a sample are collected by electron detectors and analysed by a computer. The sample for the SEM should be electrically conductive to avoid charging effects and dry to prevent its damage in the SEM vacuum chamber. The energy of the electron beam (accelerating voltage) should be chosen carefully, as if it is too low, the image might be dim, while too high energy can lead to melting of sensitive samples.

In this project, SEM was used to detect the formation and decomposition of the discharge products on the surface of carbon black cathodes from the batteries with 0.01 M

RPTIOs added to LiTFSI/DEGDME electrolyte, as well as to determine the morphology of these deposits. As the samples are air-sensitive, they were removed from the glove box immediately before the measurements in a sealed container.

2.5.7. X-ray Diffraction

X-ray diffraction was used to study the crystalline nature of materials. X-rays diffracted due to interaction with the electrons of the crystal lattice of a sample are collected by a detector, and the analysis of the diffraction pattern provides information about the atoms present in the sample and their spatial arrangement. The X-rays that form a diffraction pattern should satisfy Bragg's condition (Eq. 35):

$$n\lambda = 2d\sin\theta, \quad (35)$$

where n is an integer, λ is the wavelength of the incident X-rays, d is the spacing between planes in the atomic lattice of the sample, and θ is the angle between the incident X-ray beam and the surface of the sample.

In this work, powder XRD was used to identify the structures and to detect formation and decomposition of the discharge products on the surface of carbon black cathodes from the batteries with 0.01 M RPTIOs added to LiTFSI/DEGDME electrolyte. The obtained XRD patterns were compared with those available in the reference pattern databases of the EVA Diffraction Suite to confirm molecular structures of the deposits.

Chapter 3: TEMPO-ionic liquids as redox mediators and solvents for Li-O₂ batteries

Chapter 3: TEMPO-ionic Liquids as Redox Mediators and Solvents for Li-O₂ Batteries[†]

3.1. Introduction

For stable operation, Li-O₂ batteries require efficient protection of the lithium metal anodes, safe solvent systems, and methods to reduce charge and discharge overpotentials.⁵⁸ Methods for protection of lithium metal have been described in Section 1.2.2.1. One method uses shielding layers between the metal and electrolyte. In practice, electrochemical reactions of such layers with lithium metal and oxygen species as well as increased interfacial resistance can impede battery performance,¹⁶⁰ and so layer-forming materials must be carefully chosen. An effective approach is to utilise the reactive nature of lithium metal to produce a protective layer *in situ* by reaction with components of the electrolyte to form a solid electrolyte interface (SEI). The properties of the SEI can be tuned depending on the nature of electrolyte additives. SEI films should be thin, dense, flexible and highly conductive to lithium ions.¹⁶¹ Fluorine-containing additives including lithium bis(trifluoromethanesulfonyl)imide (LiTFSI) can form highly effective SEIs based on the formation of LiF.⁵³

Safer alternatives to aprotic organic electrolytes used in Li-O₂ batteries to date include solid electrolytes, gel electrolytes,¹³ and of relevance to the current work, ionic liquids.¹⁶²⁻¹⁶⁷ Imidazolium ionic liquids can perform as effective electrolytes.⁵⁴ There are reports that imidazolium ionic liquids are unstable in the presence of oxygen reactive species,¹⁶⁸⁻¹⁷⁰ but they can be stabilised by the use of oxygen quenchers (radical scavengers) such as

[†] A significant component of the work presented in this chapter has been published¹⁵⁹

TEMPO.¹⁷¹⁻¹⁷³ For instance, a Li-O₂ battery with a mixture of imidazolium ionic liquid and DMSO recently demonstrated 100 and 700 cycles at a capacity of 1000 and 500 mAh g⁻¹, respectively, and a current density of 500 mA g⁻¹ in an air-like atmosphere.⁵⁸ In this example, DMSO was likely to act as a radical scavenger.¹⁷⁴ Moreover, imidazolium ionic liquids with dissolved LiTFSI as electrolytes aid the formation of an effective SEI due to a facilitated reduction of LiTFSI salt near the surface of the anode.¹⁷⁵

Overpotentials caused by clogging of material on the cathode side of cells with Li₂O₂ as well as the sluggish kinetics of the oxygen evolution reaction (OER) lead to a gradual decomposition of aprotic solvents.¹² Redox mediators (RMs), which are soluble electrocatalysts, may be applied to reduce overpotentials and improve the kinetics of the OER (Section 1.2.3).^{126,176-177} Among the organic redox mediators, stable nitroxide radicals have been found to be promising for many reasons, including the highest rate of the oxidation of Li₂O₂.^{142,178}

Often a solution to one problem of Li-O₂ batteries causes other issues to arise. When a number of compounds are included to address individual issues, their interactions with each other should be considered, along with the additional increase in the weight of the battery. Therefore, multifunctional compounds that can address several aspects of battery performance simultaneously are highly attractive. A TEMPO-ionic liquid with n = 5, R = Me studied earlier in our laboratory (**Error! Reference source not found.** 20,) can effectively function as a solvent and RM for Li-O₂ batteries, and also aid the formation of a stable brush-like SEI layer capable of suppressing side reactions between the RM and Li metal.¹⁴⁴ A 1% solution of the TEMPOImIL with n = 5, R = Me in DEGDME could

improve the performance of both ORR and OER, which is not the case for some other TEMPO-based redox mediators.¹⁴²⁻¹⁴³

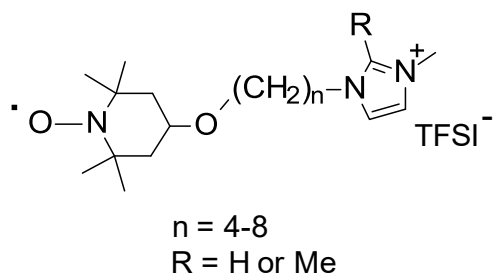
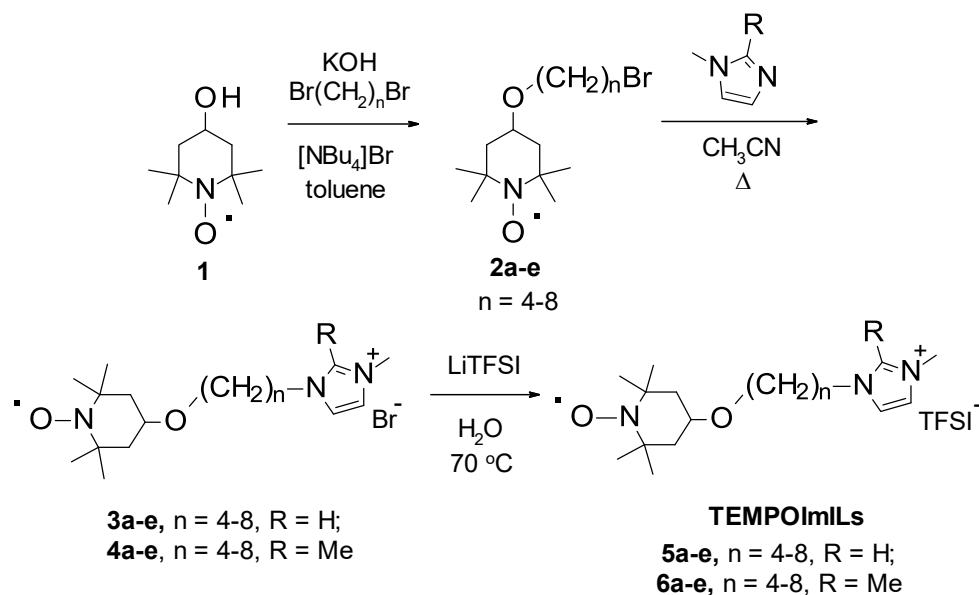


Figure 20. Structure of TEMPOImILs studied in this work.

Considering the remarkable properties of the TEMPOImIL with $n = 5$, $R = \text{Me}$ as a solvent, RM and SEI additive, we sought to determine the optimal structures for this class of compounds with regard to Li-O₂ battery performance. The present study investigates the synthesis and properties of a range of TEMPOImILs with varying lengths of the alkyl chain connecting the TEMPO and imidazole moieties and with either 1-methyl- or 1,2-dimethylimidazolium groups. Specifically, the effect of substituents on the imidazole ring and the number of alkyl chain carbon atoms on the ionic conductivity and the performance of Li-O₂ batteries using the TEMPOImILs as electrolyte solvents and RMs with no added materials is investigated.

3.2. Synthesis of TEMPOImILs



Scheme 1. Synthesis of TEMPOImILs.

The length and number of alkyl substituents in the imidazole ring can substantially affect the properties of the imidazolium ionic liquids.¹⁷⁹ To reveal the most suitable candidates among TEMPO-substituted imidazolium ionic liquids (TEMPOImILs) in terms of catalytic performance for the OER and cycle life of Li-O₂ batteries, ten compounds with different substituents at position 2 of the imidazole ring were selected. TEMPO-substituted imidazolium ionic liquids (TEMPOImILs) were synthesised using a modified literature method,¹⁴⁹ Scheme 1 (**3b-e**, **4a**, **4c-e**, **5a-e**, **6a**, **6c-e** have not been previously reported). In the first step, TEMPO-OH and α,ω -dibromoalkanes ($n = 4-8$) were reacted using potassium hydroxide as a base and the phase-transfer catalyst tetra-*n*-butylammonium bromide.¹⁴⁸ Compounds **2a-e** were prepared in yields ranging from 50 to 75%, which are more than twice those obtained using the reported procedure with sodium hydride as a base.¹⁸⁰ The reaction of **2a-e** with 1-methylimidazole gave **3a-e** as viscous oils, whereas the reaction of

2a–e with 1,2-dimethylimidazole yielded **4a–e** as powders. Bromide anions were exchanged with TFSI anions to increase the ionic conductivity of the ionic liquids. Anion exchange reactions conducted at 70 °C proceeded rapidly to yield the ionic liquids **5a–e** and **6a–e** as viscous oils.

3.3. General Characterisation of TEMPOImILs

Compounds **2–6 (a–e)** are paramagnetic. Meaningful NMR spectra were acquired after the addition of phenylhydrazine to reduce nitroxide groups to hydroxylamine groups *in situ*.¹⁵⁰ The obtained ¹H and ¹³C NMR spectra contain all of the expected characteristic signals for **2–6 (a–e)**. Exchange of the bromide counter-ions for TFSI[−] resulted in the imidazolium proton signals shifting slightly upfield.

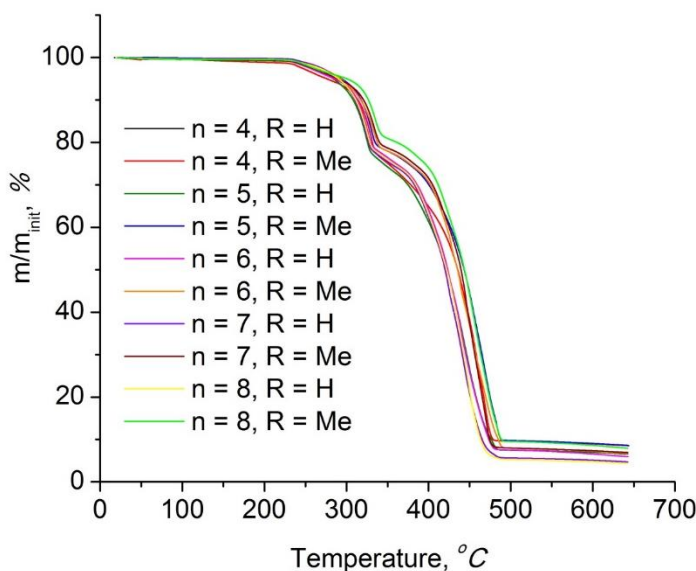


Figure 21. TGA curves of TEMPOImILs in N₂ atmosphere.

Thermogravimetric analysis (TGA) coupled with differential scanning calorimetry (DSC) were used to examine the thermal properties of **5a–e** and **6a–e** in an inert atmosphere. TGA and DSC experiments using **5a–e** and **6a–e** showed an absence of water.

No mass loss was observed from 25 to ~230 °C (Fig. 21). The first mass loss event, ~230–350 °C, is exothermic for all TEMPOImILs (Figs. 22, A1–A9), and thus cannot be attributed to the evaporation of residual moisture. This event is assigned to the decomposition of the TEMPO radical moiety based on the percentage of mass loss (17.8–21.4%). Total decomposition was complete by ~490–505 °C. For comparison, evaporation of glymes commonly used in Li-O₂ battery electrolytes starts instantly after 100 °C,¹⁸¹ while it is known that volatility of electrolyte solvents leads to graduate failure of the batteries.

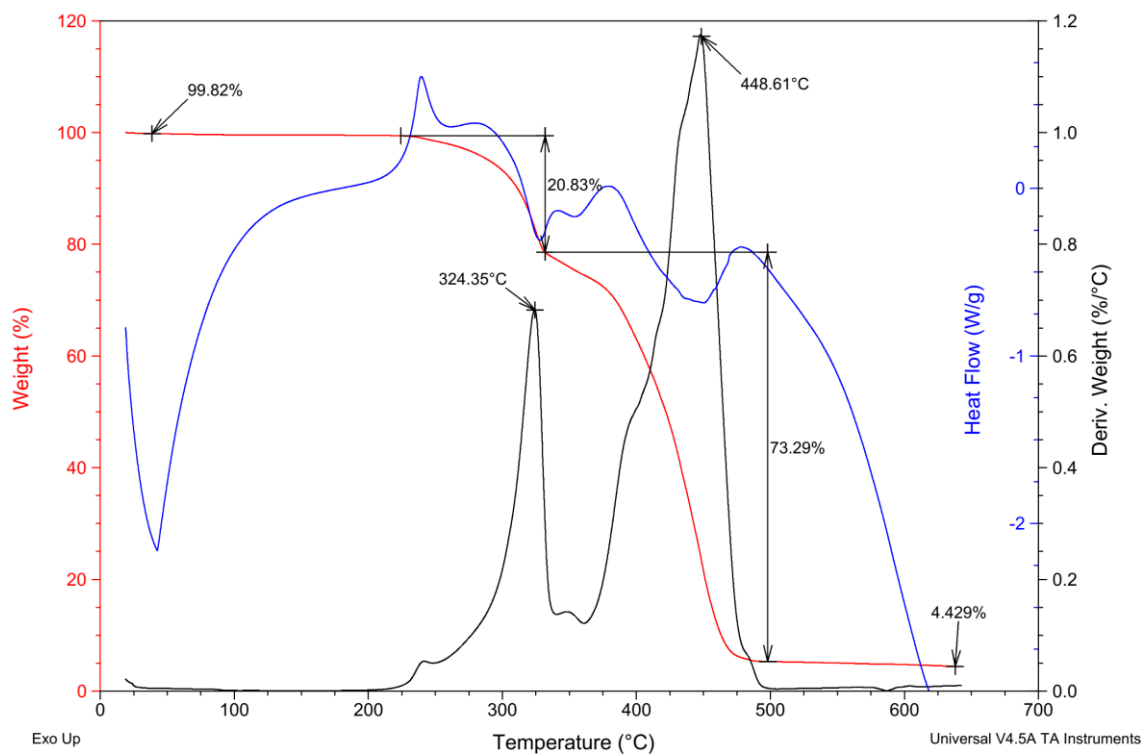


Figure 22. TGA and DSC data for TEMPOImIL 5e.

3.4. Ionic Conductivity of TEMPOImILs

For high-performance Li-O₂ batteries, an electrolyte should have an ionic conductivity of $\geq 10^{-3}$ S cm⁻¹. Ionic conductivities of the TEMPOImILs were measured using

electrochemical impedance spectroscopy (EIS, Figs. 23-25). Measurements at different temperatures were conducted using a sealed system with two stainless steel blocking electrodes soaked in pure TEMPOImILs. The values of a bulk resistance obtained from the Nyquist plots were then used to calculate the ionic conductivities.⁹² In general, compounds bearing the monomethylated imidazolium moiety (**5a–e**, R = H) had higher ionic conductivities than those with a dimethylated imidazolium group (**6a–e**, R = Me). No trend was observed in the ionic conductivity data based on the number of carbon atoms in the alkyl chains, which is in contrast to reports of linear 1,3-dialkylimidazolium ionic liquids where ionic conductivity decreased with an increased number of carbon atoms in the alkyl chains, and the odd and even effects were evident.¹⁸²⁻¹⁸⁴ The room temperature ionic conductivities of pure TEMPOImILs ranged from 1.3×10^{-5} to $4.7 \times 10^{-5} \text{ S cm}^{-1}$. At 73 °C the ionic conductivities were of the order of $10^{-3} \text{ S cm}^{-1}$, which are within an acceptable range for Li-O₂ batteries.

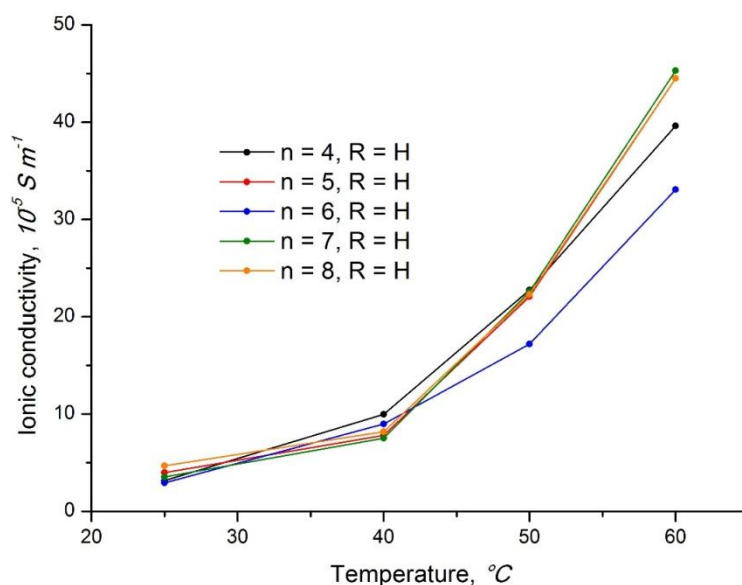


Figure 23. Temperature vs. ionic conductivity plots for pure TEMPOImILs **5a–e**.

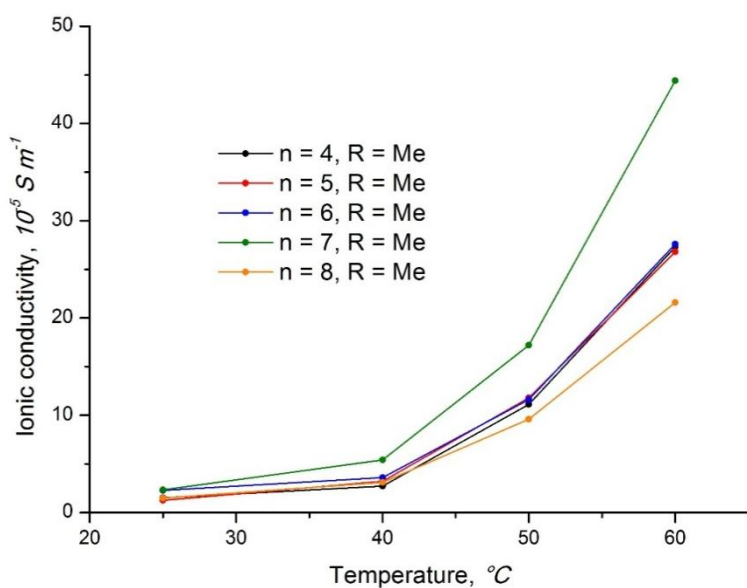


Figure 24. Temperature vs. ionic conductivity plots for pure TEMPOImILs **6a–e**.

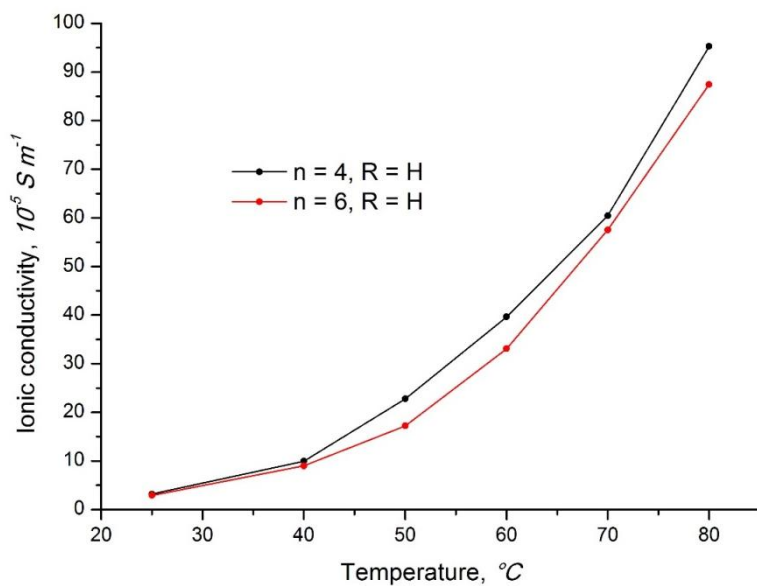


Figure 25. Temperature vs. ionic conductivity plots for pure TEMPOImILs **5a, c** tested up to 80 °C.

3.5. Cyclic Voltammetry of TEMPOImILs

Prior to battery testing, it is important to ensure that compounds satisfy basic criteria for the charging RMs, such as electrochemical stability in an oxygen atmosphere and redox

potentials for the charge process between 3 and 4 V (to provide high energy efficiency, Chapter 1.2.3).¹⁰ Electrochemical properties of TEMPOImILs were examined using cyclic voltammetry (CV) in a conventional three-electrode cell with glassy carbon, platinum wire and non-aqueous Ag/Ag⁺ as a working, counter and a reference electrode, respectively. Four representative compounds were chosen for CV experiments: TEMPOImILs **5a**, **e**, **6a**, **e**. Dilute solutions of TEMPOImILs in TEGDME were used for the CV because the high viscosity of pure TEMPOImILs was problematic at room temperature and did not provide a reasonable indication of the RMs suitability to affect the OER and ORR. In other experiments, this drawback can be overcome by increasing the temperature, but it is difficult to perform higher temperature experiments in a three-electrode setup. Nevertheless, the electrochemical performance of TEMPOImILs in TEGDME provided some insight into the performance of undiluted TEMPOImILs.

3.5.1. The Effect of Ferrocene on TEMPOImILs

During cyclic voltammetry experiments, interactions were observed between ferrocene and the TEMPOImIL **5a** when ferrocene was used as an internal standard for apparatus using a silver wire pseudo-reference electrode.¹⁶ CV experiments were conducted under an argon atmosphere with 10 mmol of TEMPOImILs dissolved in 0.1 M LiTFSI/DMA electrolyte. Upon the addition of ferrocene, a noticeable shift to higher potential values in TEMPOImIL **5a** (**Error! Reference source not found.** 26) was recorded, while it was negligible for TEMPOImILs **5b**, **e**. These preliminary tests were conducted using DMA as a solvent, because it was reported that DMA can stabilise the SEI¹¹, and initially we planned to use it to dilute the TEMPOImILs. However, for all other CV tests we chose TEGDME, which is more stable and more commonly used in Li-O₂ batteries.¹⁸⁵

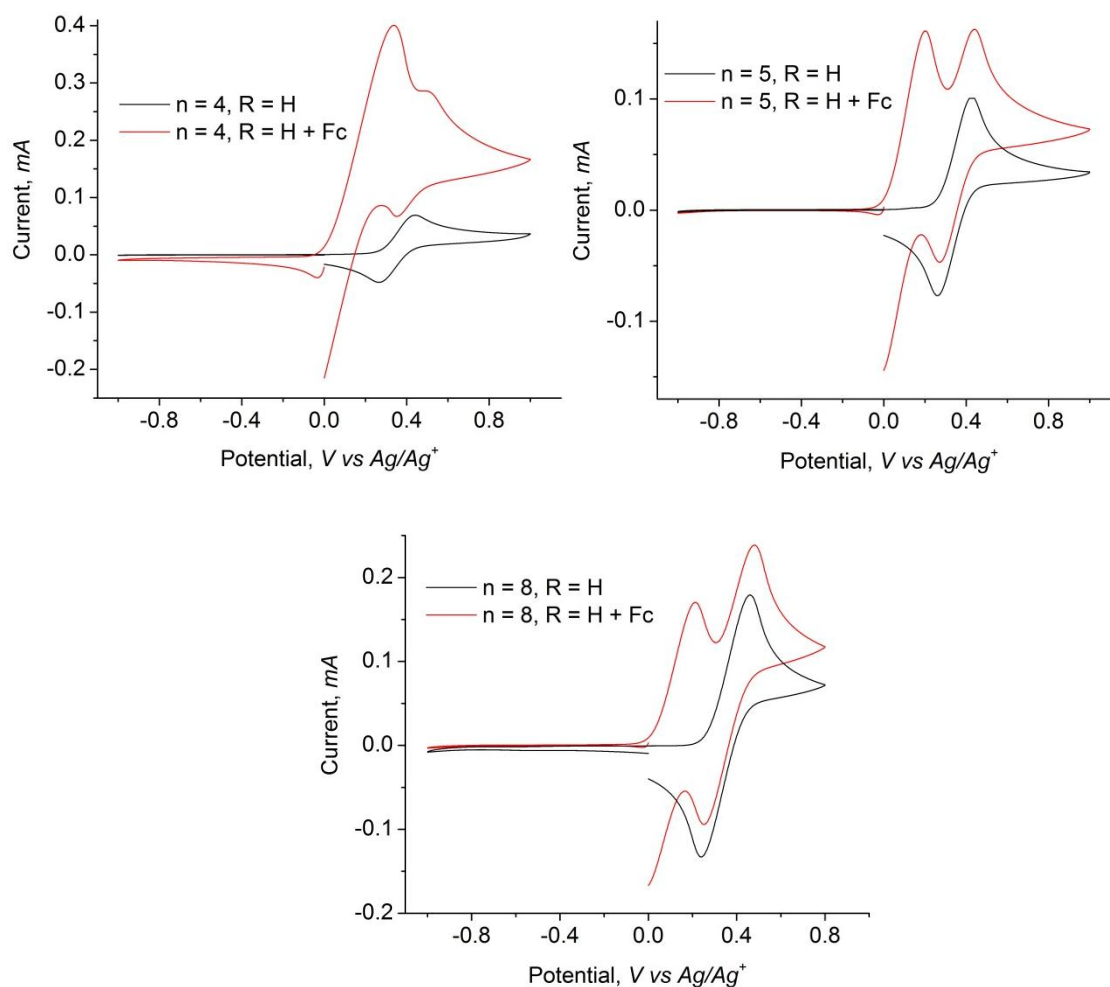


Figure 26. Cyclic voltammetry plots for 10 mmol TEMPOImILs **5a**, **b**, **e** in 0.1 M LiTFSI/DMA with and without added ferrocene.

The potential values are listed in Table 3. The positive shift of the redox potential upon oxidation of **5a** indicates the removal of electron density from the nitroxide group. One of the possible interactions is the formation of a hydrogen bond between the oxygen atom of the nitroxide group of TEMPOImIL and the hydrogen atom of the cyclopentadienyl ring of ferrocene. As the oxidation process of ferrocene occurs at lower potentials than that of the nitroxide group, the obtained oxidised form of iron (Fe^{3+}) might also interact with the nitroxide group to withdraw electron density.¹⁸⁶⁻¹⁸⁷ However, this interaction is less likely

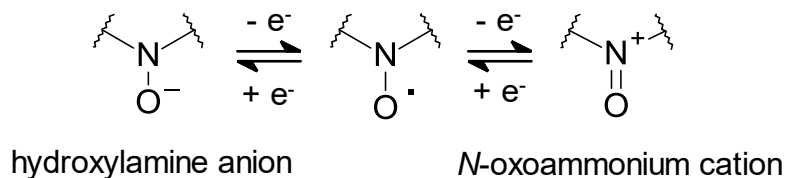
due to steric hindrance. Due to the uncertainties introduced by the use of ferrocene, it was not applied as an internal reference for further TEMPOImILs studies and a non-aqueous Ag/Ag⁺ reference electrode was used.

Table 3. Potentials of TEMPOImILs with and without added ferrocene.

	Anodic peak potential for the oxidation of TEMPO, <i>V</i> vs. Ag/Ag ⁺		Cathodic peak potential for the oxidation of TEMPO, <i>V</i> vs. Ag/Ag ⁺	
	without Fc	with Fc	without Fc	with Fc
5a	0.44	0.51	0.27	0.35
5b	0.43	0.44	0.26	0.27
5c	0.46	0.48	0.24	0.25

3.5.2. Cyclic Voltammetry Studies with LiTFSI

The redox action of TEMPOImILs is based on the oxidation of the nitroxide groups into *N*-oxoammonium cations (as is the case for TEMPO, Scheme 2).



Scheme 2. Redox processes in nitroxide radicals.

The redox potentials for the oxidation of TEMPOImILs were not assumed to be the same as that of TEMPO¹⁴² (Table 1, Section 1.2.3) and were measured before conducting other electrochemical characterization experiments. To measure the redox potentials, 10 mmol of TEMPOImILs were dissolved in a commonly used ether-based electrolyte in Li-O₂ batteries (0.1 M LiTFSI in TEGDME). As shown in Figure 27, the compounds

exhibited a reversible process at 3.90 ± 0.02 V vs. Li/Li^+ corresponding to oxidation of the nitroxide group to an oxoammonium cation, which is higher than that of TEMPO, but within the voltage range required for RMs.¹⁴²

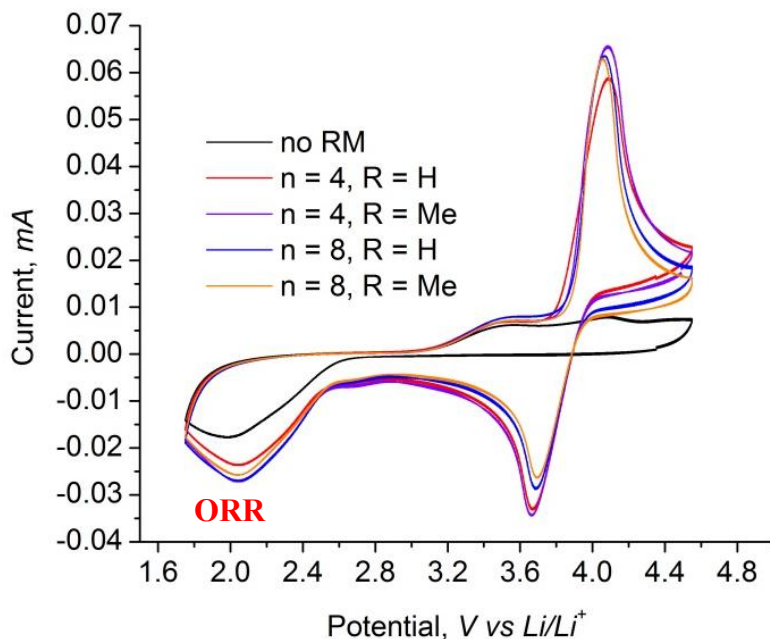


Figure 27. Cyclic voltammograms of TEMPOImILs **5a**, **e**, **6a**, **e** (10mM) in LiTFSI/TEGDME under an oxygen atmosphere, 1st cycle.

The differences in the structures of TEMPOImILs did not lead to any variation in the potentials of the redox processes across the studied range of compounds. The potential values indicate that TEMPOImILs could also aid the decomposition of Li_2CO_3 , which occurs at potentials above 3.82 V vs. Li/Li^+ .¹¹⁸ Thus, it is likely that TEMPOImILs could be used to reduce the charge overpotential in Li- CO_2 batteries.¹⁸⁸

The effect of TEMPOImILs on the OER is visible upon prolonged cycling in oxygen (positive scan direction, Figs. 28, 29). After the first cycle, the cathodic peak E_{pc} related to nitroxide group oxidation shifts to greater potential values and increases in intensity due to

interaction with Li_2O_2 deposited during the ORR, while the corresponding anodic peak E_{pa} remains the same, which means that Li_2O_2 was fully removed by the oxidised form of the redox mediator (RM^+). This observation provides strong evidence that TEMPOImILs act as effective charge RMs.¹³⁶ Shifts in cathodic peak potentials after the 1st cycle for selected TEMPOImILs averaged upon three CV tests are shown in Table 4.

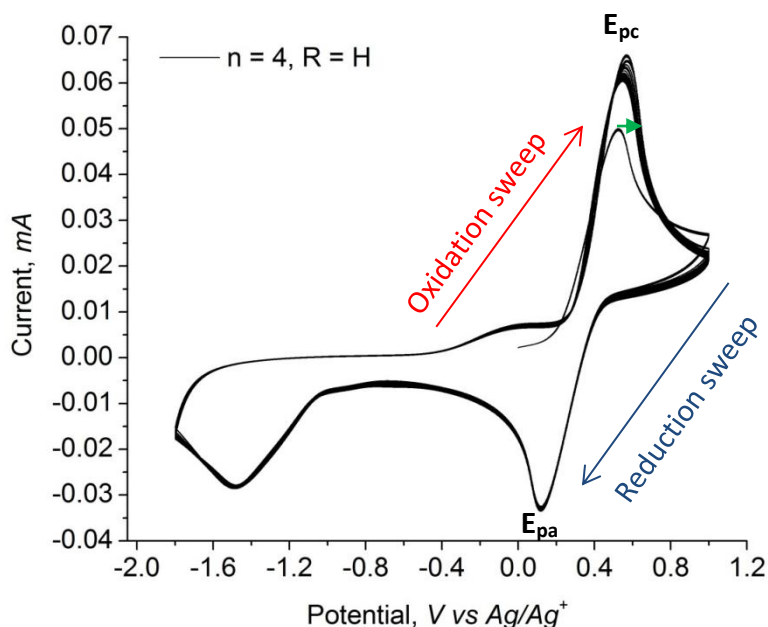


Figure 28. Cyclic voltammogram of TEMPOImIL **5a** demonstrating the effect on the OER, 10 cycles.

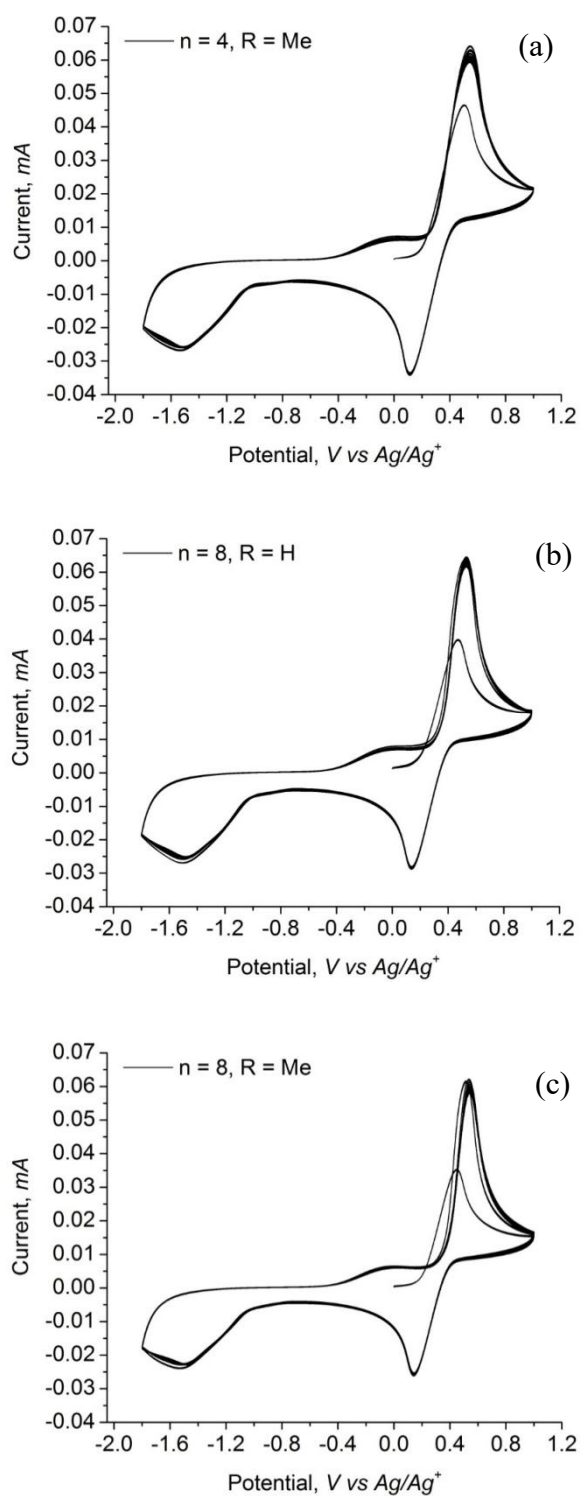
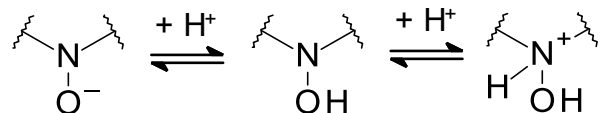


Figure 29. Cyclic voltammograms demonstrating the effect on the OER of TEMPOImILs **6a** (a), **5e** (b), **6e** (c), 10 cycles.

Table 4. Shifts in cathodic peak potentials (E_{pc}) of TEMPOImILs after the 1st cycle

TEMPOImIL	Average shift in cathodic peak potential for the oxidation of the nitroxide group, V
5a	0.03
5e	0.04
6a	0.04
6e	0.06

There are differing opinions about the reversibility of the reduction process of nitroxide radicals resulting in the formation of hydroxylamine anion (Scheme 2). Some authors claim that this process is irreversible.¹⁴² A study of the rate constant conducted in an aqueous solution with acetate-borate-phosphate buffer showed that the reduction of TEMPO is quasi-reversible with a very large anodic-to-cathodic peak separation shortening at higher pH values.¹⁸⁹⁻¹⁹⁰ This process has sluggish kinetics due to further protonation of the hydroxylamine anion (facile at lower pH) to yield hydroxylamine and hydroxylammonium cation and exhibits slow electron transfer back to the hydroxylamine anion form (Scheme 3).^{189,191} At pH<7, the anodic peak related to a re-oxidation of hydroxylamine anion (Scheme 2) was observed in the cyclic voltammograms at a potential higher than that of the oxidation process.



Scheme 3. Protonation of hydroxylamine anion.

To study the reduction process of TEMPOImILs, we conducted experiments in an argon atmosphere using acetonitrile with 0.1 M LiTFSI and 0.01 M TEMPOImIL with $n = 5$, $R = H$ as an electrolyte (Fig. 30). The use of an argon atmosphere excludes the possibility of the re-oxidation anodic peak to be confused with the OER. When the potentials were scanned down to -1.6 V vs. Ag/Ag^+ , the onset of the reduction process was observed. Still, it is unlikely that the peak that appeared at ~ 0.8 V vs. Ag/Ag^+ was a return reduction peak, as it was not present in the cyclic voltammograms depicted in Figures 28, 29. More likely, the increased current at high voltages is related to the decomposition of the electrolyte. Thus, the return reduction peak could not be observed in this study. The absence of the return reduction peak at potentials lower than the oxidation process is related to lower stability of the reduced state of TEMPOImILs compared to RPTIOs (Chapter 4). This in turn is reflected in the effect of these compounds on the ORR with less improvement of the discharge performance expected for TEMPOImILs compared to RPTIOs. The magnitude of the cathodic peak at ~ 2.0 V vs. Li/Li^+ (associated with the ORR) increased upon the addition of the RMs, Figure 27, which suggests that TEMPOImILs have some catalytic effect on the ORR when diluted with other solvents. In this case, the concentration of RM^- would reduce while catalysing the ORR, leading to a decrease in intensity or disappearance of the re-oxidation anodic peaks from the cyclic voltammograms. However, the absence of the return reduction peaks in the cyclic voltammograms does not allow unambiguous determination of the effect of TEMPOImILs on the ORR. In addition, it is not possible to calculate whether the reduction potential of TEMPOImILs is within the suitable range for discharging RMs. Hence, we focus on the action of TEMPOImILs as charging RMs.

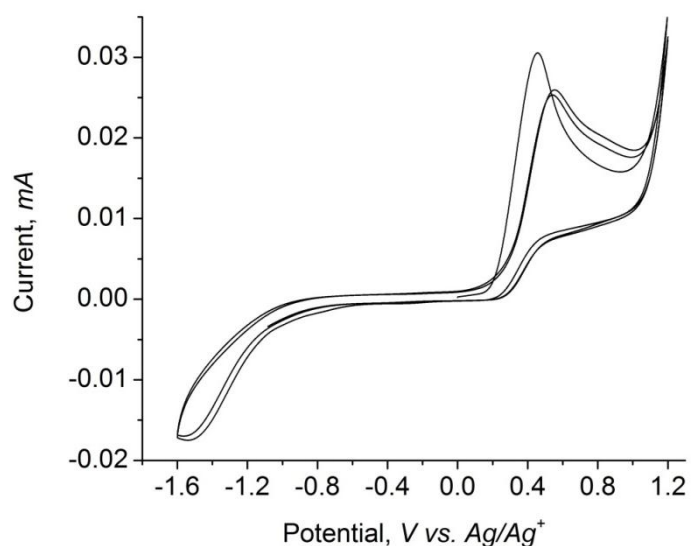


Figure 30. Cyclic voltammogram of TEMPOImIL **5b** (10mM) in LiTFSI/MeCN under an argon atmosphere.

During cycling of Li-O₂ batteries, not only oxygen but also reduced oxygen species can interact with redox mediators, electrolytes and other battery components, with nucleophilic superoxide O₂⁻ being present in reasonable concentrations. In the CV experiments, included Li⁺ ions under an oxygen atmosphere generate reactive oxygen species in a similar way to that in the Li-O₂ battery environment. The stability of TEMPO towards these highly nucleophilic species has been examined earlier by Bernger et al.,¹⁴³ who showed that the peak current ratio for the oxidation of TEMPO during the CV tests remains close to unity, which indicates high stability of TEMPO towards reduced oxygen species. This is relevant to the current work as the TEMPO moiety is an electrochemically active centre in the TEMPOImILs.

3.5.3. Cyclic Voltammetry Studies with TBATFSI

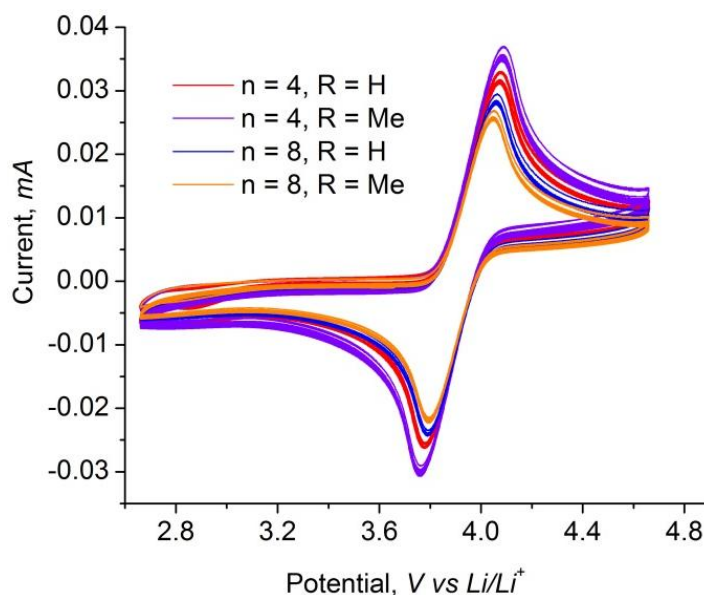


Figure 31. Cyclic voltammograms of TEMPOImILs **5a**, **e**, **6a**, **e** (10mM) in TBATFSI/TEGDME, 20 cycles.

Electrochemical stability of the four TEMPOImILs in an oxygen atmosphere was examined using TBATFSI as electrolyte rather than LiTFSI salt, as the latter may affect the formation and decomposition of Li_2O_2 on the glassy carbon electrode (Fig. 31). No significant decomposition of the TEMPOImILs was observed upon cycling for up to 20 times. For TEMPOImIL **5a**, the stability on a longer timescale was investigated (Fig. 32), and no major changes were recorded during 100 cycles. These findings indicate that the compounds are electrochemically stable in the presence of oxygen.

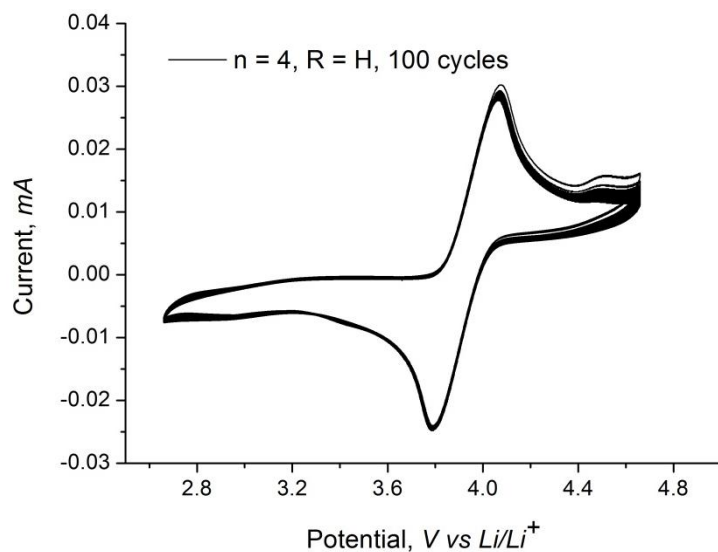


Figure 32. Cyclic voltammogram of TEMPOImIL **5a** (10mM) in TBATFSI/TEGDME, 100 cycles.

3.6. Galvanostatic Cycling of the Li-O₂ Batteries with TEMPOImILs

The performance of the TEMPOImILs as solvents and redox mediators was investigated in Li-O₂ batteries. The electrolyte was prepared by dissolving LiTFSI in TEMPOImILs. Galvanostatic charge-discharge measurements were carried out at a fixed capacity of 0.13 mAh cm⁻² in the voltage range of 2.0–4.2 V at 73 °C. Figure 33 shows terminal voltages for up to 50 cycles of the batteries with TEMPOImILs and with TEGDME/LiTFSI electrolyte cycled under the same conditions.

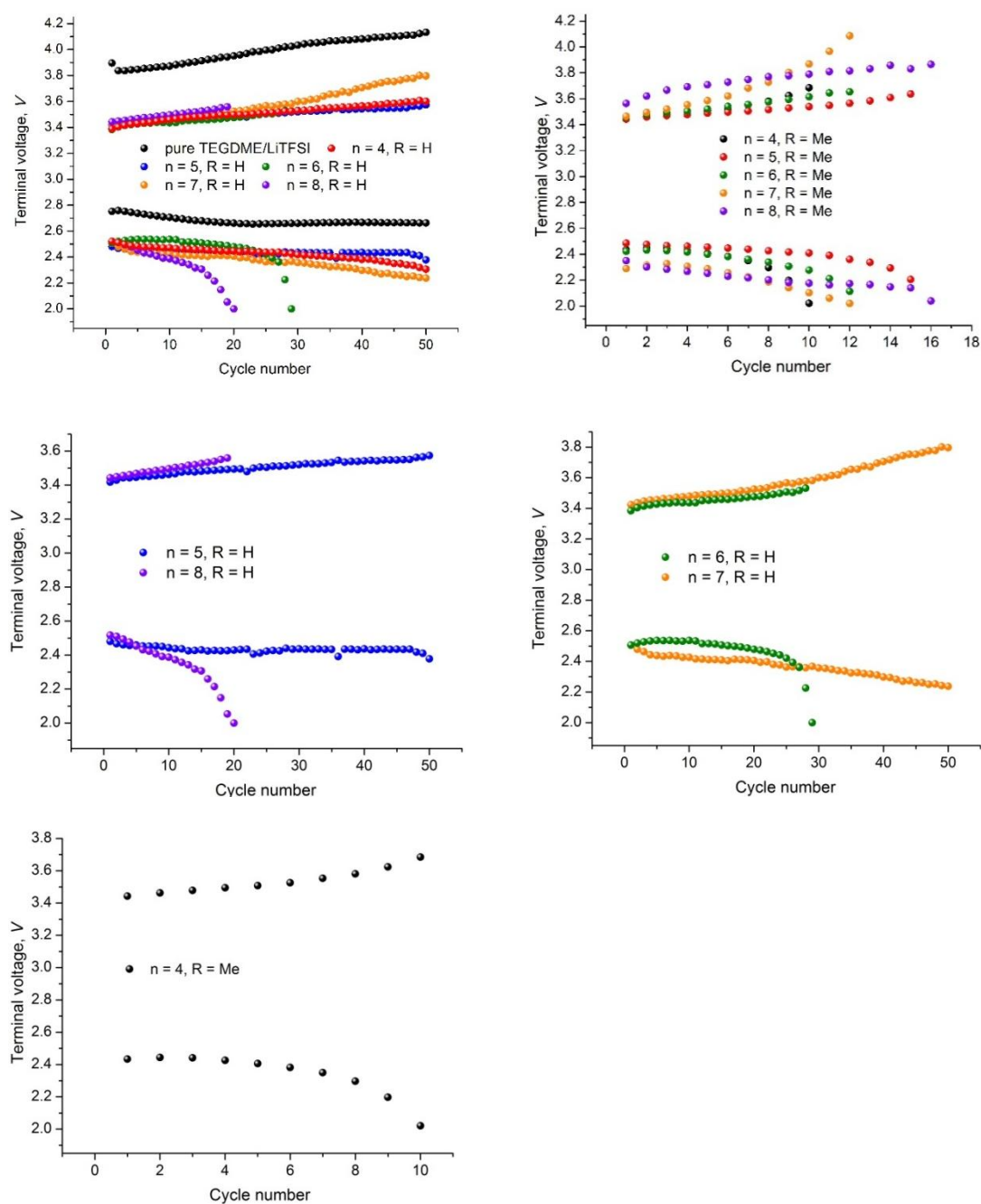


Figure 33. Cycle life of Li-O₂ batteries with TEMPOImILs/LiTFSI and TEGDME/LiTFSI operated at a fixed capacity of 0.13 mAh cm⁻² in the voltage range of 2.0–4.2 V at 73 °C.

The batteries TEMPOImILs **5a**, **b**, **d** had the longest lifetime compared to other TEMPOImILs and provided significant reduction of charge potentials of up to 0.57 V (for **5b**). The batteries using **5a–e** (R = H) had longer lifetimes than those using **6a–e** (R = Me), which is attributed to the differences in ionic conductivities. A greater ionic conductivity of the electrolyte provides faster diffusion of species within the Li-O₂ battery, thus, improving the rate performance.¹⁹² Furthermore, the morphology of the discharge product Li₂O₂ is rate dependent.¹⁹³ Change of morphology of the Li₂O₂ can affect the cyclability of the batteries (Section 1.2.2.4), e.g., solution route formation of Li₂O₂ reduces clogging of the cathode material because Li₂O₂ is formed in solution rather than on the surface of the electrode. Additional tests like SEM to analyse the morphology evolution of the discharge product would be beneficial to determine the effect of the change in ionic conductivities of TEMPOImILs on the morphology of the Li₂O₂.

In general, the batteries with TEMPOImILs ceased cycling due to an increase in discharge overpotential with the discharge voltage gradually approaching 2.0 V. The discharge overpotential can be reduced by diluting TEMPOImILs with other solvents, as in a recent example published in my group.¹⁴⁴

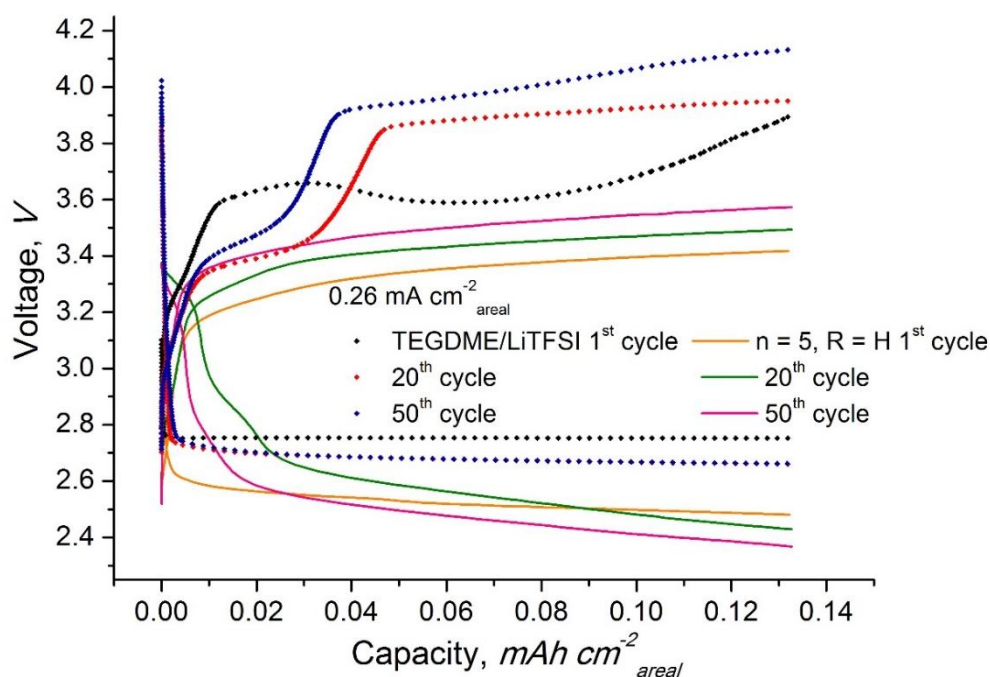


Figure 34. Galvanostatic discharge/charge profiles of Li-O₂ batteries with TEGDME/LiTFSI and TEMPOImIL **5b**/LiTFSI at 73 °C.

It has been reported that the charge overpotential is reduced in Li-O₂ batteries operated at elevated temperatures due to multiple possible reasons, one of them being the increased high-temperature ionic conductivity of Li₂O₂.¹⁹⁴ However, batteries in this work using conventional TEGDME/LiTFSI electrolyte cycled at 73 °C (Fig. 34) exhibited a different trend. During each charge process, the charge voltage remained lower than 3.7 V until the capacity reached 0.01–0.035 mAh cm⁻², and then a second plateau appeared, leading to end charge voltages of 3.8 V and above. The terminal charge voltage gradually reached the upper limit of 4.2 V. In contrast, the charge voltage of the battery with **5b** remained lower than 3.6 V.

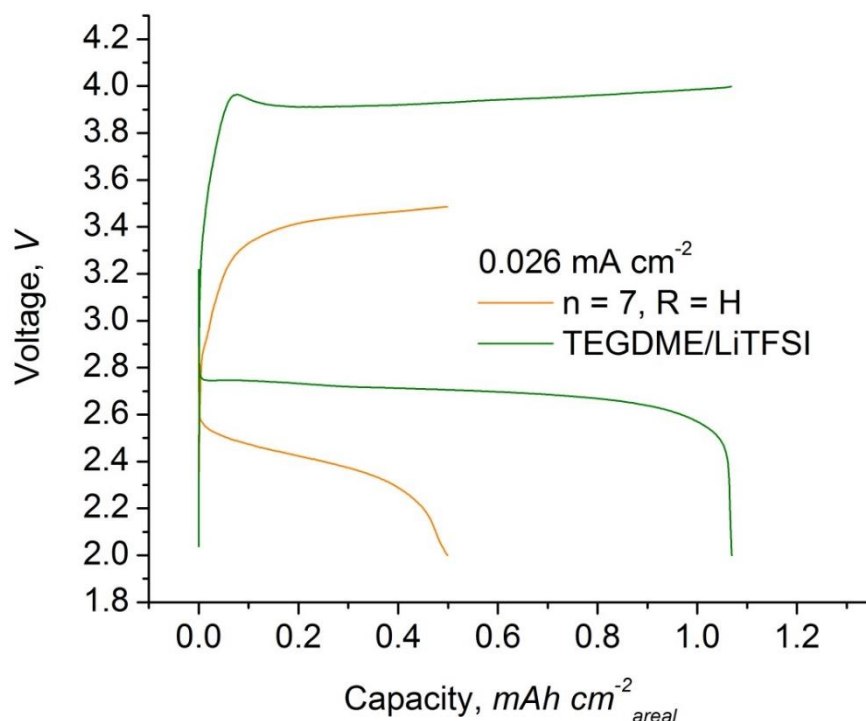


Figure 35. Full charge and discharge profiles of Li-O₂ batteries with TEGDME/LiTFSI and TEMPOImIL **5d**/LiTFSI at 73 °C.

The maximum charge and discharge capacities for the Li-O₂ batteries with TEMPOImILs were evaluated by fully discharging and then charging a battery containing LiTFSI/TEMPOImIL **5d** electrolyte at 73 °C. The results were compared to those of a battery with conventional LiTFSI/TEGDME electrolyte (Fig. 35). The battery with LiTFSI/TEGDME electrolyte demonstrated greater capacity values, but its charge voltage was close to 4 V, while the charge voltage of the battery with TEMPOImIL remained lower than 3.5 V over the course of the operation. These tests again demonstrate the effectiveness of TEMPOImILs as charge RMs. A reduction of the capacity has been previously observed with other TEMPO-based RMs and was attributed to the change in the morphology of the discharge product Li₂O₂ upon the addition of TEMPO.^{143,195} As can be seen from the CV

results, TEMPOImILs have an effect on the ORR. Presumably, their influence on the formation pathway of Li_2O_2 leads to a film-like morphology, which has an inferior capacity compared to toroid-like particles, but provides lower charge overpotential (Section 1.2.2.4).

Recently, Freunberger et al. demonstrated that it is most likely singlet oxygen $^1\text{O}_2$ that initiates most parasitic reactions in metal- O_2 batteries.¹⁹⁶⁻¹⁹⁸ Meanwhile, it has been reported that nitroxide radicals can act as singlet oxygen quenchers, which means that the nitroxide group can suppress the decomposition of TEMPOImILs and other battery components.¹⁷¹⁻¹⁷³

TEMPOImILs **5a–e** ($\text{R} = \text{H}$) have the potential to degrade through side reactions involving abstraction of an acidic hydrogen in the 2-position of the imidazole ring by lithium metal and further dimerisation of the resulting heterocyclic carbene.¹⁹⁹ However, the superior performance of these compounds compared to 2-methylated analogs (**6a–e**, $\text{R} = \text{Me}$) suggested that any such reaction was suppressed.

3.7. Summary

Nine new compounds that perform as redox mediators and solvents for Li-O_2 batteries have been synthesised and characterised. Electrochemical experiments revealed that compounds **5a, b** ($n = 4, 5$; $\text{R} = \text{H}$) were the most effective TEMPOImILs in the series for the use in Li-O_2 batteries and reduce the charge overpotential by ~ 0.6 V after 50 cycles. No improvement of the discharge performance (ORR) was observed in these experiments. The performance of the batteries with TEMPOImILs was mostly consistent with the ionic conductivities of the compounds, and suggests that side reactions were suppressed presumably by the protective action of the nitroxide group and that continuous reaction of

TEMPOImILs **5a–e** with Li metal does not occur. TEMPOImILs are also effective when used in mixtures with aprotic solvents that can improve the ionic conductivity of the TEMPOImILs.¹⁴⁴ Owing to the large and adjustable size of the molecules, TEMPOImILs can be used in studies where a membrane is applied to prevent the crossover of the redox mediators towards the anode. Importantly, these materials provide safer alternatives to current liquid electrolytes.

Chapter 4: Nitronyl- nitroxide-based redox mediators for Li-O₂ batteries

Chapter 4: Nitronyl-nitroxide-based Redox Mediators for Li-O₂ Batteries[‡]

4.1. Introduction

In Li-O₂ batteries, charging redox mediators (RMs) can help to effectively decompose the solid insulating discharge product Li₂O₂, which clogs the cathode surface leading to high charge voltages and short cycle life (Section 1.2.3 and Chapter 3). An effective charging RM can provide significant improvement to the oxygen evolution reaction (OER). However, low discharge capacity, poor rate performance and high discharge overpotentials remain serious drawbacks preventing the commercial use of Li-O₂ batteries. RMs that can facilitate the discharge reaction (discharging RMs) by assisting the formation of Li₂O₂ either by interacting with Li ions or with oxygen, are important to combat these issues. Systems where both discharging and charging RMs are added are known as dual RM systems.^{135,137,178,200} Dual RMs can transfer the discharge and charge reactions from the cathode surface into the solution, avoiding the passivation of the cathode surface and thus increasing the capacity and rate, and reducing overpotentials. The solution pathway also provides greater stability of the carbon electrode material, which is the most favourable material for porous cathodes but is prone to decomposition with the formation of Li₂CO₃ upon interaction with Li₂O₂ or LiO₂ at higher voltages.^{9,39,135}

Discharging RMs reported to date include 2,5-di-*tert*-butyl-1,4-benzoquinone (DBBQ),^{135,178,201} other quinone derivatives,¹³⁹⁻¹⁴¹ iron phthalocyanine,¹³⁴ and ethyl viologens^{133,137-138}. Among the reported charging RMs there are nitroxide radicals,^{115,142,159}

[‡] A significant component of the work presented in this chapter has been submitted to *JPhysChemC*

tetrathiafulvalene, *N*-methylphenothiazine, *tris*[4-(diethylamino)-phenyl]amine,¹²⁶ *N,N,N',N'*-tetramethyl-*p*-phenylenediamine, 5,10-dimethylphenazine, ferrocene,¹⁰ cobalt(II) *bis*(terpyridine),¹²⁹ metal porphyrins, metal phthalocyanines,^{126,145} LiI,¹⁰ CsI,¹⁴⁶ InI₃,²⁰² LiBr, and LiNO₃.¹²⁶ PTIO (2-phenyl-4,4,5,5-tetramethylimidazoline-1-oxyl 3-oxide) is a phenyl-substituted nitronyl nitroxide (Fig. 36) that combines charging and discharging redox mediation functions in one molecule; there are two redox processes occurring at 2.1 and 3.7 V vs. Li/Li⁺.¹³² PTIO also has high solubility and fast diffusion in common battery electrolytes.^{132,203}

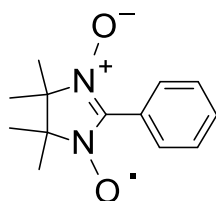
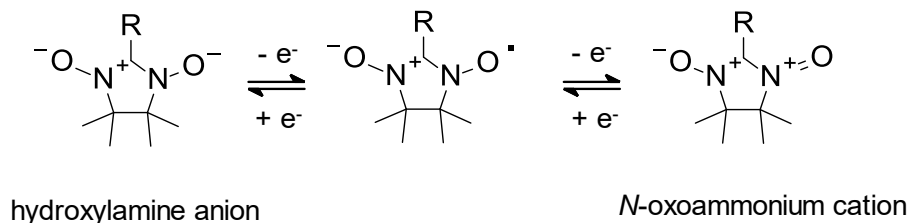


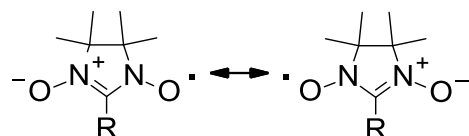
Figure 36. The structure of PTIO.

The electrocatalytic action of PTIO is similar to that of nitroxide radicals (Scheme 4), which have received extensive attention as RMs for Li-O₂ batteries (Table 1 in Section 1.2.3 and Chapter 3). As explained in Section 3.5.2, the reduction of a nitroxide radical into a hydroxylamine anion is a quasi-reversible process and has sluggish kinetics. Thus, nitroxide radicals are commonly used only as charging RMs.



Scheme 4. Redox processes in nitronyl nitroxide radicals.

In nitronyl nitroxides (NNs), an unpaired electron is delocalised between five atoms with the positive spin density spread almost evenly between the two nitrogen and two oxygen atoms. The system may be represented by the resonance structures shown in Scheme 5.²⁰⁴⁻²⁰⁶



Scheme 5. Resonance structures in nitronyl nitroxide radicals.

Due to the effective distribution of the electron density, the reduced state of NN radicals (Scheme 4) has been proposed to be more stable than that of nitroxides.²⁰⁷⁻²⁰⁸ It is therefore feasible that these molecules act as dual RMs. However, as with any radical compounds in this context, overall stability is important. To avoid side reactions involving the nitroxide group, nitronyl nitroxides should not contain heteroatoms or multiple carbon-carbon bonds attached to the C(4) and C(5) atoms of the imidazoline ring (in the α -position to a radical centre).²⁰⁹ In this case, delocalisation of an unpaired electron density would create a new reaction centre for dimerisation. In addition, the presence of α -hydrogens allows for disproportionation of the nitroxide group to nitron and hydroxylamine. Hence, fully substituted 4,4,5,5-tetraalkyl NNs (Scheme 5) exhibit significant stability compared to other NNs.

The stability of the reduced state and reversibility of the reduction of nitronyl nitroxides is significantly affected by the structure of the substituents.²¹⁰⁻²¹¹ For example, the reduction processes associated with pyrazolyl-based tetramethyl-substituted NNs,²¹² poly(4-nitronyl nitroxylstyrene),^{207,213} triarylamine-substituted NN,²¹⁴ biphenyl-based

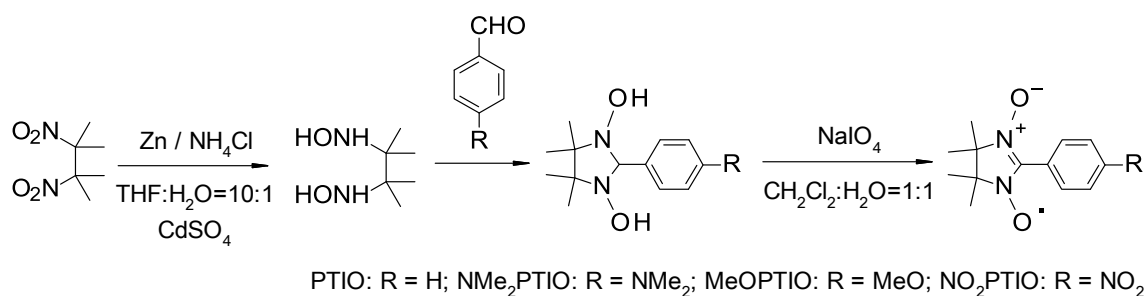
NN,²⁰⁸ and NN mono- and disubstituted norbornenes²¹⁵ were reported to be reversible. Thiophene-based NN demonstrated an irreversible reduction.²¹⁶ Among the NN biradicals, it is uncommon to have a reversible reduction process. For instance, in studies of the biradical consisting of two PTIO moieties linked by a short chain of ethylene glycol polymer, the reduction process is quasi-reversible and some by-products are formed.²¹⁷ Quasi-reversible reduction was also reported for three NN biradicals with fused-thiophene couplers²¹⁸. Other tetramethyl-substituted NN biradicals, including oligopyridine²¹⁹, pyrene-pyrazole-, anthracene-based compounds, biphenyl or bipyridine bridged NNs with one or two acetylene fragments connecting the aromatic rings²¹¹ exhibited irreversible reduction following the same pathway as depicted in Scheme 4, with the exception of a bromoanthracene-based derivative in which reduction waves appeared to be quasi-reversible, possibly due to an electron-withdrawing effect of the bromine substituent.²¹¹ Apart from the abovementioned tetramethyl-substituted NNs, the redox processes of annelated nitronyl nitroxides have also been investigated. Phenyl-substituted pyrene-based NN and phenyl-substituted benzonitronyl nitroxide (BNN) also exhibited a reversible reduction process, while phenanthrene- and pyridine-based phenyl-substituted NNs, as well as anisole-, *N*-ethylcarbazole- and triphenylamine-substituted BNNs had quasi-reversible reduction waves; although, the stability of these compounds was markedly lower than that of tetraalkyl-substituted NNs.²¹⁰ As seen from these reports, a correlation between the structures of the NNs and reversibility of the reduction process is not obvious. However, of importance to the current work, the reduction process of PTIO was reported as reversible.^{132,203}

A recent study demonstrated that the addition of PTIO to a Li-O₂ battery as a redox mediator not only reduced the charge overpotential but also increased the discharge capacity, because PTIO is capable of improving the oxygen solubility.¹³² Here, we report the findings of our studies into PTIO analogues as RMs for Li-O₂ batteries.

PTIO and its analogues benefit from straightforward synthetic methods that allow variation of substituents that can modify the redox potentials of the compounds.^{191,212,214} Thus, the potential of the RMs can be gradually adjusted until the desired battery performance is achieved. In the current study, we have chosen PTIO as a model compound and three analogues with different substituents on the 4-position of the benzene ring. We have investigated the effect of altering the substituents on the redox potential of the compounds and the performance of Li-O₂ batteries incorporating these RMs.

4.2. Synthesis of RPTIOs

PTIO analogues (RPTIOs) were chosen with R = MeO and NMe₂ due to their strong electron-donating effect, which could provide lower oxidation potentials. In addition, these groups are less likely to react with Li metal. A strong electron withdrawing group, NO₂, was included for comparison and to possibly enhance the stability of the reduced state.



Scheme 6. Synthesis of RPTIO compounds.

The synthesis of RPTIOs was achieved using the Ullman method modified by other researchers (Scheme 6).^{152,154,220} Due to the instability of *N,N'*-dihydroxy-2,3-diamino-2,3-dimethylbutane and *N,N'*-dihydroxy-2-phenyl-4,4,5,5-tetramethylimidazolidine, these compounds were used in the subsequent synthetic step immediately after collection by filtration and drying in vacuo. The reduction of *N,N'*-dihydroxy-2,3-diamino-2,3-dimethylbutane was followed by nucleophilic addition of *N,N'*-dihydroxy-2-phenyl-4,4,5,5-tetramethylimidazolidine to the corresponding aldehyde and oxidation of the resulting dihydroxyimidazolidines with NaIO₄ to obtain the RPTIOs.

Crystals of the obtained RPTIOs are shown in Figure 37. The crystals of NMe₂PTIO are greenish-blue, NO₂PTIO – dark green, while MeOPTIO and PTIO are blue colour, typical for NNs with an aromatic substituent.²²¹ All of the prepared RPTIOs are soluble in ether-based electrolyte solvents DEGDME and TEGDME, which are preferred due to their stability in a Li-O₂ battery environment.¹⁸⁵

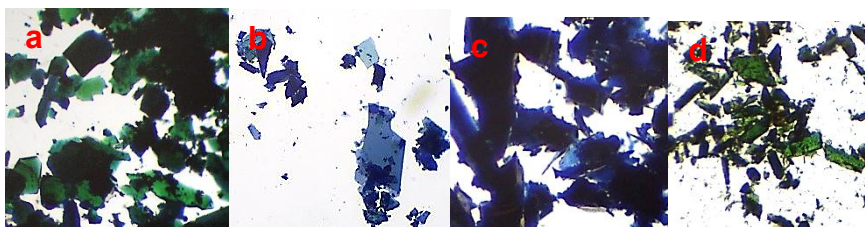


Figure 37. Photographs of the crushed crystals of RPTIO compounds: (a) NMe₂PTIO, (b) MeOPTIO, (c) PTIO, (d) NO₂PTIO.

4.3. Cyclic Voltammetry Studies with LiTFSI

The suitability of the electrochemistry of RPTIOs as RMs for Li-O₂ batteries was investigated. To effectively decompose Li₂O₂, the redox potential for the oxidation of RPTIOs should be higher than 2.96 V, while to catalyse the formation of Li₂O₂, the redox

potential for the reduction should be lower than 2.96 V. To maximize energy efficiency, both processes should be as close to 2.96 V as possible. The redox characteristics of RPTIOs were measured using cyclic voltammetry (CV) performed in a three-electrode setup with glassy carbon, platinum wire and non-aqueous Ag/Ag^+ as a working, counter and a reference electrode, respectively. Cyclic voltammograms of RPTIOs obtained under an argon atmosphere (Fig. 38) revealed two redox processes: an oxidation into the *N*-oxoammonium salt (RM^+) and a reduction into the hydroxylamine anion (RM^-).

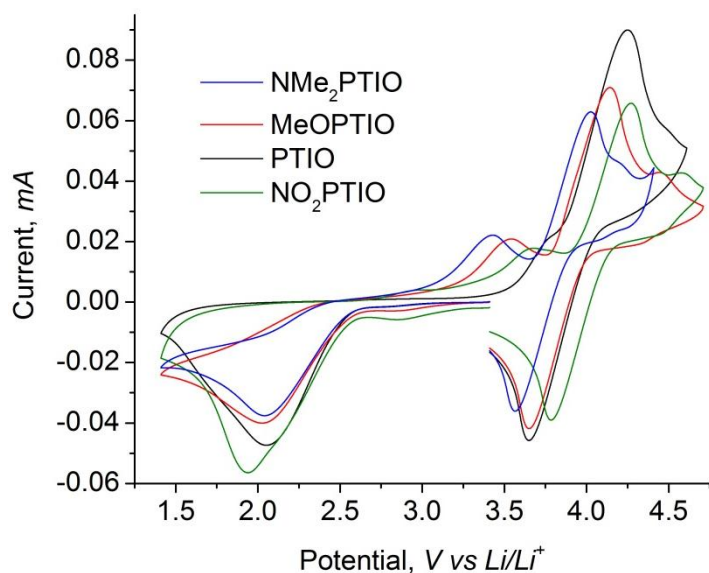


Figure 38. Cyclic voltammograms of RPTIOs (10 mM), LiTFSI (0.1 M) in TEGDME under an argon atmosphere.

Formal redox potentials for the oxidation process of RPTIOs ($E^{\circ'}_{\text{ox}}$) were calculated by averaging the potentials of the cathodic and anodic peaks (Table 5). As expected, the values of $E^{\circ'}_{\text{ox}}$ were the lowest for the compounds with electron-donating substituents NMe_2 and MeO .

Table 5. Redox potentials for the oxidation of RPTIOs.

Redox mediator	$E^{\circ'}_{ox}$, V vs. Li/Li^+
NMe ₂ PTIO	3.79
MeOPTIO	3.91
PTIO	3.95
NO ₂ PTIO	4.03

Regarding the reduction process, cyclic voltammograms obtained using LiTFSI under an argon atmosphere (Fig. 38) did not contain any anodic peaks at ~ 2.4 V vs. Li/Li^+ , which have been reported by others and assigned to re-oxidation of RM^- . Instead, we observed low-intensity peaks at 3.4–3.8 V vs. Li/Li^+ . We attribute these differences to the solvent (TEGDME vs. DMSO or acetonitrile).^{132,203} It is likely that the CV in Figure 38 is a result of a coupled chemical reaction (Scheme 3, Section 3.5.2), while the reduction process in TEGDME remains reversible or quasi-reversible.^{189,222} However, it would not be correct to calculate the redox potentials for the reduction, unless the nature of these chemical and electrochemical processes is unambiguously determined, as there is a possibility that the peaks at 3.4–3.8 V vs. Li/Li^+ are related to an oxidation of hydroxylamine instead of a re-oxidation of RM^- . The separation of the anodic and cathodic peaks for the reduction of RPTIOs is less than that of nitroxides,¹⁸⁹ indicating greater reversibility possibly due to higher stability of the reduced state.

To determine the onset potential of the reduction of RPTIOs, we conducted the CV tests in argon by changing the potential range stepwise until the return reduction peak started appearing (Fig. 39). The value of the onset potential for the reduction is ≈ 2.3 V vs. Li/Li^+ .

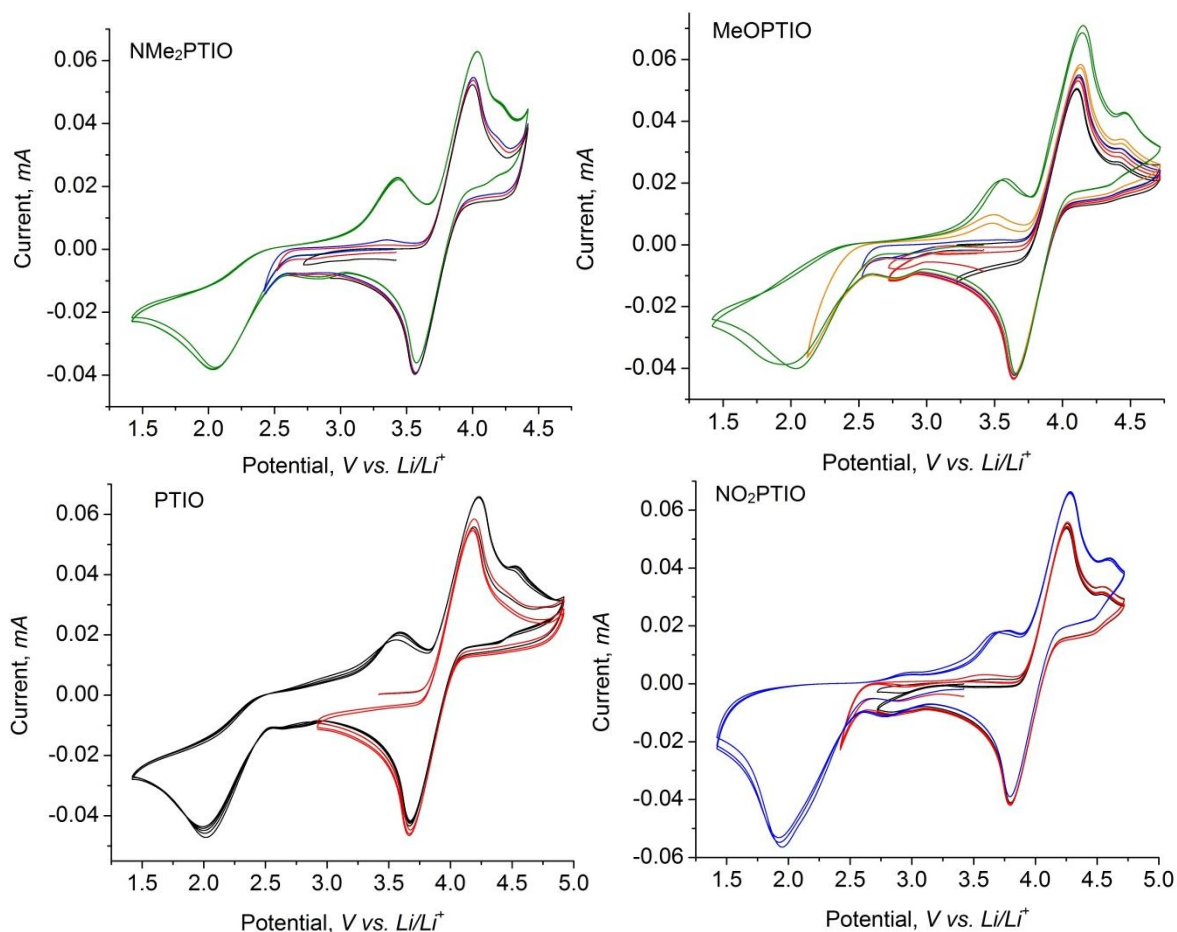


Figure 39. Cyclic voltammograms of RPTIOs (10 mM) in LiTFSI/TEGDME under an argon atmosphere in different potential ranges.

Figure 40 shows that upon the addition of RPTIOs under oxygen the anodic traces at 3.4–3.8 V vs. Li/Li^+ disappear, which suggests that the concentration of RM^- was reduced while catalysing the oxygen reduction reaction (ORR). However, the low reduction potentials of the RPTIOs reported here may not significantly improve the performance of the ORR and the reduction potentials of discharging RMs reported to date are greater than 2.4 V vs. Li/Li^+ .^{133-135,137-141,178,201} Generally, the voltage in Li- O_2 batteries does not reach such low values unless the battery is close to failure. In addition, there was only a slight increase in the intensity of the ORR peak upon the addition of RPTIOs in an oxygen

atmosphere (Fig. 40). Thus, the action of RPTIOs as charging RMs was investigated in greater detail.

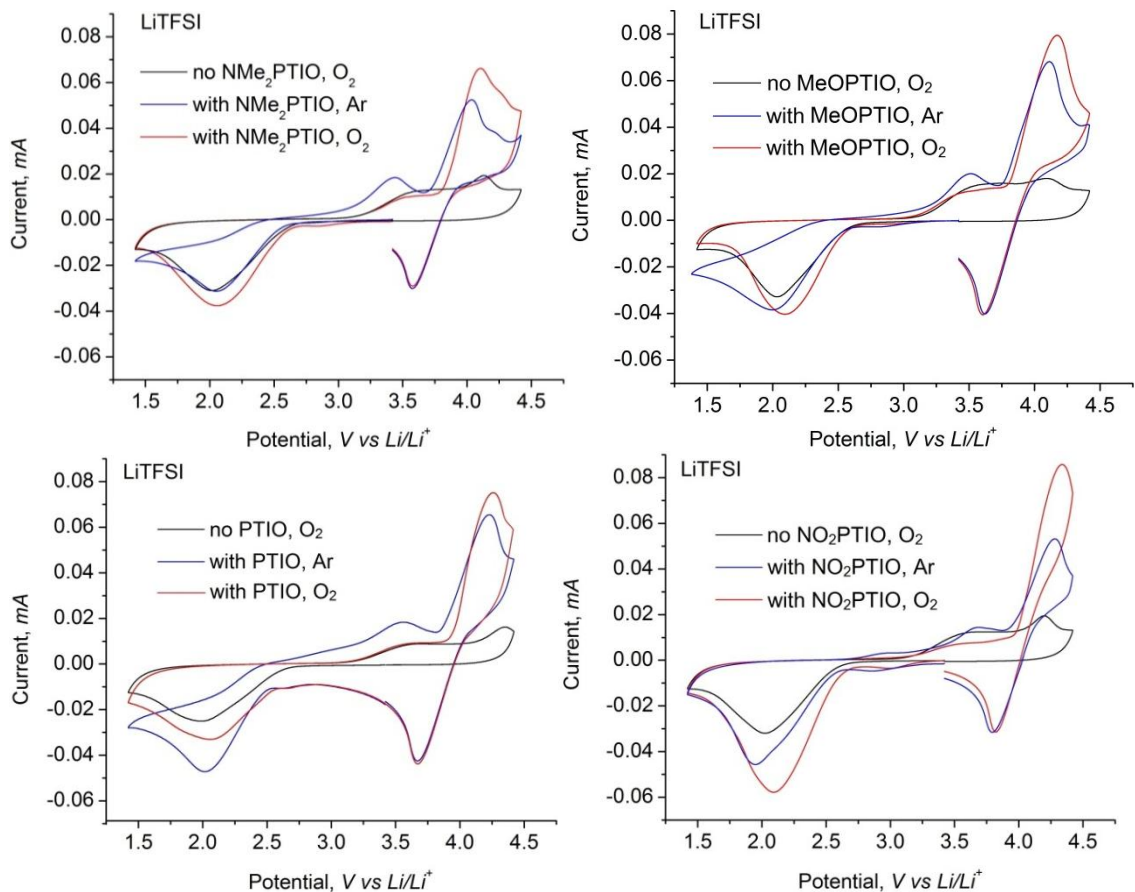


Figure 40. Cyclic voltammograms with and without RPTIOs (10 mM) in LiTFSI/TEGDME under an O_2 and Ar atmosphere. “No RM” refers to 0.1 M LiTFSI in TEGDME.

4.4. Cyclic Voltammetry Studies with TBATFSI

The long-term electrochemical stability of PTIO under an oxygen atmosphere (Fig. 41) was examined using TBATFSI (instead of LiTFSI) to avoid clogging of the glassy carbon electrode with Li_2O_2 , which leads to a gradual shift in the potentials. The increase in the intensity of the anodic peak related to the oxidation of PTIO and its shift to higher potential

values indicates a pronounced effect of this compound on the OER. There were no significant changes in the peaks during the subsequent 50 cycles, which demonstrates high electrochemical stability of PTIO in oxygen.

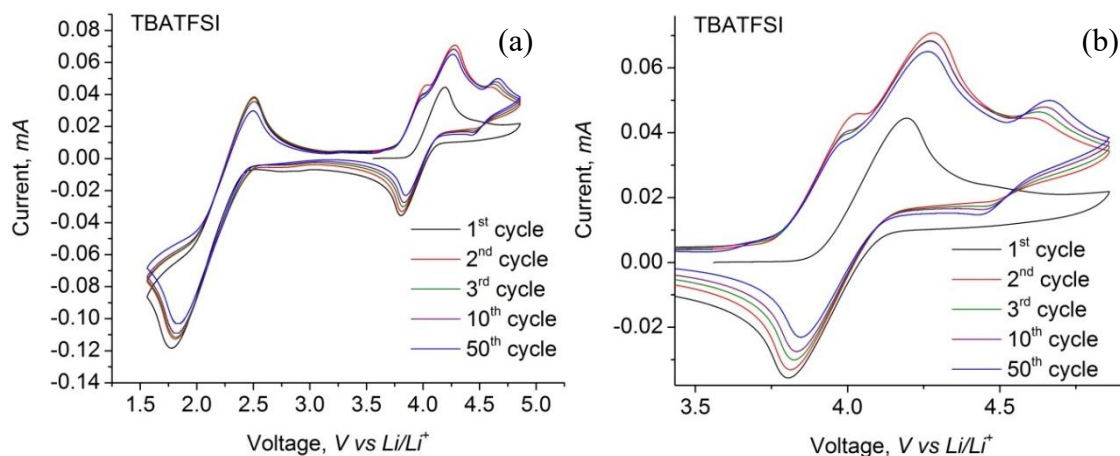


Figure 41. Cyclic voltammograms of PTIO (10 mM) in TBATFSI/TEGDME under an oxygen atmosphere: (a) full scan range, (b) enlarged region at higher positive potentials.

4.5. Spectroelectrochemistry of PTIO

UV-visible spectroelectrochemistry of PTIO under an O₂ atmosphere was performed to investigate the reversibility of the oxidation process (Fig. 42). UV-visible absorption spectra of $3 \cdot 10^{-7}$ M solutions of PTIO in 0.3 M TBAPF₆/MeCN were collected at 60 s intervals after the potential was applied. The voltage step was 0.1 V. The first spectrum was recorded before applying a potential. The electrolyte system TBAPF₆/MeCN was selected due to a very high potential window, which excludes contributions from electrolyte decomposition.²²³

The initial UV-visible absorption spectrum of PTIO contains two characteristic bands at 361 and ~605 nm related to $n \rightarrow \pi^*$ and $\pi \rightarrow \pi^*$ electronic transitions (Fig. 42).²²⁴⁻²²⁵

During oxidation, these bands gradually decreased in intensity and disappeared indicating the removal of an unpaired electron, while two new bands arose at 310 and ~445 nm. The three isosbestic points at 338, 377 and 540 nm were observed, and the spectra obtained at the conclusion of the experiment were almost identical to those collected initially, which shows the reversibility of the oxidation process.

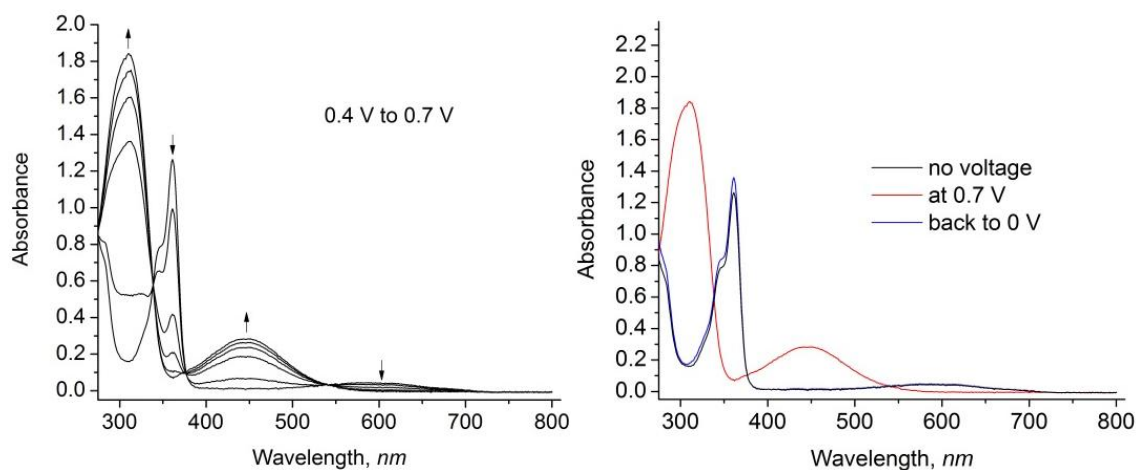


Figure 42. UV-Visible spectral changes during stepwise electrochemical oxidation of PTIO solution in TBAPF₆/MeCN. The potential was recorded vs. Ag/Ag⁺ reference electrode.

When the potential was scanned in the negative direction (Fig. 43), the band at ~605 nm disappeared and the peak at 361 nm decreased in intensity. The formation of a new band was recorded at ~310 nm. Upon applying 0 V, the curves did not fully regain their original appearance, which is likely due to the formation of hydroxylamine and/or hydroxylammonium cation (Scheme 3, Section 3.5.2), while the reverse reactions are slow compared to the timescale of the experiment. The voltage at which this process occurs is ~2.3 V vs. Li/Li⁺, which suggests that it will not affect the stability of RPTIOs during cycling of the Li-O₂ batteries.

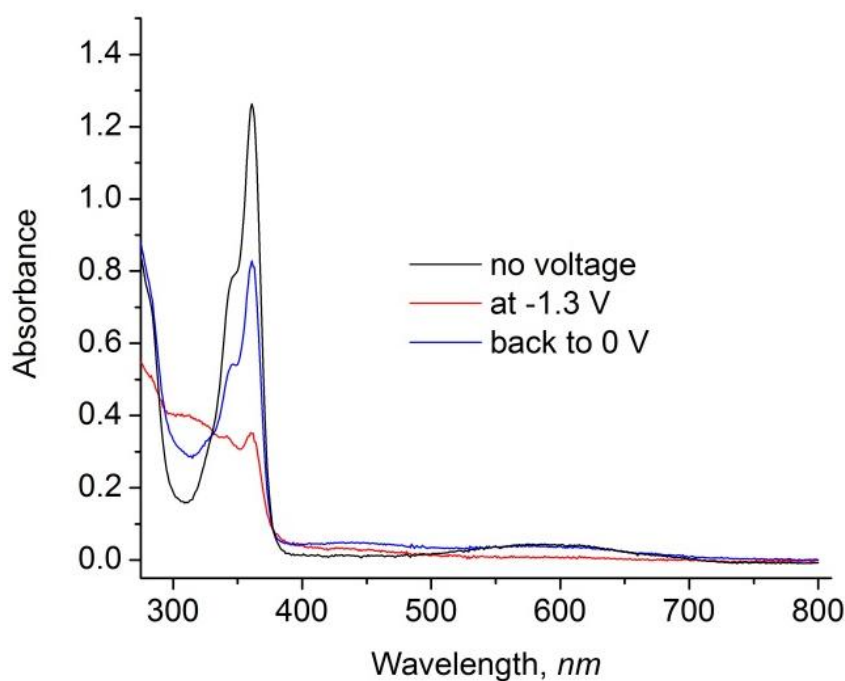


Figure 43. UV-Visible spectral changes during stepwise electrochemical reduction of PTIO solution in TBAPF₆/MeCN. The potential was recorded vs. Ag/Ag⁺ reference electrode.

4.6. Reactions in Li-O₂ Batteries upon the Addition of the Redox Mediators

Before testing the performance of RPTIOs in Li-O₂ batteries, it was crucial to demonstrate that the new RMs do not contribute to the capacity of a battery by shuttling from the cathode to anode, but are indeed catalysing the decomposition of Li₂O₂. The contribution from the redox shuttling of the RM can be considered insignificant if the redox reactions in the Li-O₂ batteries upon the addition of the RM follow the Equations 5 and 6 (Section 1.2.1.1) with the formation of Li₂O₂ as the main discharge product, and if the RM does not provide high capacity on its own (in the absence of oxygen). For this purpose, SEM, XRD and battery tests in an argon atmosphere were conducted.

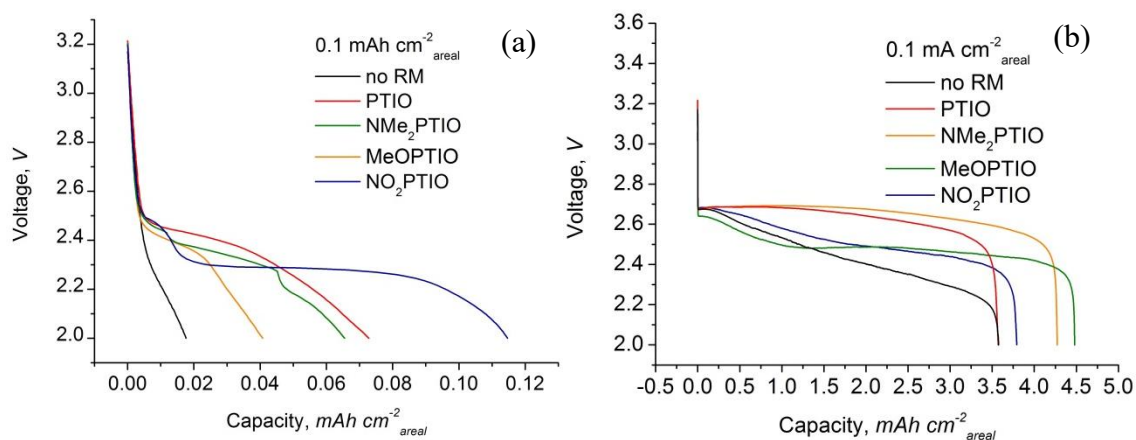


Figure 44. Full discharge curves of the batteries with RPTIOs (10 mM) in LiTFSI/DEGDME and pure LiTFSI/DEGDME electrolyte in argon (a) and oxygen (b).

Battery tests in argon were performed in Swagelok cells with a sealed O₂ inlet using Li metal, carbon black (CB) and glass fibre as anode, cathode and separator, respectively. The electrolyte was composed of 10 mM RPTIO dissolved in 0.5 M LiTFSI/DEGDME (Fig. 44a). The obtained capacity was negligible enough to affirm that the addition of the RPTIO does not significantly affect the overall capacity of the Li-O₂ batteries.

SEM images of the cathodes with and without RMs showed the morphology of the battery discharge product and the action of the RMs towards it (Figs. 45 and 46). With the addition of PTIO, thin plates of the discharge product were formed (Fig. 45b), which fully decomposed upon charging (Fig. 45d). Without PTIO, the formation of larger particles was recorded (Fig. 45c). The same effect was observed for the other RPTIOs.

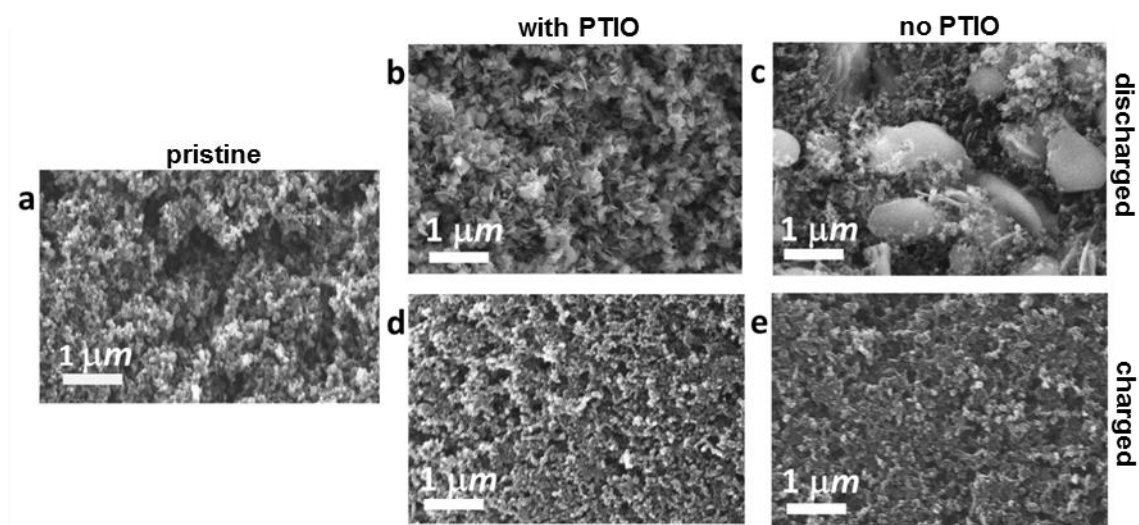


Figure 45. SEM images of CB cathodes: (a) pristine, (b) discharged containing PTIO, (c) discharged without PTIO, (d) charged containing PTIO, (e) charged without PTIO.

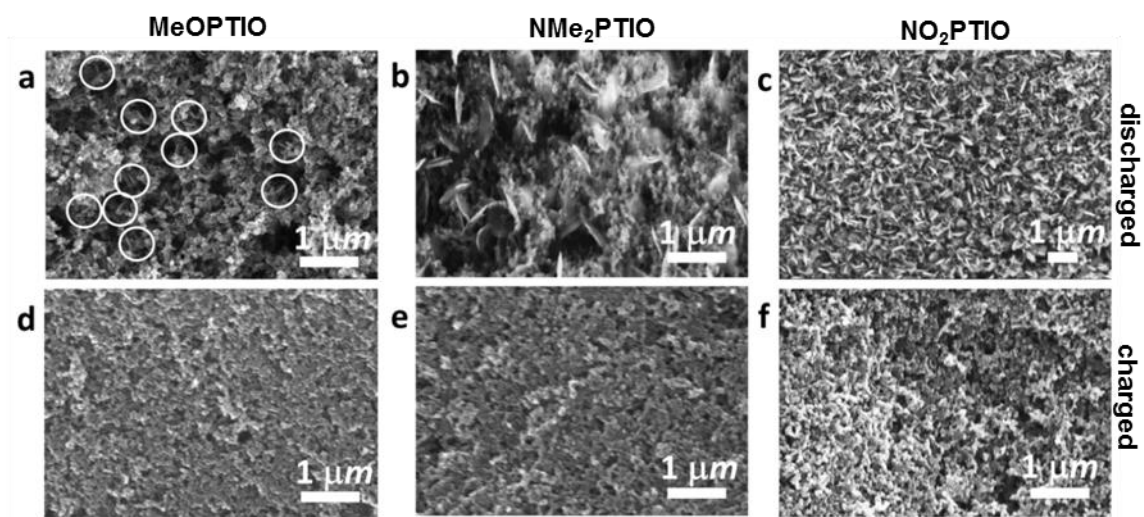


Figure 46. SEM images of discharged (top) and charged (bottom) CB cathodes with RPTIOs: a), d) MeOPTIO; b), e) NMe₂PTIO; c), f) NO₂PTIO.

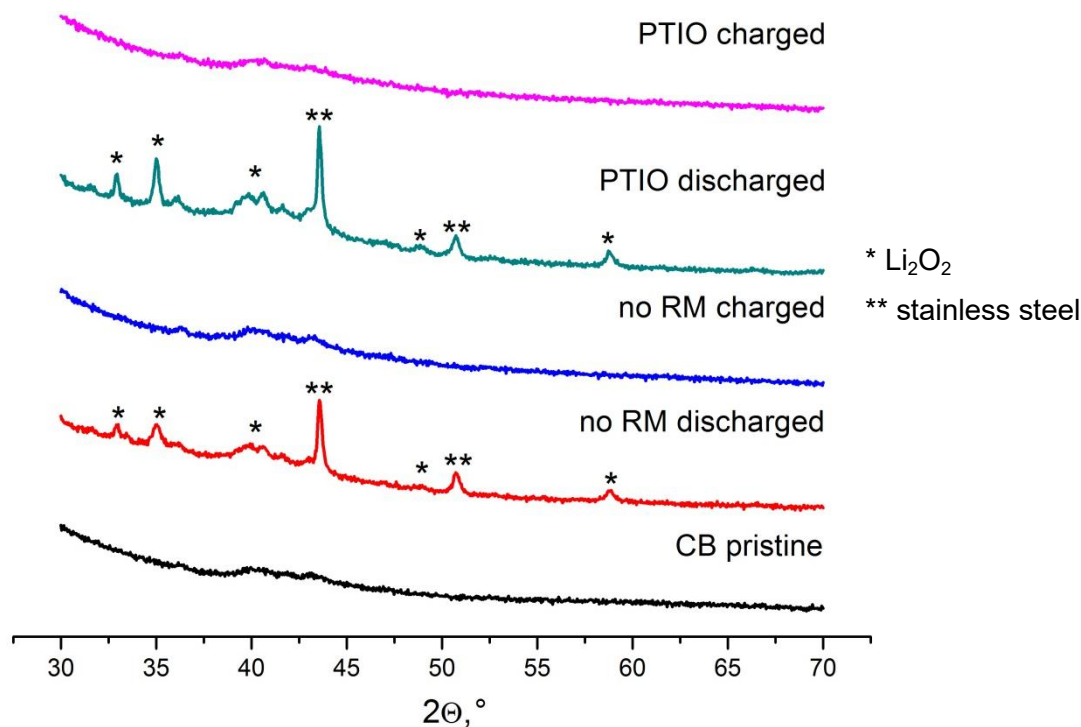


Figure 47. XRD patterns of pristine, discharged and charged CB cathodes with and without PTIO. Note: discharged cathodes remained attached to the stainless steel current collectors, peaks assigned to stainless steel are indicated in the diffraction patterns by **.

XRD studies showed that the particles observed in the SEM images belonged to the discharge product Li_2O_2 (Figs. 47 and 48). XRD patterns of the discharged cathodes with and without PTIO contained all of the characteristic signals assigned to Li_2O_2 , and no other signals were apparent. These results suggest that the overall reaction in the batteries with RPTIOs is the same as in Li- O_2 batteries cycled without RMs.

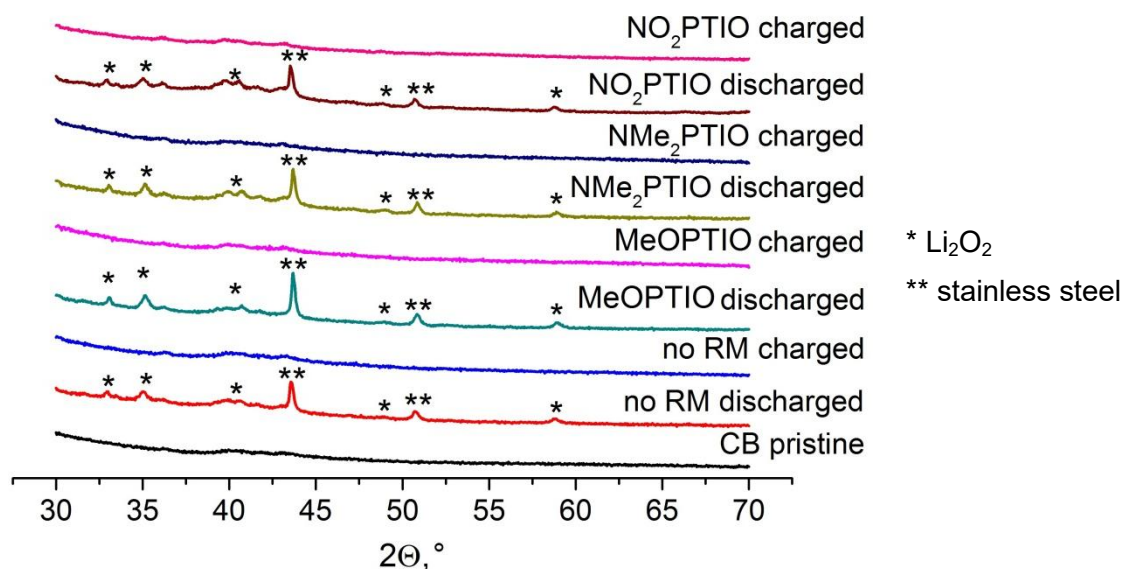


Figure 48. XRD patterns of pristine, discharged and charged CB cathodes with and without RPTIOs.

4.7. Performance of Li-O₂ Batteries with RPTIOs

To test the effect of RPTIOs on the ORR, Li-O₂ batteries with CB cathodes and 10 mM RPTIOs in LiTFSI/DEGDME electrolyte were discharged until 2 V (Fig. 44b). The discharge curves of all RPTIOs, except for PTIO, demonstrated a slight increase in the discharge capacity compared to the battery with a pure LiTFSI/DEGDME electrolyte, up to 0.9 mAh cm⁻² for MeOPTIO, while the batteries with PTIO and NMe₂PTIO showed notably lower discharge overpotentials. Unlike some TEMPO-containing RMs,¹⁹⁵ the RPTIOs did not reduce the discharge capacity. The discharge capacities for batteries containing each of the RPTIOs were much greater when discharged in an oxygen atmosphere compared to argon (Fig. 44a) indicating that the compounds facilitate the reactions in the Li-O₂ battery, rather than contributing to the capacity by redox shuttling.

The action of RPTIOs on the OER was investigated by discharging and then charging Li-O₂ batteries with the same composition to 0.25 mAh cm⁻² in the voltage range of 2–4.1 V (Fig. 49). Batteries containing RPTIOs exhibited an improvement in the OER, decreasing the charge overpotential by up to 0.3 V for NMe₂PTIO in the studied voltage window and with a more than double charge capacity. Importantly, the battery charge potentials followed the same order as the oxidation potentials for the RPTIOs ($E(\text{NMe}_2\text{PTIO}) < E(\text{MeOPTIO}) < E(\text{PTIO}) < E(\text{NO}_2\text{PTIO})$), consistent with our hypothesis that changes in the structures of RPTIOs will have a direct and predictable effect on the charge overpotential.

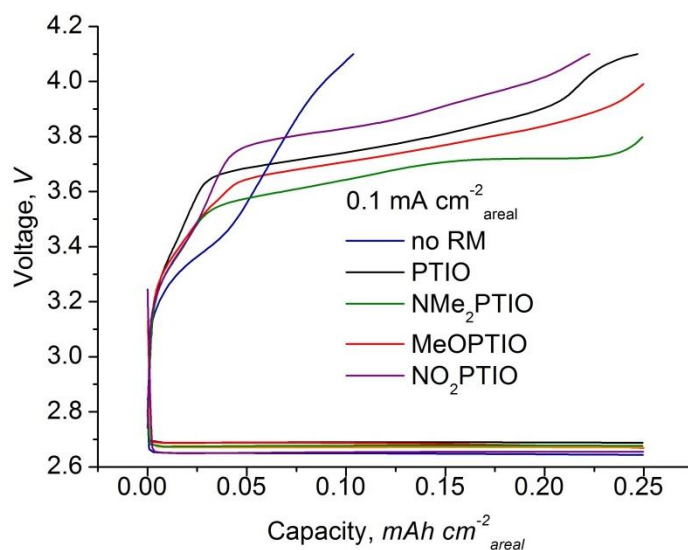


Figure 49. Galvanostatic discharge/charge curves of RPTIOs (10 mM) in LiTFSI/DEGDME (1st cycle).

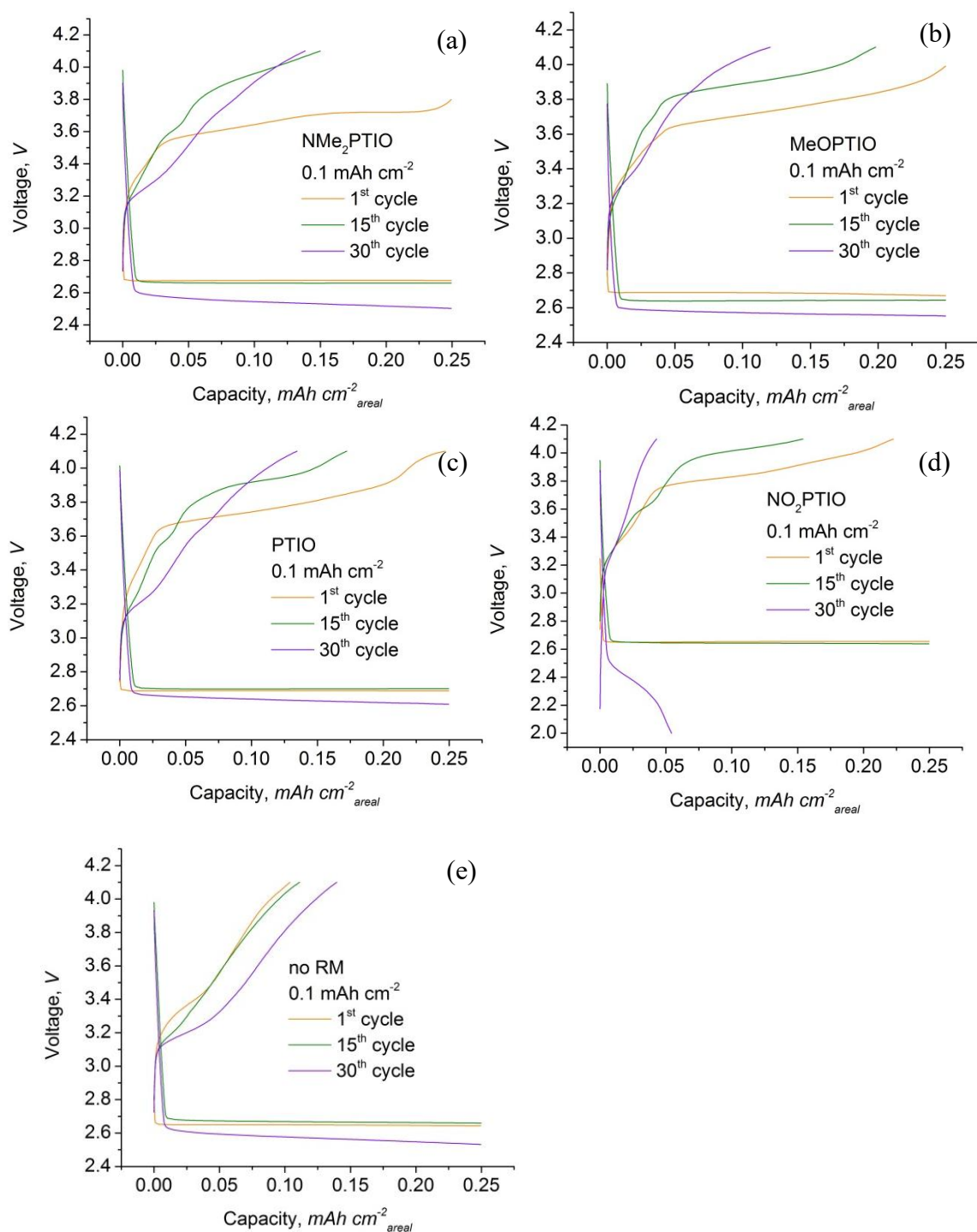


Figure 50. Galvanostatic cycling profiles of batteries (RPTIO (10 mM) in LiTFSI/DEGDME): (a) NMe₂PTIO, (b) MeOPTIO, (c) PTIO, (d) NO₂PTIO, and (e) pure LiTFSI/DEGDME electrolyte.

The long-term effect of the RMs on battery performance was investigated by cycling the Li-O₂ batteries with and without RPTIOs for 30 cycles in the voltage range of 2–4.1 V at a fixed capacity of 0.25 mAh cm⁻² (Fig. 50). The batteries containing RPTIOs maintained lower charge voltages than the battery without added RM for at least 15 cycles. The discharge capacity of the battery with NO₂PTIO dropped after the 25th cycle, and the battery ceased cycling earlier than that without RM, possibly due to a high oxidation redox potential of this RM.

The battery with MeOPTIO had the longest cycle life and cycled slightly longer than the battery without RM at fixed capacities of 0.25 mAh cm⁻² and 0.5 mAh cm⁻² (Fig. 51). The catalytic action of MeOPTIO leads to the formation of very thin plates of Li₂O₂ that were observed in SEM images (Fig. 46a). These particles are easier to be decomposed during discharge than larger particles formed in the battery with a pure LiTFSI/DEGDME electrolyte, leading to lower charge overpotentials and longer cycle life.

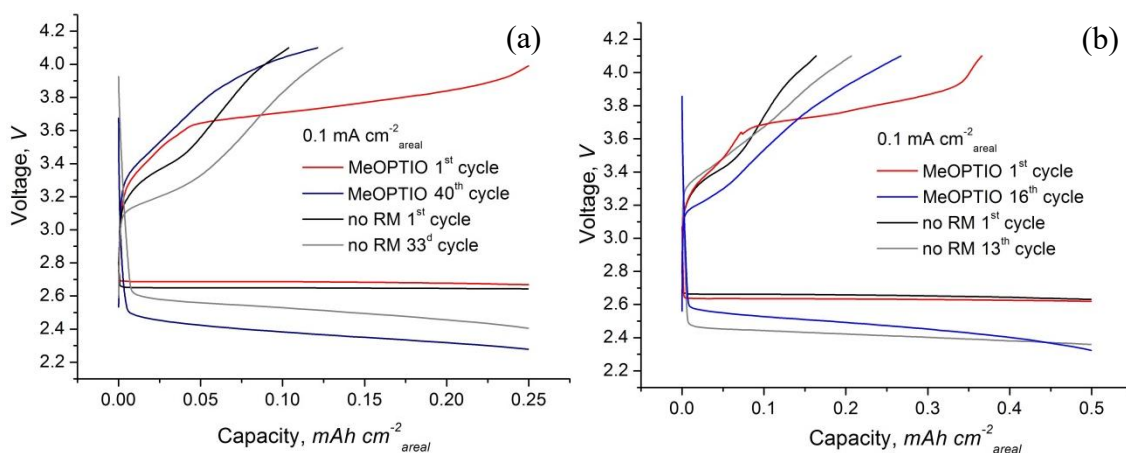


Figure 51. Galvanostatic cycling profiles of the batteries with 10 mM MeOPTIO in LiTFSI/DEGDME and pure LiTFSI/DEGDME electrolyte at fixed capacities of 0.25 mAh cm⁻² (a) and 0.5 mAh cm⁻² (b).

4.8. Summary

In conclusion, three new RMs for Li-O₂ batteries were proposed and synthesized. The stability of the reduced state of the RPTIOs was greater than that of nitroxides with the return peak for the reduction observed in CV experiments at lower voltages than the oxidation process, suggesting that they can operate as charging and discharging RMs combined in one molecule. The addition of RPTIOs to Li-O₂ batteries led to a lower discharge overpotential with a slight increase of the discharge capacity, unlike some other nitroxide-group-based RMs. More importantly, RPTIOs provided a significant decrease of the charge overpotential (up to 0.3 V in the studied voltage window), and the order of the obtained charge voltages was the same as the redox potentials for the oxidation calculated from the CV curves, which proves a pronounced catalytic effect of RPTIOs on the OER. This study demonstrated a clear dependence of the charge potential on the character of the substituent on the position 2 of imidazoline moiety in nitronyl-nitroxide-based RMs. The advantage of this type of RMs is that the synthetic method allows for an easy adjustment of the structures and correction of the redox potentials to the optimum values. A variation of the structures could decrease the peak separation for the reduction process, which might lead to a more significant increase of the discharge capacity. For example, it is worth considering to replace a benzene ring with a pyrazole as in pyrazolyl-based tetramethyl-substituted NNs²¹² (Section 4.1) which were reported to have a reversible reduction process with lower peak separation than observed for PRTIOs in our group.

Chapter 5: Conclusions

Chapter 5: Conclusions

This thesis proposed and examined new redox mediators (RMs) to improve the performance of Li-O₂ batteries. Selected compounds were also investigated for their stability as electrolyte solvents. The thesis aims (described in detail in the Overview) have been achieved by designing and synthesising twelve new RMs that decreased the charge overpotential and, in some cases, enhanced cyclability of the batteries, and nine new electrolyte solvents based on ionic liquids.

TEMPO-substituted imidazolium ionic liquids (TEMPOImILs) were examined as RMs and electrolyte solvents for Li-O₂ batteries (Chapter 3). Nine of ten TEMPOImILs are new compounds. TGA and DSC studies of TEMPOImILs demonstrated that they are less volatile than conventional aprotic electrolytes, which proves their increased safety. It was found that, unlike other imidazolium ionic liquids, TEMPOImILs are sufficiently stable in an oxygen atmosphere, which was assigned to a radical scavenging action of the TEMPO moiety. TEMPOImILs used solely as electrolyte solvents in Li-O₂ batteries provided a significant and stable decrease of the charge overpotential, which confirms their catalytic activity towards the oxygen evolution reaction (OER). Diluting TEMPOImILs with less viscous aprotic solvents and using them in combination with discharging RMs (Section 1.2.3) might help to increase the discharge capacity, decrease discharge overpotential and further improve the cycle life of the batteries.

In this chapter, the effect of changing the structure of TEMPOImILs on the battery performance was also elucidated. We varied the number of carbon atoms in the alkyl chain connecting the TEMPO moiety and imidazolium cation and the substituents on the 2-

position of imidazole ring (either methyl or hydrogen). The length of alkyl chains did not have any noticeable effect on the battery performance. Meanwhile, the replacement of the methyl group on the 2-position of imidazole ring with the hydrogen atom resulted in substantially longer cycle life of the Li-O₂ batteries.

The second part of this thesis presents phenyl-substituted nitronyl nitroxides (RPTIOs) as RMs for Li-O₂ batteries (Chapter 4). In this chapter, we investigated the effect of introducing substituents with different electron affinity into the benzene ring on the redox potentials of RPTIOs and the performance of Li-O₂ batteries with catalytic amounts of these compounds. PTIO (2-phenyl-4,4,5,5-tetramethylimidazoline-1-oxyl 3-oxide, no substituents on the benzene ring) was reported to have two reversible redox processes, and thus, was proposed as RM for both discharge and charge reactions. However, the reduction waves of RPTIOs obtained during cyclic voltammetry experiments did not replicate the ones published for PTIO, possibly due to the use of a different solvent. Measurements of the rate constant would provide further insight into the nature of the reduction process of RPTIOs. Regarding the oxidation process, a clear dependence of the redox potential on the donating character of the substituent was observed, where RPTIOs with electron-donating groups had a lower oxidation potential.

Three of four RPTIOs were not reported previously as RMs for Li-O₂ batteries; thus, XRD, SEM studies and battery tests in argon were conducted to prove that they can indeed catalyse the formation and decomposition of Li₂O₂, rather than redox shuttling from the cathode to the anode. When added to Li-O₂ batteries, RPTIOs not only enhanced the performance of the OER but also provided a slight improvement to the oxygen reduction reaction (ORR). The reduction of the charge overpotential was in direct correlation with the

redox potentials for the oxidation and electron donating character of the substituents, which proved the hypothesis that the value of the charge potential of Li-O₂ batteries with nitronyl-nitroxide-based RMs can be easily tuned by changing the structures of the RMs.

Overall, nitroxide-group-based RMs studied in this thesis are capable of facilitating the charge process more than the discharge. The directions for future research include altering the structures of the RPTIOs, *e.g.*, using pyrazolyl-based nitronyl nitroxides with lower peak separation for the reduction process than in RPTIOs. Enhanced reversibility of the reduction process might provide a more significant improvement of the discharge reaction and allow to achieve dual redox mediator function in one molecule. In terms of applications of the proposed compounds, future studies for RPTIOs include using higher concentrations of the RMs that could lead to a more significant decrease of the overpotentials and increase of the charge and discharge capacities. The use of a membrane separating the anode and cathode compartments with a TEMPOImIL added only to the cathode will eliminate the crossover of the RMs towards the anode and might increase the cycle life and coulombic efficiency of the batteries. In combination with the protection of the Li metal discussed in Section 1.2.2.1 and other additives for the ORR, *e.g.*, effective discharging RMs (Section 1.2.3) TEMPOImILs and RPTIOs can be used to provide high-performance Li-O₂ batteries for energy storage, electric vehicles and various electronic devices.

Appendix

A.1. TGA and DSC Data for TEMPOImILs

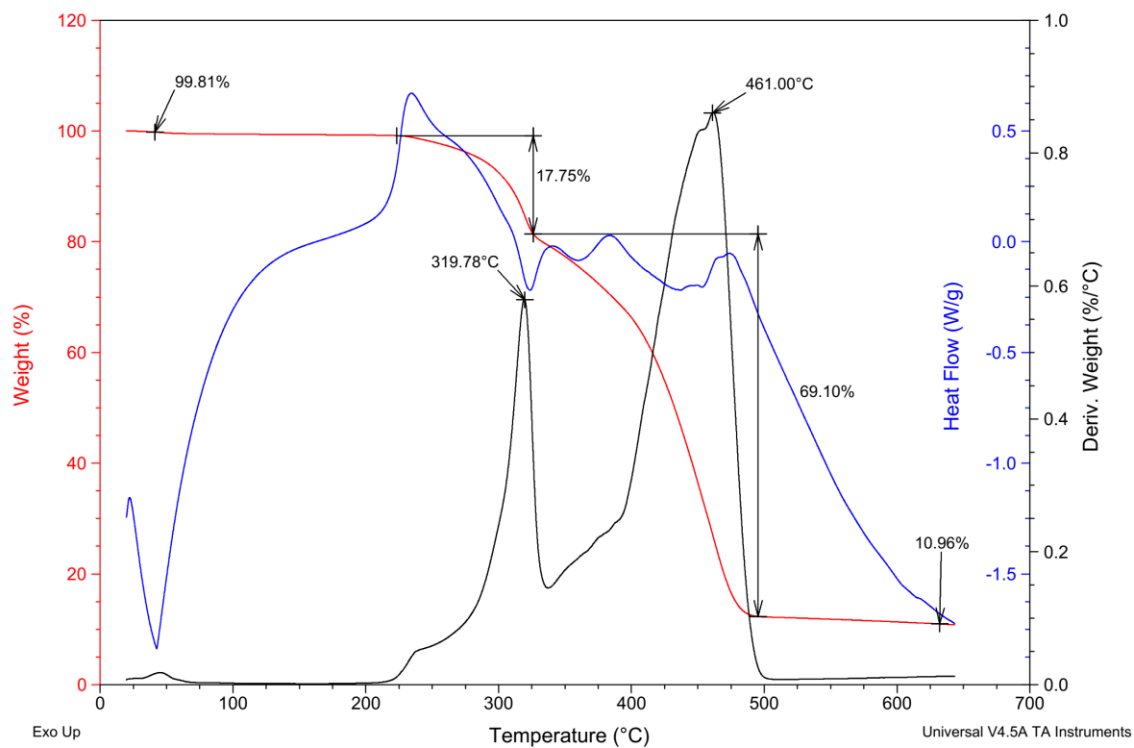


Figure A1. TGA and DSC data for TEMPOImIL with $n = 4$, $R = H$.

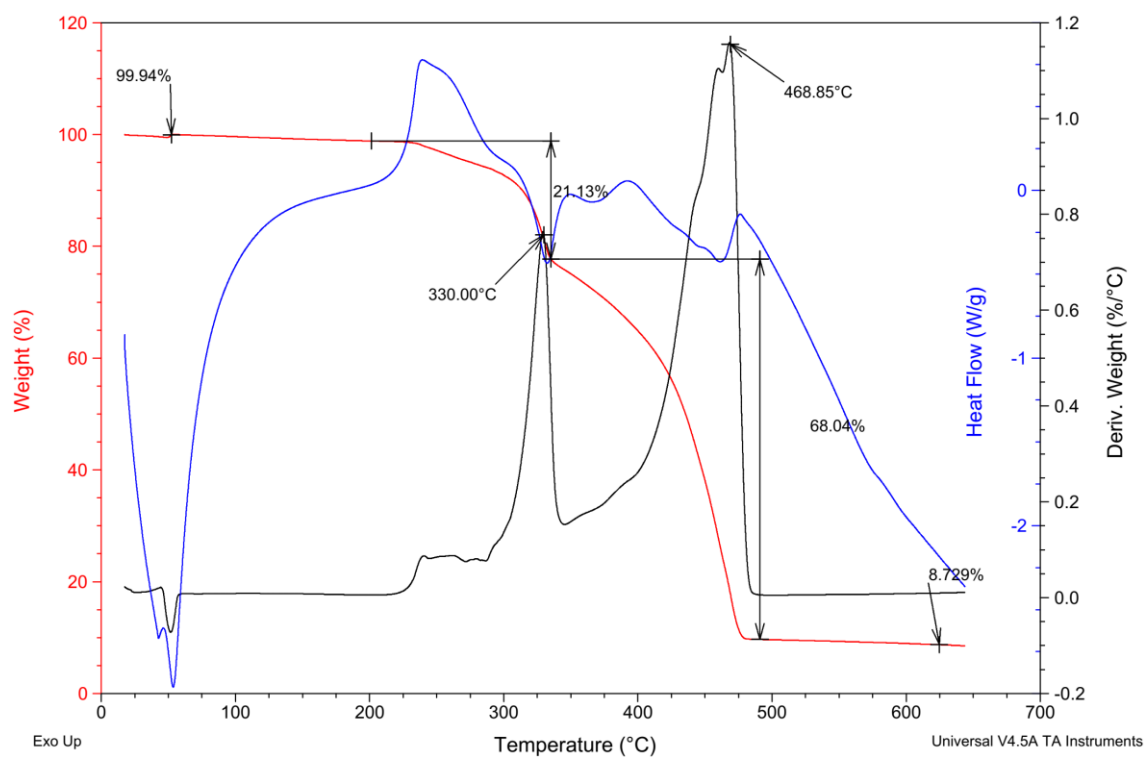


Figure A2. TGA and DSC data for TEMPOImIL with $n = 4$, $R = \text{Me}$.

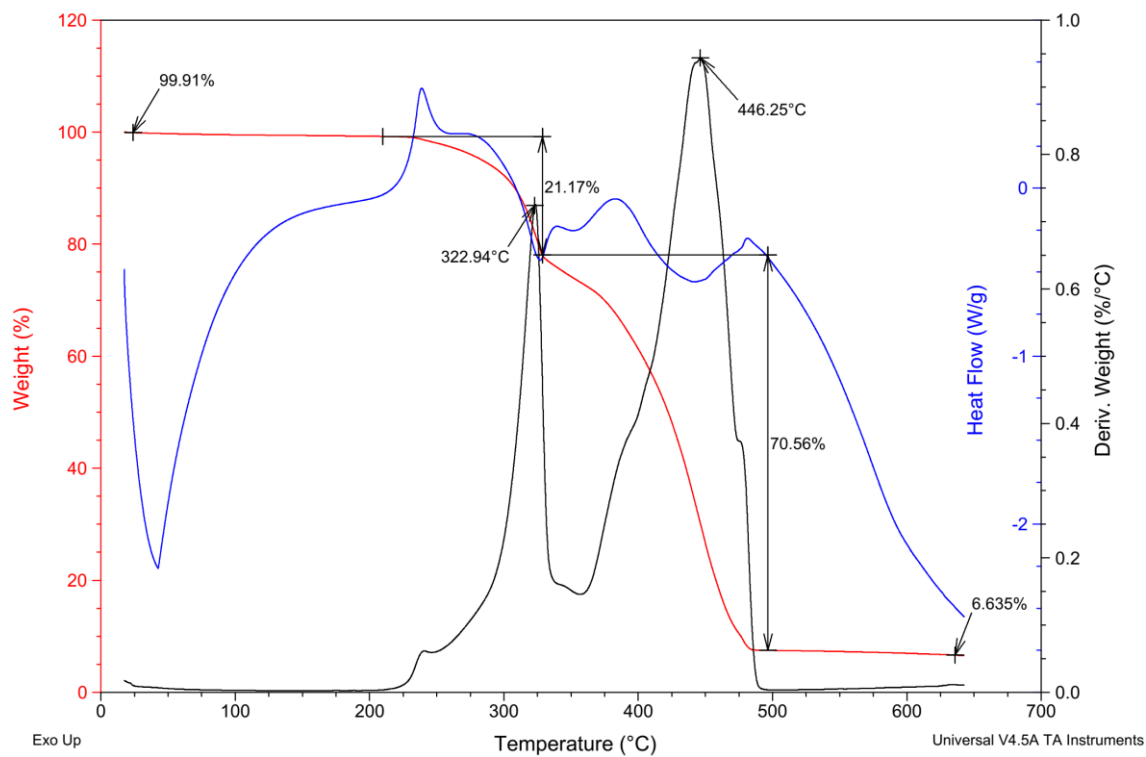


Figure A3. TGA and DSC data for TEMPOImIL with $n = 5$, $R = \text{H}$.

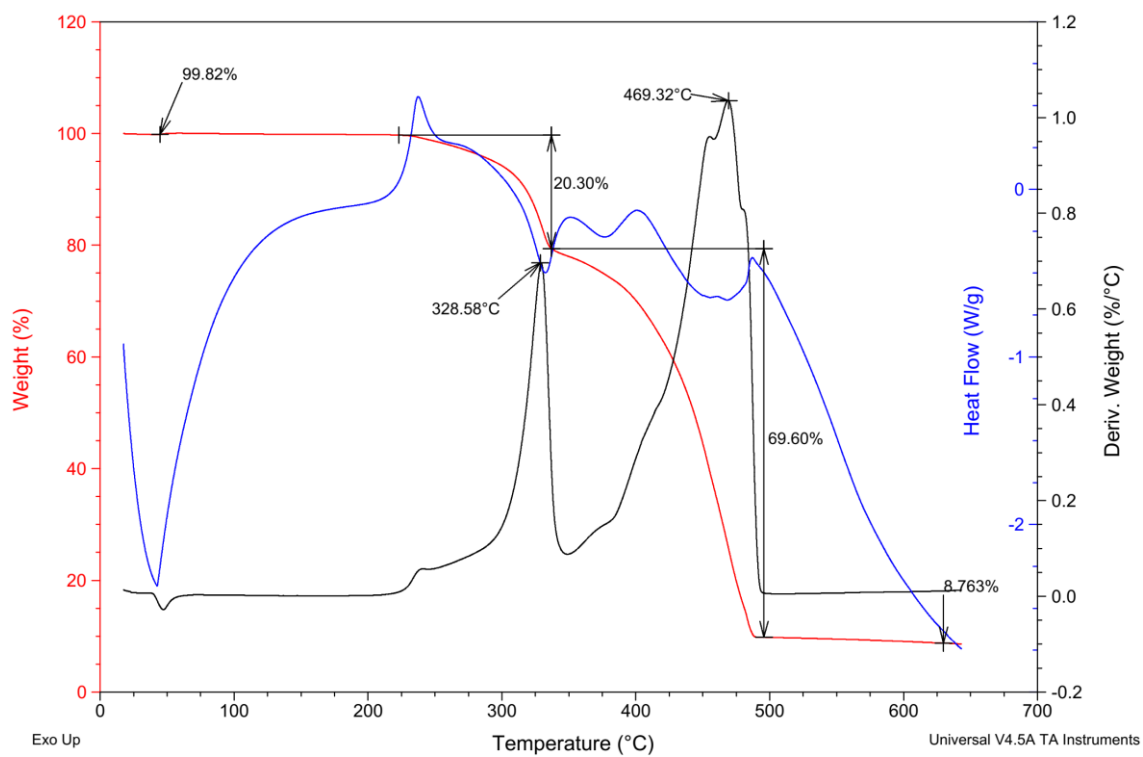


Figure A4. TGA and DSC data for TEMPOImIL with $n = 5$, $R = \text{Me}$.

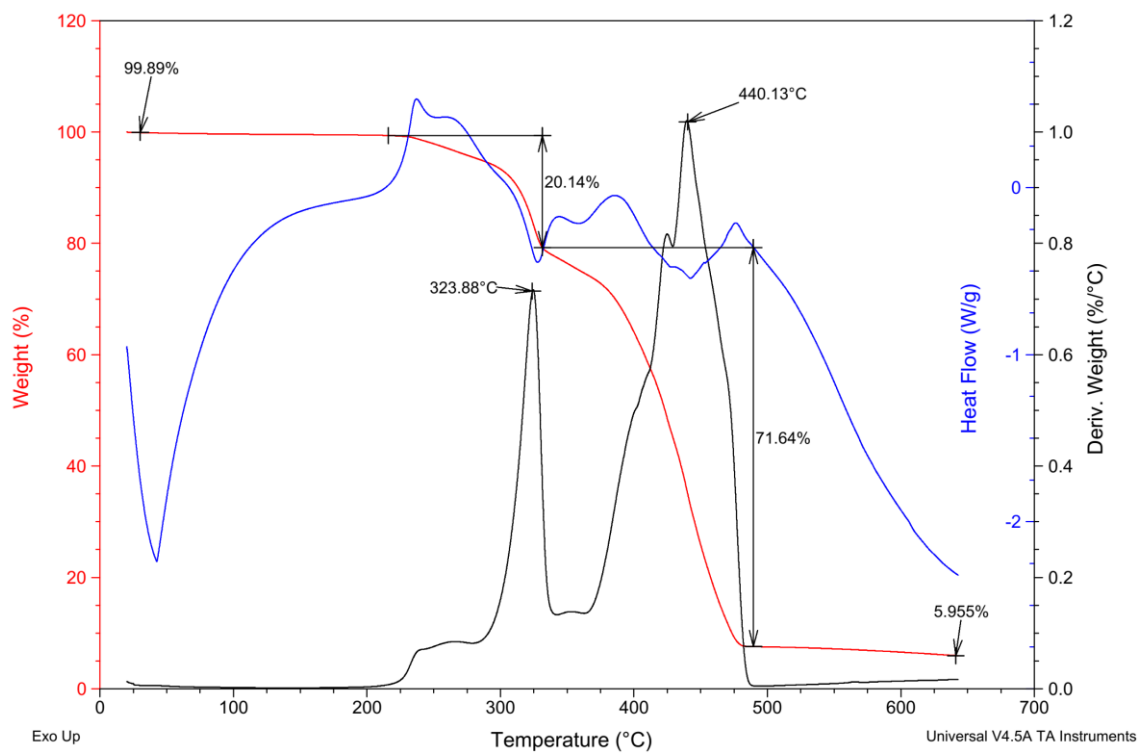


Figure A5. TGA and DSC data for TEMPOImIL with $n = 6$, $R = \text{H}$.

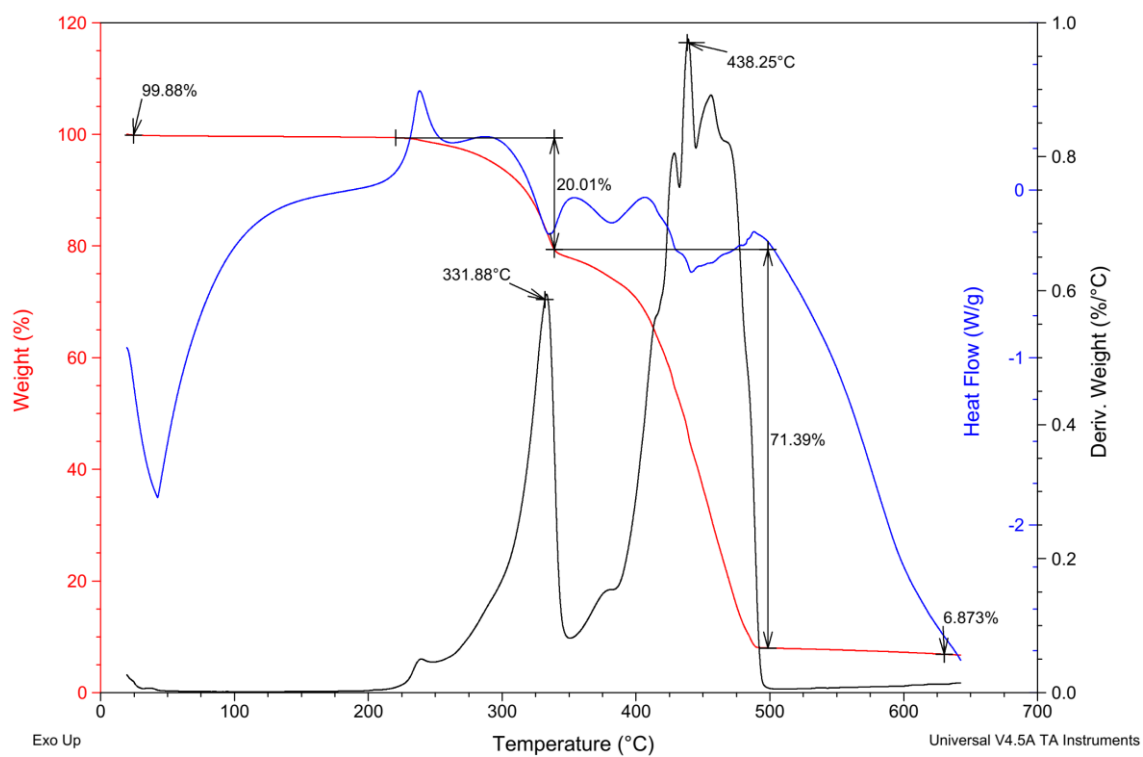


Figure A6. TGA and DSC data for TEMPOImIL with $n = 6$, $R = \text{Me}$.

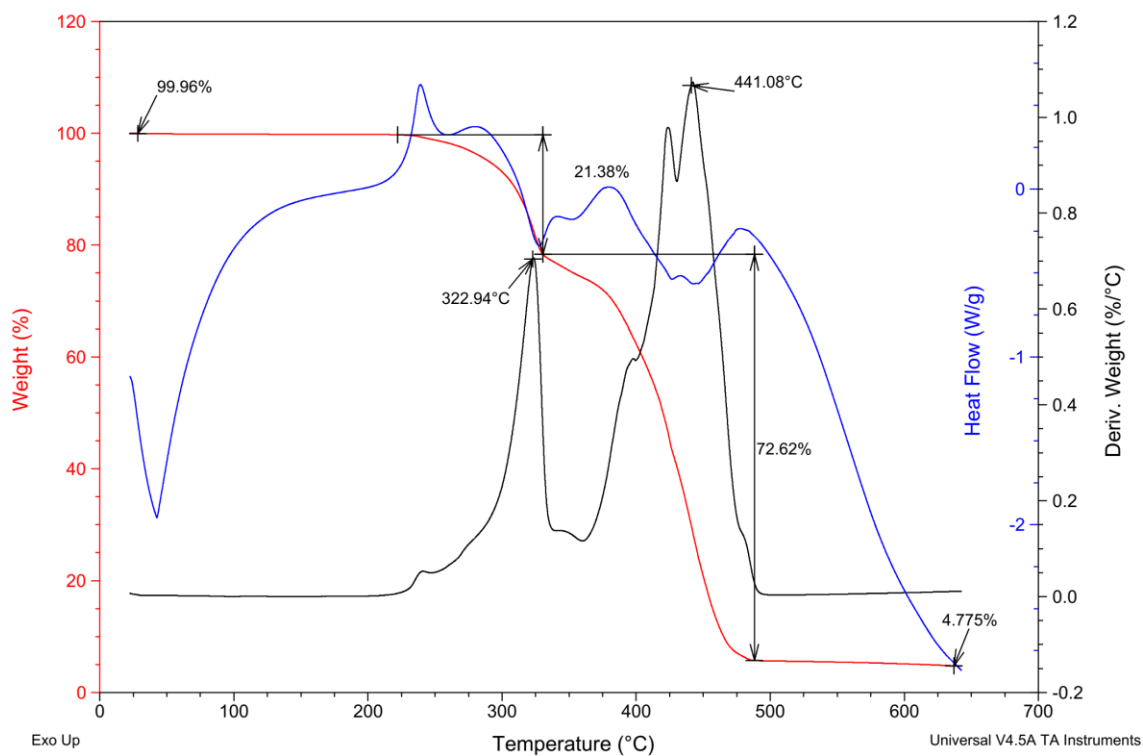


Figure A7. TGA and DSC data for TEMPOImIL with $n = 7$, $R = \text{H}$.

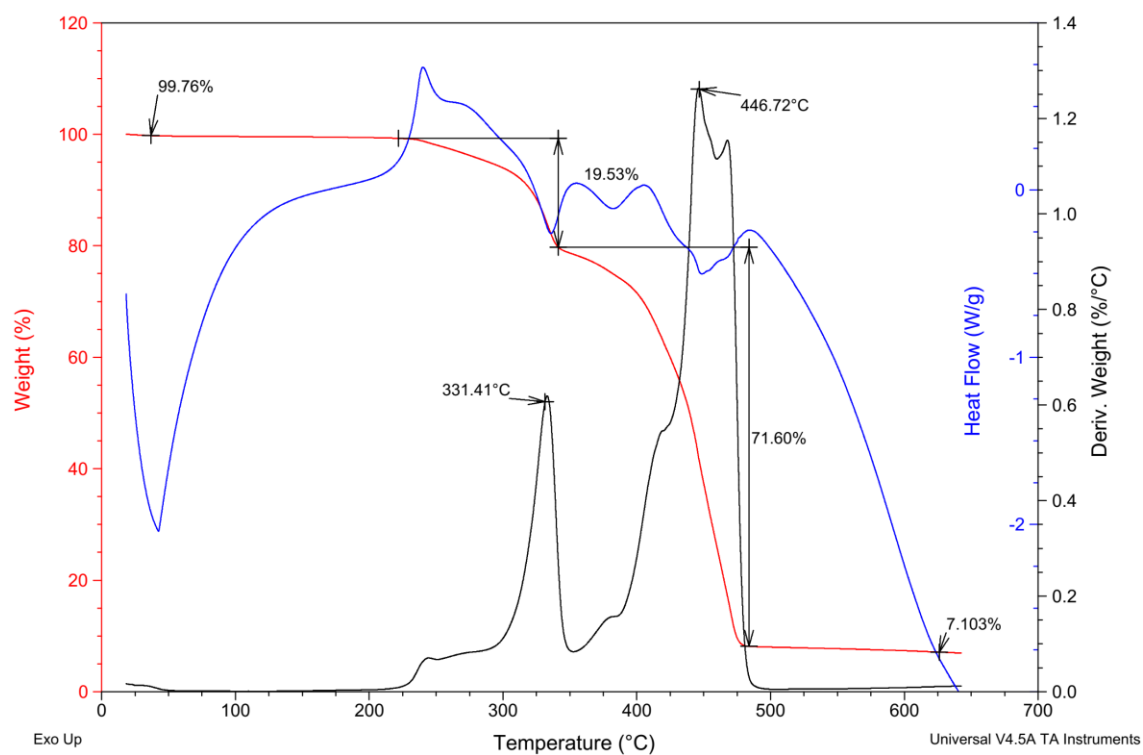


Figure A8. TGA and DSC data for TEMPOImIL with $n = 7$, $R = \text{Me}$.

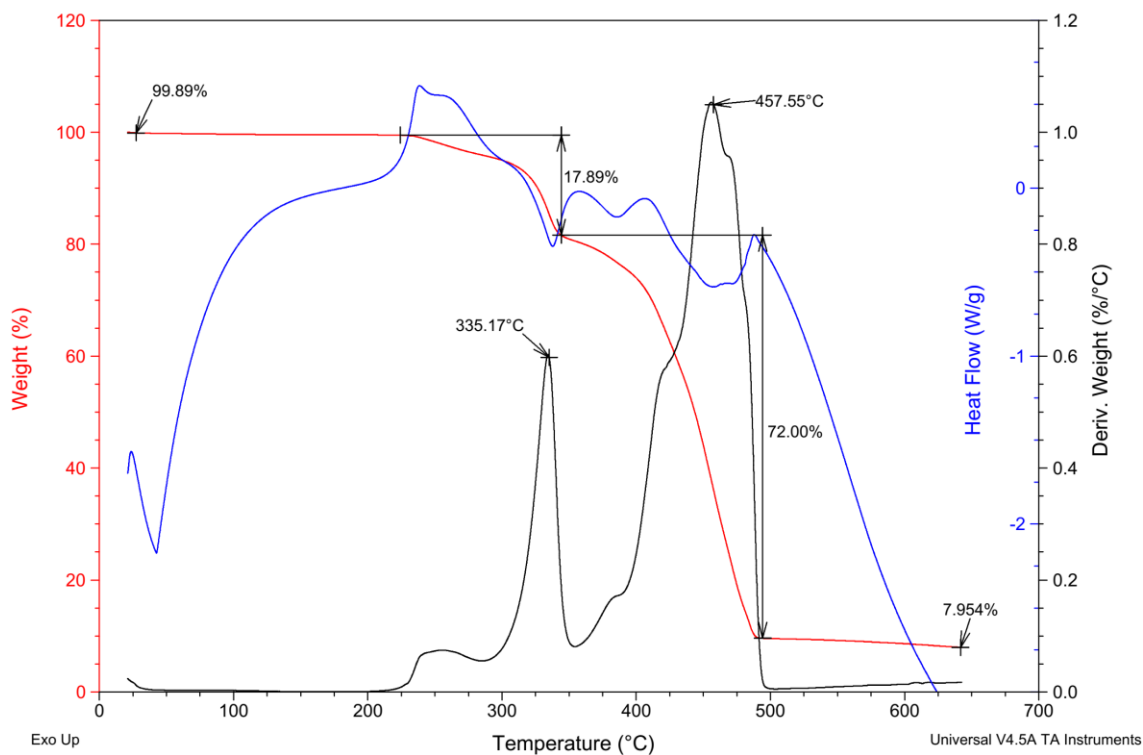


Figure A9. TGA and DSC data for TEMPOImIL with $n = 8$, $R = \text{Me}$.

A.2. An Investigation of Methylated Ferrocenes as RMs for Li-O₂ Batteries

A.2.1. Introduction

Ferrocene (Fc) has been previously investigated as a charging RM for Li-O₂ batteries with the work published by Bruce *et al* 2012.¹⁷⁶ Even though the redox potential for the oxidation of Fc is within the suitable range (3.6 V vs. Li/Li⁺, Chapter 1.2.3), the compound is unstable in the presence of oxygen. The instability of Fc and other metallocenes undergoing redox processes in an oxygen atmosphere is related to the formation of dimers where oxygen atoms form bridges between the cyclopentadienyl rings.²²⁶⁻²²⁷ Thus, Fc is not a particularly suitable RM for use in Li-O₂ batteries.

Octa- and decamethylferrocenes (OMeFc and DMeFc) are more kinetically stable in oxygen due to steric hindrance created by the methyl substituents. The introduction of electron donating methyl groups also lowers the redox potentials in comparison with Fc²²⁸⁻²²⁹ making OMeFc and DMeFc more favourable candidates for Li-O₂ batteries. With these considerations in mind, the effect of introducing OMeFc and DMeFc as electrocatalysts in Li-O₂ batteries on the discharge and charge capacities and on the associated overpotentials was investigated.

A.2.2. Results and Discussion

The catalytic action of OMeFc and DMeFc was investigated by assembling Li-O₂ batteries with Li metal anodes, glass fibre separators and 0.01 M solutions of the compounds in LiTFSI/DEGDME electrolyte. For OMeFc, carbon paper (CP) cathodes were used. CP allows clear visualisation of the discharge product. Data recorded for experiments conducted with and without RM under Ar and O₂ atmospheres are shown in

Figure A10. The charge capacities of the batteries with 0.01 M OMeFc in argon and oxygen are almost identical. Clearly, OMeFc is not a suitable RM for Li-O₂ batteries, as it not only decreases the discharge capacity but also contributes to the charge capacity of the battery, which indicates that the compound is acting as a redox shuttle instead of catalysing the decomposition or formation of Li₂O₂.

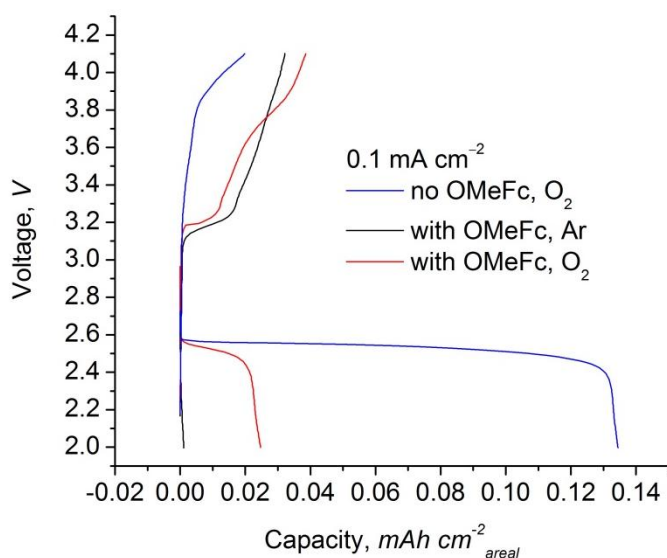


Figure A10. Full discharge/charge curves of the Li-O₂ batteries with pure LiTFSI/DEGDME electrolyte (“no OMeFc”) and 0.01 M OMeFc in LiTFSI/DEGDME electrolyte.

For the experiments with DMeFc, carbon black (CB) cathodes were used and the current density was 1 mA h cm⁻² to enable rapid screening (Fig. A11). The capacity of the battery commonly decreases with increasing current density, which was observed on the discharge/charge curves. Unlike OMeFc, DMeFc provided only a small capacity under an argon atmosphere, which indicates that it does not act as a redox shuttle. DMeFc had a noticeable effect on the OER with the charge potential lower by up to 0.3 V at the beginning of the charging process and the charge capacity four times greater in the batteries

with the RM compared to those without within the chosen voltage range. The discharge capacity was twice lower in the batteries containing the RM compared to those without, which has been observed in batteries with other charging RMs (Section 3.6) and might be improved by the addition of a discharging RM.

A battery with DMeFc added only to the cathode (50 μL) and pure LiTFSI/DEGDME electrolyte added on the separator (100 μL) had a similar performance to the battery without the RM. It is likely that diffusion of the RM occurred over time, and the overall concentration of DMeFc in the bulk electrolyte was too low to have any effect on the OER.

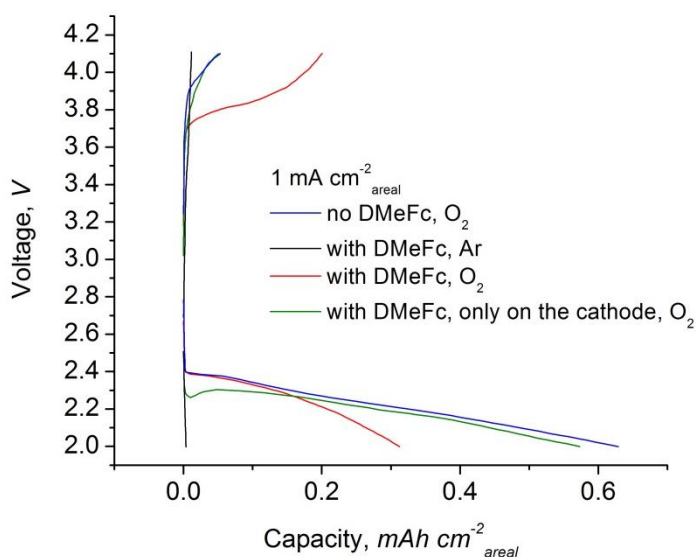


Figure A11. Full discharge/charge curves of the Li-O₂ batteries with pure LiTFSI/DEGDME electrolyte (“no DMeFc”), 0.01 M DMeFc in LiTFSI/DEGDME electrolyte, and a mixture of both.

A.2.3. Summary

Octa- and decamethylferrocene (OMeFc and DMeFc) were tested as RMs for Li-O₂ batteries. Galvanostatic cycling tests of the batteries with these compounds showed that

OMeFc is unsuitable as it significantly contributes to the charge capacity of the battery. This was not the case for DMeFc, which provided a decrease of the charge overpotential. Further studies are required to confirm that DMeFc can be used as a charging RM, such as SEM, XRD of the cathodes, and CV tests to check the redox potentials in the chosen electrolyte.

References

1. Ellis, B. L.; Lee, K. T.; Nazar, L. F., Positive Electrode Materials for Li-Ion and Li-Batteries. *Chemistry of Materials* **2010**, *22* (3), 691-714.
2. *Encyclopedia of Electrochemical Power Sources*. Elsevier Science & Technology: 2009; p 4538.
3. Herrmann, F.; Rothfuss, F., Introduction to hybrid electric vehicles, battery electric vehicles, and off-road electric vehicles. In *Advances in Battery Technologies for Electric Vehicles*, Scrosati, B.; Garche, J.; Tillmetz, W., Eds. Woodhead Publishing Ltd: Cambridge, United Kingdom, 2015; pp 3-16.
4. Gandoman, F. H.; Jaguemont, J.; Goutam, S.; Gopalakrishnan, R.; Firouz, Y.; Kalogiannis, T.; Omar, N.; Van Mierlo, J., Concept of reliability and safety assessment of lithium-ion batteries in electric vehicles: Basics, progress, and challenges. *Applied Energy* **2019**, *251*, 113343.
5. Young, K.; Wang, C.; Wang, L. Y.; Strunz, K., Electric Vehicle Battery Technologies. In *Electric Vehicle Integration into Modern Power Networks*, 2013; pp 15-56.
6. Yamamoto, O., Introduction. In *The Lithium Air Battery: Fundamentals*, Imanishi, N.; Luntz, A. C.; Bruce, P. G., Eds. Springer Science+Business Media: New York, 2014; pp 1-21.
7. Cao, Y.; Lu, H.; Hong, Q.; Xu, B.; Wang, J.; Deng, Y.; Yang, W.; Cai, W., Synthesis of Ag/Co@CoO NPs anchored within N-doped hierarchical porous hollow carbon nanofibers as a superior free-standing cathode for Li-O₂ batteries. *Carbon* **2019**, *144*, 280-288.
8. Surya, K.; Michael, M. S.; Prabakaran, S. R. S., A review on advancement in non-noble metal based oxides as bifunctional catalysts for rechargeable non-aqueous Li/air battery. *Solid State Ionics* **2018**, *317*, 89-96.
9. Feng, N.; He, P.; Zhou, H., Critical Challenges in Rechargeable Aprotic Li-O₂ Batteries. *Advanced Energy Materials* **2016**, *6* (9), 1502303.
10. Lim, H.-D.; Lee, B.; Zheng, Y.; Hong, J.; Kim, J.; Gwon, H.; Ko, Y.; Lee, M.; Cho, K.; Kang, K., Rational design of redox mediators for advanced Li-O₂ batteries. *Nature Energy* **2016**, *1* (6), 16066.
11. Francia, C.; Amici, J.; Tasarkuyu, E.; Çoşkun, A.; Gül, Ö. F.; Şener, T., What do we need for the lithium-air batteries: A promoter or a catalyst? *International Journal of Hydrogen Energy* **2016**, *41* (45), 20583-20591.
12. Choudhury, S.; Wan, C. T.-C.; Al Sadat, W. I.; Tu, Z.; Lau, S.; Zachman, M. J.; Kourkoutis, L. F.; Archer, L. A., Designer interphases for the lithium-oxygen electrochemical cell. *Science Advances* **2017**, *3* (4), e1602809.
13. Yi, J.; Guo, S.; He, P.; Zhou, H., Status and prospects of polymer electrolytes for solid-state Li-O₂ (air) batteries. *Energy & Environmental Science* **2017**, *10* (4), 860-884.
14. Linden, D.; Reddy, T. B., *Handbook of batteries*. McGraw-Hill Companies, Inc.: US, New York, 2001; p 1456.
15. Crompton, T. R., Introduction to battery technology. In *Battery Reference Book*, 3rd ed.; Newnes: Great Britain, Oxford, 2000; pp 3-28.
16. *Handbook of Reference Electrodes*. Inzelt, G.; Lewenstam, A.; Scholz, F., Eds. Springer Berlin Heidelberg: 2013.
17. Goldman, J. L. Directed Lithium Transport in High Capacity Lithium-Ion Battery Electrodes. Dissertation, Urbana, Illinois, 2014.
18. Bruce, P. G.; Freunberger, S. A.; Hardwick, L. J.; Tarascon, J. M., Li-O₂ and Li-S batteries with high energy storage. *Nature Materials* **2011**, *11* (1), 19-29.

19. Lu, J.; Li, L.; Park, J. B.; Sun, Y. K.; Wu, F.; Amine, K., Aprotic and aqueous Li-O₂ batteries. *Chemical Reviews* **2014**, *114* (11), 5611-5640.
20. Shao, Y.; Ding, F.; Xiao, J.; Zhang, J.; Xu, W.; Park, S.; Zhang, J.-G.; Wang, Y.; Liu, J., Making Li-Air Batteries Rechargeable: Material Challenges. *Advanced Functional Materials* **2013**, *23* (8), 987-1004.
21. Grande, L.; Paillard, E.; Hassoun, J.; Park, J. B.; Lee, Y. J.; Sun, Y. K.; Passerini, S.; Scrosati, B., The lithium/air battery: still an emerging system or a practical reality? *Advanced Materials* **2015**, *27* (5), 784-800.
22. Littauer, E. L.; Tsai, K. C., Corrosion of Lithium in Alkaline Solution. *Journal of The Electrochemical Society* **1977**, *124* (6), 850-855.
23. Blurton, K. F.; Sammels, A. F., Metal/air batteries: their status and potential - a review. *Journal of Power Sources* **1979**, *4*, 263-279.
24. Balaish, M.; Kraytsberg, A.; Ein-Eli, Y., A critical review on lithium-air battery electrolytes. *Physical Chemistry Chemical Physics* **2014**, *16* (7), 2801-2822.
25. *Metal-Air Batteries. Fundamentals and Applications*. Wiley-VCH: Weinheim, Germany, 2018.
26. Kumar, B.; Kumar, J.; Leese, R.; Fellner, J. P.; Rodrigues, S. J.; Abraham, K. M., A Solid-State, Rechargeable, Long Cycle Life Lithium-Air Battery. *Journal of The Electrochemical Society* **2010**, *157* (1), A50.
27. Girishkumar, G.; McCloskey, B.; Luntz, A. C.; Swanson, S.; Wilcke, W., Lithium-Air Battery: Promise and Challenges. *The Journal of Physical Chemistry Letters* **2010**, (1), 2193-2203.
28. Das, U.; Lau, K. C.; Redfern, P. C.; Curtiss, L. A., Structure and Stability of Lithium Superoxide Clusters and Relevance to Li-O₂ Batteries. *The Journal of Physical Chemistry Letters* **2014**, *5* (5), 813-819.
29. He, P.; Zhang, T.; Jiang, J.; Zhou, H., Lithium-Air Batteries with Hybrid Electrolytes. *The Journal of Physical Chemistry Letters* **2016**, *7* (7), 1267-1280.
30. Lu, J.; Lee, Y. J.; Luo, X.; Lau, K. C.; Asadi, M.; Wang, H. H.; Brombosz, S.; Wen, J.; Zhai, D.; Chen, Z.; Miller, D. J.; Jeong, Y. S.; Park, J. B.; Fang, Z. Z.; Kumar, B.; Salehi-Khojin, A.; Sun, Y. K.; Curtiss, L. A.; Amine, K., A lithium-oxygen battery based on lithium superoxide. *Nature* **2016**, *529* (7586), 377-382.
31. Papp, J. K.; Forster, J. D.; Burke, C. M.; Kim, H. W.; Luntz, A. C.; Shelby, R. M.; Urban, J. J.; McCloskey, B. D., Poly(vinylidene fluoride) (PVDF) Binder Degradation in Li-O₂ Batteries: A Consideration for the Characterization of Lithium Superoxide. *The Journal of Physical Chemistry Letters* **2017**, 1169-1174.
32. Christensen, J.; Albertus, P.; Sanchez-Carrera, R. S.; Lohmann, T.; Kozinsky, B.; Liedtke, R.; Ahmed, J.; Kojic, A., A Critical Review of Li/Air Batteries. *Journal of The Electrochemical Society* **2011**, *159* (2), R1-R30.
33. Ye, L.; Lv, W.; Cui, J.; Liang, Y.; Wu, P.; Wang, X.; He, H.; Lin, S.; Wang, W.; Dickerson, J. H.; He, W., Lithium-Air Batteries: Performance Interplays with Instability Factors. *ChemElectroChem* **2015**, *2* (3), 312-323.
34. Lim, H. D.; Lee, B.; Bae, Y.; Park, H.; Ko, Y.; Kim, H.; Kim, J.; Kang, K., Reaction chemistry in rechargeable Li-O₂ batteries. *Chemical Society Reviews* **2017**, *46* (10), 2873-2888.
35. Yao, X.; Dong, Q.; Cheng, Q.; Wang, D., Why Do Lithium-Oxygen Batteries Fail: Parasitic Chemical Reactions and Their Synergistic Effect. *Angewandte Chemie International Edition* **2016**, *55* (38), 11344-11353.
36. Ling, C.; Zhang, R.; Takechi, K.; Mizuno, F., Intrinsic Barrier to Electrochemically Decompose Li₂CO₃ and LiOH. *The Journal of Physical Chemistry C* **2014**, *118* (46), 26591-26598.

37. Gallagher, K. G.; Goebel, S.; Greszler, T.; Mathias, M.; Oelerich, W.; Eroglu, D.; Srinivasan, V., Quantifying the promise of lithium–air batteries for electric vehicles. *Energy & Environmental Science* **2014**, 7 (5), 1555-1563.
38. Giordani, V.; Tozier, D.; Tan, H.; Burke, C. M.; Gallant, B. M.; Uddin, J.; Greer, J. R.; McCloskey, B. D.; Chase, G. V.; Addison, D., A Molten Salt Lithium-Oxygen Battery. *Journal of the American Chemical Society* **2016**, 138 (8), 2656-2663.
39. Chang, Z.-w.; Xu, J.-j.; Liu, Q.-c.; Li, L.; Zhang, X.-b., Recent Progress on Stability Enhancement for Cathode in Rechargeable Non-Aqueous Lithium-Oxygen Battery. *Advanced Energy Materials* **2015**, 5 (21), 1500633.
40. Aetukuri, N. B.; McCloskey, B. D.; Garcia, J. M.; Krupp, L. E.; Viswanathan, V.; Luntz, A. C., Solvating additives drive solution-mediated electrochemistry and enhance toroid growth in non-aqueous Li-O₂ batteries. *Nature Chemistry* **2015**, 7 (1), 50-56.
41. Wu, S.; Tang, J.; Li, F.; Liu, X.; Yamauchi, Y.; Ishida, M.; Zhou, H., A Synergistic System for Lithium-Oxygen Batteries in Humid Atmosphere Integrating a Composite Cathode and a Hydrophobic Ionic Liquid-Based Electrolyte. *Advanced Functional Materials* **2016**, 26 (19), 3291-3298.
42. Guo, Z.; Dong, X.; Yuan, S.; Wang, Y.; Xia, Y., Humidity effect on electrochemical performance of Li–O₂ batteries. *Journal of Power Sources* **2014**, 264, 1-7.
43. Li, F.; Wu, S.; Li, D.; Zhang, T.; He, P.; Yamada, A.; Zhou, H., The water catalysis at oxygen cathodes of lithium-oxygen cells. *Nature Communications* **2015**, 6, 7843.
44. Liu, T.; Leskes, M.; Yu, W.; Moore, A. J.; Zhou, L.; Bayley, P. M.; Kim, G.; Grey, C. P., Cycling Li-O₂ batteries via LiOH formation and decomposition. *Science* **2015**, 350 (6260), 530-533.
45. Wu, S.; Tang, J.; Li, F.; Liu, X.; Zhou, H., Low charge overpotentials in lithium-oxygen batteries based on tetraglyme electrolytes with a limited amount of water. *Chemical Communications* **2015**, 51 (94), 16860-16863.
46. Schwenke, K. U.; Metzger, M.; Restle, T.; Piana, M.; Gasteiger, H. A., The Influence of Water and Protons on Li₂O₂ Crystal Growth in Aprotic Li-O₂ Cells. *Journal of The Electrochemical Society* **2015**, 162 (4), A573-A584.
47. Dai, A.; Li, Q.; Liu, T.; Amine, K.; Lu, J., Fundamental Understanding of Water-Induced Mechanisms in Li-O₂ Batteries: Recent Developments and Perspectives. *Advanced Materials* **2018**, e1805602.
48. Huang, Z.; Zeng, H.; Xie, M.; Lin, X.; Huang, Z.; Shen, Y.; Huang, Y., A Stable Lithium-Oxygen Battery Electrolyte Based on Fully Methylated Cyclic Ether. *Angewandte Chemie International Edition* **2019**, 58 (8), 2345-2349.
49. Wang, Y.; Zhong, W.-H., Development of Electrolytes towards Achieving Safe and High-Performance Energy-Storage Devices: A Review. *ChemElectroChem* **2015**, 2 (1), 22-36.
50. Nasybulin, E.; Xu, W.; Engelhard, M. H.; Nie, Z.; Burton, S. D.; Cosimbescu, L.; Gross, M. E.; Zhang, J.-G., Effects of Electrolyte Salts on the Performance of Li–O₂ Batteries. *The Journal of Physical Chemistry C* **2013**, 117 (6), 2635-2645.
51. Younesi, R.; Veith, G. M.; Johansson, P.; Edström, K.; Vegge, T., Lithium salts for advanced lithium batteries: Li–metal, Li–O₂, and Li–S. *Energy & Environmental Science* **2015**, 8 (7), 1905-1922.
52. Tong, B.; Huang, J.; Zhou, Z.; Peng, Z., The Salt Matters: Enhanced Reversibility of Li-O₂ Batteries with a Li[(CF₃SO₂)(n-C₄F₉SO₂)N]-Based Electrolyte. *Advanced Materials* **2018**, 30 (1), 1704841.
53. Tikekar, M. D.; Choudhury, S.; Tu, Z.; Archer, L. A., Design principles for electrolytes and interfaces for stable lithium-metal batteries. *Nature Energy* **2016**, 1 (9), 1-7.

54. Das, S. K.; Xu, S.; Emwas, A.-H.; Lu, Y. Y.; Srivastava, S.; Archer, L. A., High energy lithium–oxygen batteries – transport barriers and thermodynamics. *Energy & Environmental Science* **2012**, 5 (10), 8927.
55. Zhang, T.; Wen, Z.-Y., A High-Rate Ionic Liquid Lithium-O₂ Battery with LiOH Product. *The Journal of Physical Chemistry C* **2017**, 121 (11), 5968-5973.
56. Kwon, H. M.; Thomas, M. L.; Tatara, R.; Oda, Y.; Kobayashi, Y.; Nakanishi, A.; Ueno, K.; Dokko, K.; Watanabe, M., Stability of Glyme Solvate Ionic Liquid as an Electrolyte for Rechargeable Li-O₂ Batteries. *ACS Applied Materials & Interfaces* **2017**, 9 (7), 6014-6021.
57. Jung, K. N.; Lee, J. I.; Jung, J. H.; Shin, K. H.; Lee, J. W., A quasi-solid-state rechargeable lithium-oxygen battery based on a gel polymer electrolyte with an ionic liquid. *Chemical Communications* **2014**, 50 (41), 5458-5461.
58. Asadi, M.; Sayahpour, B.; Abbasi, P.; Ngo, A. T.; Karis, K.; Jokisaari, J. R.; Liu, C.; Narayanan, B.; Gerard, M.; Yasaei, P.; Hu, X.; Mukherjee, A.; Lau, K. C.; Assary, R. S.; Khalili-Araghi, F.; Klie, R. F.; Curtiss, L. A.; Salehi-Khojin, A., A lithium-oxygen battery with a long cycle life in an air-like atmosphere. *Nature* **2018**, 555 (7697), 502-506.
59. He, P.; Zhang, T.; Jiang, J.; Zhou, H., Lithium-Air Batteries with Hybrid Electrolytes. *The Journal of Physical Chemistry Letters* **2016**, 7, 1267-80.
60. Zhang, T.; Imanishi, N.; Takeda, Y.; Yamamoto, O., Aqueous Lithium/Air Rechargeable Batteries. *Chemistry Letters* **2011**, 40 (7), 668-673.
61. Wang, Y.; Zhou, H., A lithium-air battery with a potential to continuously reduce O₂ from air for delivering energy. *Journal of Power Sources* **2010**, 195 (1), 358-361.
62. Zhang, T.; Imanishi, N.; Shimonishi, Y.; Hirano, A.; Takeda, Y.; Yamamoto, O.; Sammes, N., A novel high energy density rechargeable lithium/air battery. *Chemical Communications* **2010**, 46 (10), 1661-1663.
63. Nong, J.; Xie, P.; Zhu, A. S.; Rong, M. Z.; Zhang, M. Q., Highly conductive doped carbon framework as binder-free cathode for hybrid Li-O₂ battery. *Carbon* **2019**, 142, 177-189.
64. Manthiram, A.; Li, L., Hybrid and Aqueous Lithium-Air Batteries. *Advanced Energy Materials* **2015**, 5 (4), 1401302.
65. Kim, B. G.; Kim, J.-S.; Min, J.; Lee, Y.-H.; Choi, J. H.; Jang, M. C.; Freunberger, S. A.; Choi, J. W., A Moisture- and Oxygen-Impermeable Separator for Aprotic Li-O₂ Batteries. *Advanced Functional Materials* **2016**, 26 (11), 1747-1756.
66. Matsui, M.; Wada, A.; Matsuda, Y.; Yamamoto, O.; Takeda, Y.; Imanishi, N., A novel aqueous lithium-oxygen cell based on the oxygen-peroxide redox couple. *Chemical Communications* **2015**, 51 (15), 3189-3192.
67. Qiao, Y.; Wu, S.; Yi, J.; Sun, Y.; Guo, S.; Yang, S.; He, P.; Zhou, H., From O₂⁻ to HO₂⁻: Reducing By-Products and Overpotential in Li-O₂ Batteries by Water Addition. *Angewandte Chemie International Edition* **2017**, 56 (18), 4960-4964.
68. Sunahiro, S.; Matsui, M.; Takeda, Y.; Yamamoto, O.; Imanishi, N., Rechargeable aqueous lithium–air batteries with an auxiliary electrode for the oxygen evolution. *Journal of Power Sources* **2014**, 262, 338-343.
69. Zhou, D.; Shanmukaraj, D.; Tkacheva, A.; Armand, M.; Wang, G., Polymer Electrolytes for Lithium-Based Batteries: Advances and Prospects. *Chem* **2019**, 5, 1-27.
70. Li, F.; Kitaura, H.; Zhou, H., The pursuit of rechargeable solid-state Li–air batteries. *Energy & Environmental Science* **2013**, 6 (8), 2302.
71. Bachman, J. C.; Muy, S.; Grimaud, A.; Chang, H. H.; Pour, N.; Lux, S. F.; Paschos, O.; Maglia, F.; Lupart, S.; Lamp, P.; Giordano, L.; Shao-Horn, Y., Inorganic Solid-State Electrolytes for Lithium

Batteries: Mechanisms and Properties Governing Ion Conduction. *Chemical Reviews* **2016**, *116* (1), 140-162.

72. Kitaura, H.; Zhou, H., Reaction and degradation mechanism in all-solid-state lithium-air batteries. *Chemical Communications* **2015**, *51* (99), 17560-17563.
73. Lu, Y.-C.; Crumlin, E. J.; Carney, T. J.; Baggetto, L.; Veith, G. M.; Dudney, N. J.; Liu, Z.; Shao-Horn, Y., Influence of Hydrocarbon and CO₂ on the Reversibility of Li–O₂ Chemistry Using In Situ Ambient Pressure X-ray Photoelectron Spectroscopy. *The Journal of Physical Chemistry C* **2013**, *117* (49), 25948-25954.
74. Hassoun, J.; Croce, F.; Armand, M.; Scrosati, B., Investigation of the O₂ electrochemistry in a polymer electrolyte solid-state cell. *Angewandte Chemie International Edition* **2011**, *50* (13), 2999-3002.
75. Balaish, M.; Peled, E.; Golodnitsky, D.; Ein-Eli, Y., Liquid-Free Lithium-Oxygen Batteries. *Angewandte Chemie International Edition* **2015**, *127* (2), 446-450.
76. Bonnet-Mercier, N.; Wong, R. A.; Thomas, M. L.; Dutta, A.; Yamanaka, K.; Yogi, C.; Ohta, T.; Byon, H. R., A structured three-dimensional polymer electrolyte with enlarged active reaction zone for Li–O₂ batteries. *Scientific Reports* **2014**, *4*, 7127.
77. Cheng, H.; Scott, K., Improving performance of rechargeable Li-air batteries from using Li-Nafion® binder. *Electrochimica Acta* **2014**, *116*, 51-58.
78. Noor, I. S.; Majid, S. R.; Arof, A. K., Poly(vinyl alcohol)–LiBOB complexes for lithium–air cells. *Electrochimica Acta* **2013**, *102*, 149-160.
79. Balaish, M.; Peled, E.; Golodnitsky, D.; Ein-Eli, Y., Liquid-free lithium-oxygen batteries. *Angewandte Chemie International Edition* **2015**, *54* (2), 436-440.
80. Amanchukwu, C. V.; Harding, J. R.; Shao-Horn, Y.; Hammond, P. T., Understanding the Chemical Stability of Polymers for Lithium–Air Batteries. *Chemistry of Materials* **2015**, *27* (2), 550-561.
81. Nasybulin, E.; Xu, W.; Engelhard, M. H.; Nie, Z.; Li, X. S.; Zhang, J.-G., Stability of polymer binders in Li–O₂ batteries. *Journal of Power Sources* **2013**, *243*, 899-907.
82. Yi, J.; Wu, S.; Bai, S.; Liu, Y.; Lia, N.; Zhou, H., Interfacial construction of Li₂O₂ for a performance improved polymer Li–O₂ battery. *Journal of Materials Chemistry A* **2016**, *4*, 2403-2407.
83. Croce, F.; Appetecchi, G. B.; Persi, L.; Scrosati, B., Nanocomposite polymer electrolytes for lithium batteries. *Nature* **1998**, *395*, 456-458.
84. Liu, S.; Imanishi, N.; Zhang, T.; Hirano, A.; Takeda, Y.; Yamamoto, O.; Yang, J., Effect of nano-silica filler in polymer electrolyte on Li dendrite formation in Li/poly(ethylene oxide)–Li(CF₃SO₂)₂N/Li. *Journal of Power Sources* **2010**, *195* (19), 6847-6853.
85. Luo, W. B.; Chou, S. L.; Wang, J. Z.; Kang, Y. M.; Zhai, Y. C.; Liu, H. K., A hybrid gel-solid-state polymer electrolyte for long-life lithium oxygen batteries. *Chemical Communications* **2015**, *51* (39), 8269-8272.
86. Yi, J.; Liu, X.; Guo, S.; Zhu, K.; Xue, H.; Zhou, H., Novel Stable Gel Polymer Electrolyte: Toward a High Safety and Long Life Li-Air Battery. *ACS Applied Materials & Interfaces* **2015**, *7* (42), 23798-23804.
87. Yi, J.; Liu, Y.; Qiao, Y.; He, P.; Zhou, H., Boosting the Cycle Life of Li–O₂ Batteries at Elevated Temperature by Employing a Hybrid Polymer–Ceramic Solid Electrolyte. *ACS Energy Letters* **2017**, *2* (6), 1378-1384.
88. Zhang, J.; Sun, B.; McDonagh, A. M.; Zhao, Y.; Kretschmer, K.; Guo, X.; Wang, G., A multi-functional gel co-polymer bridging liquid electrolyte and solid cathode nanoparticles: An efficient route to Li–O₂ batteries with improved performance. *Energy Storage Materials* **2017**, *7*, 1-7.

89. Anju, V. G.; Sampath, S., Stable, Rechargeable Lithium – Oxygen Battery in Liquid and Gel-Based Electrolytes. *Electrochimica Acta* **2017**, *252*, 119-126.
90. Kufian, M. Z.; Arof, A. K., Effect of Calix[6]arene on charge discharge behaviour of lithium air cell based on PAN-LiBOB gel polymer electrolyte. *Materials Technology: Advanced Functional Materials* **2014**, *29* (A2), A114-A117.
91. Abraham, K. M.; Jiang, Z., A Polymer Electrolyte-Based Rechargeable Lithium/Oxygen Battery. *Journal of the Electrochemical Society* **1996**, *143* (1), 1-5.
92. Zhang, J.; Sun, B.; Xie, X.; Kretschmer, K.; Wang, G., Enhancement of stability for lithium oxygen batteries by employing electrolytes gelled by poly(vinylidene fluoride-co-hexafluoropropylene) and tetraethylene glycol dimethyl ether. *Electrochimica Acta* **2015**, *183*, 56-62.
93. Guo, Z.; Li, C.; Liu, J.; Wang, Y.; Xia, Y., A Long-Life Lithium-Air Battery in Ambient Air with a Polymer Electrolyte Containing a Redox Mediator. *Angewandte Chemie International Edition* **2017**, *56* (26), 7505-7509.
94. Leng, L.; Zeng, X.; Chen, P.; Shu, T.; Song, H.; Fu, Z.; Wang, H.; Liao, S., A novel stability-enhanced lithium-oxygen battery with cellulose-based composite polymer gel as the electrolyte. *Electrochimica Acta* **2015**, *176*, 1108-1115.
95. Elia, G. A.; Hassoun, J., A Polymer Lithium-Oxygen Battery. *Scientific Reports* **2015**, *5*, 12307.
96. Wu, C.; Liao, C.; Li, T.; Shi, Y.; Luo, J.; Li, L.; Yang, J., A polymer lithium–oxygen battery based on semi-polymeric conducting ionomers as the polymer electrolyte. *Journal of Materials Chemistry A* **2016**, *4* (39), 15189-15196.
97. Yi, J.; Zhou, H., A Unique Hybrid Quasi-Solid-State Electrolyte for Li-O₂ Batteries with Improved Cycle Life and Safety. *ChemSusChem* **2016**, *9* (17), 2391-2396.
98. Chamaani, A.; Chawla, N.; Safa, M.; El-Zahab, B., One-Dimensional Glass Micro-Fillers in Gel Polymer Electrolytes for Li-O₂ Battery Applications. *Electrochimica Acta* **2017**, *235*, 56-63.
99. Liu, T.; Liu, Q. C.; Xu, J. J.; Zhang, X. B., Cable-Type Water-Survivable Flexible Li-O₂ Battery. *Small* **2016**, *12* (23), 3101-3105.
100. Liu, Q. C.; Liu, T.; Liu, D. P.; Li, Z. J.; Zhang, X. B.; Zhang, Y., A Flexible and Wearable Lithium-Oxygen Battery with Record Energy Density achieved by the Interlaced Architecture inspired by Bamboo Slips. *Advanced Materials* **2016**, *28* (38), 8413-8418.
101. Liu, J.-Y.; Li, X.-X.; Huang, J.-R.; Li, J.-J.; Zhou, P.; Liu, J.-H.; Huang, X.-J., Three-dimensional graphene-based nanocomposites for high energy density Li-ion batteries. *Journal of Materials Chemistry A* **2017**, *5* (13), 5977-5994.
102. Golodnitsky, D.; Strauss, E.; Peled, E.; Greenbaum, S., Review—On Order and Disorder in Polymer Electrolytes. *Journal of The Electrochemical Society* **2015**, *162* (14), A2551-A2566.
103. Lee, H. C.; Park, J. O.; Kim, M.; Kwon, H. J.; Kim, J.-H.; Choi, K. H.; Kim, K.; Im, D., High-Energy-Density Li-O₂ Battery at Cell Scale with Folded Cell Structure. *Joule* **2019**, *3* (2), 542-556.
104. Kraytsberg, A.; Ein-Eli, Y., Review on Li–air batteries—Opportunities, limitations and perspective. *Journal of Power Sources* **2011**, *196* (3), 886-893.
105. Betz, J.; Bieker, G.; Meister, P.; Placke, T.; Winter, M.; Schmuck, R., Theoretical versus Practical Energy: A Plea for More Transparency in the Energy Calculation of Different Rechargeable Battery Systems. *Advanced Energy Materials* **2018**, *9* (6), 1803170.
106. Kim, H.; Jeong, G.; Kim, Y. U.; Kim, J. H.; Park, C. M.; Sohn, H. J., Metallic anodes for next generation secondary batteries. *Chemical Society Reviews* **2013**, *42* (23), 9011-9034.
107. Zhou, D.; Tkacheva, A.; Tang, X.; Sun, B.; Shanmukaraj, D.; Li, P.; Zhang, F.; Armand, M.; Wang, G., Stable Conversion Chemistry-Based Lithium Metal Batteries Enabled by Hierarchical

Multifunctional Polymer Electrolytes with Near-Single Ion Conduction. *Angewandte Chemie International Edition* **2019**, *58* (18), 6001-6006.

108. Cheng, X. B.; Zhang, R.; Zhao, C. Z.; Wei, F.; Zhang, J. G.; Zhang, Q., A Review of Solid Electrolyte Interphases on Lithium Metal Anode. *Advanced science (Weinheim, Baden-Württemberg, Germany)* **2016**, *3* (3), 1500213.

109. Lin, D.; Liu, Y.; Cui, Y., Reviving the lithium metal anode for high-energy batteries. *Nat Nanotechnology* **2017**, *12* (3), 194-206.

110. Zhang, R.; Li, N. W.; Cheng, X. B.; Yin, Y. X.; Zhang, Q.; Guo, Y. G., Advanced Micro/Nanostructures for Lithium Metal Anodes. *Advanced science (Weinheim, Baden-Württemberg, Germany)* **2017**, *4* (3), 1600445.

111. Walker, W.; Giordani, V.; Uddin, J.; Bryantsev, V. S.; Chase, G. V.; Addison, D., A rechargeable Li-O₂ battery using a lithium nitrate/*N,N*-dimethylacetamide electrolyte. *Journal of the American Chemical Society* **2013**, *135* (6), 2076-2079.

112. Bryantsev, V. S.; Giordani, V.; Walker, W.; Uddin, J.; Lee, I.; van Duin, A. C. T.; Chase, G. V.; Addison, D., Investigation of Fluorinated Amides for Solid-Electrolyte Interphase Stabilization in Li-O₂ Batteries Using Amide-Based Electrolytes. *The Journal of Physical Chemistry C* **2013**, *117* (23), 11977-11988.

113. Ding, F.; Xu, W.; Graff, G. L.; Zhang, J.; Sushko, M. L.; Chen, X.; Shao, Y.; Engelhard, M. H.; Nie, Z.; Xiao, J.; Liu, X.; Sushko, P. V.; Liu, J.; Zhang, J. G., Dendrite-free lithium deposition via self-healing electrostatic shield mechanism. *Journal of the American Chemical Society* **2013**, *135* (11), 4450-4456.

114. Tikekar, M. D.; Choudhury, S.; Tu, Z.; Archer, L. A., Design principles for electrolytes and interfaces for stable lithium-metal batteries. *Nature Energy* **2016**, *1* (9), 16114.

115. Wang, D.; Zhang, F.; He, P.; Zhou, H., A Versatile Halide Ester Enabling Li-Anode Stability and a High Rate Capability in Lithium-Oxygen Batteries. *Angewandte Chemie International Edition* **2019**, *58* (8), 2355-2359.

116. Huang, Z.; Ren, J.; Zhang, W.; Xie, M.; Li, Y.; Sun, D.; Shen, Y.; Huang, Y., Protecting the Li-Metal Anode in a Li-O₂ Battery by using Boric Acid as an SEI-Forming Additive. *Advanced Materials* **2018**, *30* (39), e1803270.

117. Zhang, Y.-T.; Liu, Z.-J.; Wang, J.-W.; Wang, L.; Peng, Z.-Q., Recent Advances in Li Anode for Aprotic Li-O₂ Batteries. *Acta Physica Sinica (Overseas Edition)* **2017**, *33* (3), 486-499.

118. Lee, D. J.; Lee, H.; Kim, Y. J.; Park, J. K.; Kim, H. T., Sustainable Redox Mediation for Lithium-Oxygen Batteries by a Composite Protective Layer on the Lithium-Metal Anode. *Advanced Materials* **2016**, *28* (5), 857-863.

119. Song, S.; Xu, W.; Zheng, J.; Luo, L.; Engelhard, M. H.; Bowden, M. E.; Liu, B.; Wang, C. M.; Zhang, J. G., Complete Decomposition of Li₂CO₃ in Li-O₂ Batteries Using Ir/B₄C as Noncarbon-Based Oxygen Electrode. *Nano Letters* **2017**, *17* (3), 1417-1424.

120. Lyu, Z.; Yang, L.; Luan, Y.; Renshaw Wang, X.; Wang, L.; Hu, Z.; Lu, J.; Xiao, S.; Zhang, F.; Wang, X.; Huo, F.; Huang, W.; Hu, Z.; Chen, W., Effect of oxygen adsorbability on the control of Li₂O₂ growth in Li-O₂ batteries: Implications for cathode catalyst design. *Nano Energy* **2017**, *36*, 68-75.

121. Johnson, L.; Li, C.; Liu, Z.; Chen, Y.; Freunberger, S. A.; Ashok, P. C.; Praveen, B. B.; Dholakia, K.; Tarascon, J. M.; Bruce, P. G., The role of LiO₂ solubility in O₂ reduction in aprotic solvents and its consequences for Li-O₂ batteries. *Nature Chemistry* **2014**, *6* (12), 1091-1099.

122. Matsuda, S.; Kubo, Y.; Uosaki, K.; Nakanishi, S., Potassium Ions Promote Solution-Route Li₂O₂ Formation in the Positive Electrode Reaction of Li-O₂ Batteries. *The Journal of Physical Chemistry Letters* **2017**, *8* (6), 1142-1146.

123. Das, S. K.; Xu, S.; Emwas, A.-H.; Lu, Y. Y.; Srivastava, S.; Archer, L. A., High energy lithium–oxygen batteries – transport barriers and thermodynamics. *Energy Environmental Science* **2012**, 5 (10), 8927-8931.
124. Liang, Z.; Lu, Y. C., Critical Role of Redox Mediator in Suppressing Charging Instabilities of Lithium–Oxygen Batteries. *Journal of the American Chemical Society* **2016**, 138 (24), 7574-83.
125. Feng, N.; Mu, X.; Zhang, X.; He, P.; Zhou, H., Intensive Study on the Catalytical Behavior of N-Methylphenothiazine as a Soluble Mediator to Oxidize the Li₂O₂ Cathode of the Li–O₂ Battery. *ACS Applied Materials & Interfaces* **2017**, 9 (4), 3733-3739.
126. Park, J. B.; Lee, S. H.; Jung, H. G.; Aurbach, D.; Sun, Y. K., Redox Mediators for Li–O₂ Batteries: Status and Perspectives. *Adv. Mater.* **2018**, 30 (1), 1704162.
127. Zhang, T.; Liao, K.; He, P.; Zhou, H., A self-defense redox mediator for efficient lithium–O₂ batteries. *Energy Environ. Sci.* **2016**, 9 (3), 1024-1030.
128. Qiao, Y.; Ye, S., Spectroscopic Investigation for Oxygen Reduction and Evolution Reactions with Tetrathiafulvalene as a Redox Mediator in Li–O₂ Battery. *The Journal of Physical Chemistry C* **2016**, 120 (29), 15830-15845.
129. Yao, K. P. C.; Frith, J. T.; Sayed, S. Y.; Bardé, F.; Owen, J. R.; Shao-Horn, Y.; Garcia-Araez, N., Utilization of Cobalt Bis(terpyridine) Metal Complex as Soluble Redox Mediator in Li–O₂ Batteries. *The Journal of Physical Chemistry C* **2016**, 120 (30), 16290-16297.
130. Zhang, S. S.; Ren, X.; Tran, D. T.; Read, J., Catalytic Effect of Heat-treated Iron and Copper Phthalocyanines in Non-aqueous Electrolyte Li/air Batteries – A Review. *Green* **2012**, 2 (2-3), 63-69.
131. Matsuda, S.; Mori, S.; Kubo, Y.; Uosaki, K.; Hashimoto, K.; Nakanishi, S., Cobalt phthalocyanine analogs as soluble catalysts that improve the charging performance of Li–O₂ batteries. *Chemical Physics Letters* **2015**, 620, 78-81.
132. Xu, C.; Xu, G.; Zhang, Y.; Fang, S.; Nie, P.; Wu, L.; Zhang, X., Bifunctional Redox Mediator Supported by an Anionic Surfactant for Long-Cycle Li–O₂ Batteries. *ACS Energy Letters* **2017**, 2 (12), 2659-2666.
133. Lacey, M. J.; Frith, J. T.; Owen, J. R., A redox shuttle to facilitate oxygen reduction in the lithium air battery. *Electrochemistry Communications* **2013**, 26, 74-76.
134. Sun, D.; Shen, Y.; Zhang, W.; Yu, L.; Yi, Z.; Yin, W.; Wang, D.; Huang, Y.; Wang, J.; Wang, D.; Goodenough, J. B., A solution-phase bifunctional catalyst for lithium-oxygen batteries. *Journal of the American Chemical Society* **2014**, 136 (25), 8941-8946.
135. Gao, X.; Chen, Y.; Johnson, L. R.; Jovanov, Z. P.; Bruce, P. G., A rechargeable lithium–oxygen battery with dual mediators stabilizing the carbon cathode. *Nature Energy* **2017**, 2 (9).
136. Kundu, D.; Black, R.; Adams, B.; Nazar, L. F., A Highly Active Low Voltage Redox Mediator for Enhanced Rechargeability of Lithium–Oxygen Batteries. *ACS Central Science* **2015**, 1 (9), 510-5.
137. Zhu, Y. G.; Jia, C.; Yang, J.; Pan, F.; Huang, Q.; Wang, Q., Dual redox catalysts for oxygen reduction and evolution reactions: towards a redox flow Li–O₂ battery. *Chemical Communications* **2015**, 51 (46), 9451-9454.
138. Yang, L.; Frith, J. T.; Garcia-Araez, N.; Owen, J. R., A new method to prevent degradation of lithium-oxygen batteries: reduction of superoxide by viologen. *Chemical Communications* **2015**, 51 (9), 1705-1708.
139. Zhang, Y.; Wang, L.; Zhang, X.; Guo, L.; Wang, Y.; Peng, Z., High-Capacity and High-Rate Discharging of a Coenzyme Q10 -Catalyzed Li–O₂ Battery. *Advanced Materials* **2018**, 30 (5), 1705571.

140. Ko, Y.; Park, H.; Kim, J.; Lim, H.-D.; Lee, B.; Kwon, G.; Lee, S.; Bae, Y.; Park, S. K.; Kang, K., Biological Redox Mediation in Electron Transport Chain of Bacteria for Oxygen Reduction Reaction Catalysts in Lithium-Oxygen Batteries. *Advanced Functional Mater* **2019**, 29 (5), 1805623.
141. Matsuda, S.; Hashimoto, K.; Nakanishi, S., Efficient Li₂O₂ Formation via Aprotic Oxygen Reduction Reaction Mediated by Quinone Derivatives. *The Journal of Physical Chemistry C* **2014**, 118 (32), 18397-18400.
142. Bergner, B. J.; Hofmann, C.; Schurmann, A.; Schroder, D.; Peppler, K.; Schreiner, P. R.; Janek, J., Understanding the fundamentals of redox mediators in Li-O₂ batteries: a case study on nitroxides. *Physical Chemistry Chemical Physics* **2015**, 17 (47), 31769-31779.
143. Bergner, B. J.; Schurmann, A.; Peppler, K.; Garsuch, A.; Janek, J., TEMPO: a mobile catalyst for rechargeable Li-O₂ batteries. *Journal of the American Chemical Society* **2014**, 136 (42), 15054-15064.
144. Zhang, J.; Sun, B.; Zhao, Y.; Tkacheva, A.; Liu, Z.; Yan, K.; Guo, X.; McDonagh, A. M.; Shanmukaraj, D.; Wang, C.; Rojo, T.; Armand, M.; Peng, Z.; Wang, G., A versatile functionalized ionic liquid to boost the solution-mediated performances of lithium-oxygen batteries. *Nature Communications* **2019**, 10 (1), 602.
145. Matsuda, S.; Mori, S.; Hashimoto, K.; Nakanishi, S., Transition Metal Complexes with Macrocyclic Ligands Serve as Efficient Electrocatalysts for Aprotic Oxygen Evolution on Li₂O₂. *The Journal of Physical Chemistry C* **2014**, 118 (49), 28435-28439.
146. Lee, C. K.; Park, Y. J., Csl as Multifunctional Redox Mediator for Enhanced Li-Air Batteries. *ACS Applied Materials & Interfaces* **2016**, 8 (13), 8561-8567.
147. Sharon, D.; Hirsberg, D.; Afri, M.; Chesneau, F.; Lavi, R.; Frimer, A. A.; Sun, Y. K.; Aurbach, D., Catalytic Behavior of Lithium Nitrate in Li-O₂ Cells. *ACS Applied Materials & Interfaces* **2015**, 7 (30), 16590-16600.
148. Gorityala, B. K.; Guchhait, G.; Fernando, D. M.; Deo, S.; McKenna, S. A.; Zhanel, G. G.; Kumar, A.; Schweizer, F., Adjuvants Based on Hybrid Antibiotics Overcome Resistance in *Pseudomonas aeruginosa* and Enhance Fluoroquinolone Efficacy. *Angewandte Chemie International Edition* **2016**, 55 (2), 555-559.
149. Chen, X.; Xu, D.; Qiu, L.; Li, S.; Zhang, W.; Yan, F., Imidazolium functionalized TEMPO/iodide hybrid redox couple for highly efficient dye-sensitized solar cells. *Journal of Materials Chemistry A* **2013**, 1 (31), 8759-8765.
150. Haugland, M. M.; El-Sagheer, A. H.; Porter, R. J.; Pena, J.; Brown, T.; Anderson, E. A.; Lovett, J. E., 2'-Alkynyl nucleotides: A Sequence- and Spin Label-Flexible Strategy for EPR Spectroscopy in DNA. *Journal of the American Chemical Society* **2016**, 138 (29), 9069-9072.
151. Lee, S. H.; Kim, J.-K.; Cheruvally, G.; Choi, J.-W.; Ahn, J.-H.; Chauhan, G. S.; Song, C. E., Electrochemical properties of new organic radical materials for lithium secondary batteries. *Journal of Power Sources* **2008**, 184 (2), 503-507.
152. Artiukhova, N. A.; Maryunina, K. Y.; Fokin, S. V.; Tretyakov, E. V.; Romanenko, G. V.; Polushkin, A. V.; Bogomyakov, A. S.; Sagdeev, R. Z.; Ovcharenko, V. I., Spirocyclic derivatives of nitronyl nitroxides in the design of heterospin Cu^{II} complexes manifesting spin transitions. *Russian Chemical Bulletin, International Edition* **2013**, 62 (10), 2132-2140.
153. Zhao, M.; Li, Z.; Peng, L.; Tang, Y. R.; Wang, C.; Zhang, Z.; Peng, S., A new class of analgesic agents toward prostacyclin receptor inhibition: synthesis, biological studies and QSAR analysis of 1-hydroxyl-2-substituted phenyl-4,4,5,5-tetramethylimidazolines. *European Journal of Medicinal Chemistry* **2008**, 43 (5), 1048-1058.

154. Stroh, C.; Mayor, M.; von Hänisch, C., Suzuki Reactions with Stable Organic Radicals - Synthesis of Biphenyls Substituted with Nitronyl-Nitroxide Radicals. *European Journal of Organic Chemistry* **2005**, 2005 (17), 3697-3703.
155. Wu, Y.; Bi, L.; Bi, W.; Li, Z.; Zhao, M.; Wang, C.; Ju, J.; Peng, S., Novel 2-substituted nitronyl nitroxides as free radical scavengers: synthesis, biological evaluation and structure-activity relationship. *Bioorganic & Medicinal Chemistry* **2006**, 14 (16), 5711-5720.
156. Cheng, J.; Jiang, Y.; Zou, L.; Zhang, M.; Zhang, G.; Wang, Z.; Huang, Y.; Chi, B.; Pu, J.; Jian, L., Efficiency of 3D-Ordered Macroporous $\text{La}_{0.6}\text{Sr}_{0.4}\text{Co}_{0.2}\text{Fe}_{0.8}\text{O}_3$ as an Electrocatalyst for Aprotic Li-O₂ Batteries. *ChemistryOpen* **2019**, 8 (2), 206-209.
157. Zhang, X.; Zhang, Q.; Wang, X. G.; Wang, C.; Chen, Y. N.; Xie, Z.; Zhou, Z., An Extremely Simple Method for Protecting Lithium Anodes in Li-O₂ Batteries. *Angewandte Chemie International Edition* **2018**, 57 (39), 12814-12818.
158. Zhang, J.; Sun, B.; Xie, X.; Zhao, Y.; Wang, G., A Bifunctional Organic Redox Catalyst for Rechargeable Lithium-Oxygen Batteries with Enhanced Performances. *Advanced science (Weinheim, Baden-Württemberg, Germany)* **2016**, 3 (4), 1500285.
159. Tkacheva, A.; Zhang, J.; Sun, B.; Zhou, D.; Wang, G.; McDonagh, A. M., TEMPO-Ionic Liquids as Redox Mediators and Solvents for Li-O₂ Batteries. *The Journal of Physical Chemistry C* **2020**, 124 (9), 5087-5092.
160. Yu, Y.; Yin, Y.-B.; Ma, J.-L.; Chang, Z.-W.; Sun, T.; Zhu, Y.-H.; Yang, X.-Y.; Liu, T.; Zhang, X.-B., Designing a self-healing protective film on a lithium metal anode for long-cycle-life lithium-oxygen batteries. *Energy Storage Materials* **2019**, 18, 382-388.
161. Xu, W.; Wang, J.; Ding, F.; Chen, X.; Nasybulin, E.; Zhang, Y.; Zhang, J.-G., Lithium metal anodes for rechargeable batteries. *Energy Environ. Sci.* **2014**, 7 (2), 513-537.
162. Knipping, E.; Aucher, C.; Guirado, G.; Aubouy, L., Room temperature ionic liquids versus organic solvents as lithium-oxygen battery electrolytes. *New J. Chem.* **2018**, 42 (6), 4693-4699.
163. MacFarlane, D. R.; Chong, A. L.; Forsyth, M.; Kar, M.; Vijayaraghavan, R.; Somers, A.; Pringle, J. M., New dimensions in salt-solvent mixtures: a 4th evolution of ionic liquids. *Faraday Discuss* **2017**, 206, 9-28.
164. Periyapperuma, K.; Zhang, Y.; MacFarlane, D. R.; Forsyth, M.; Pozo-Gonzalo, C.; Howlett, P. C., Towards Higher Energy Density Redox-Flow Batteries: Imidazolium Ionic Liquid for Zn Electrochemistry in Flow Environment. *ChemElectroChem* **2017**, 4 (5), 1051-1058.
165. Begic, S.; Jonsson, E.; Chen, F.; Forsyth, M., Molecular dynamics simulations of pyrrolidinium and imidazolium ionic liquids at graphene interfaces. *Physical Chemistry Chemical Physics* **2017**, 19 (44), 30010-30020.
166. MacFarlane, D. R.; Forsyth, M.; Howlett, P. C.; Kar, M.; Passerini, S.; Pringle, J. M.; Ohno, H.; Watanabe, M.; Yan, F.; Zheng, W.; Zhang, S.; Zhang, J., Ionic liquids and their solid-state analogues as materials for energy generation and storage. *Nature Reviews Materials* **2016**, 1 (2).
167. Pozo-Gonzalo, C.; Howlett, P. C.; MacFarlane, D. R.; Forsyth, M., Highly reversible oxygen to superoxide redox reaction in a sodium-containing ionic liquid. *Electrochemistry Communications* **2017**, 74, 14-18.
168. Katayama, Y.; Onodera, H.; Yamagata, M.; Miura, T., Electrochemical Reduction of Oxygen in Some Hydrophobic Room-Temperature Molten Salt Systems. *Journal of The Electrochemical Society* **2004**, 151 (1), A59-A63.
169. Allen, C. J.; Hwang, J.; Kautz, R.; Mukerjee, S.; Plichta, E. J.; Hendrickson, M. A.; Abraham, K. M., Oxygen Reduction Reactions in Ionic Liquids and the Formulation of a General ORR Mechanism for Li-Air Batteries. *The Journal of Physical Chemistry C* **2012**, 116 (39), 20755-20764.

170. Wang, B.; Qin, L.; Mu, T.; Xue, Z.; Gao, G., Are Ionic Liquids Chemically Stable? *Chemical Reviews* **2017**, *117* (10), 7113-7131.
171. Darmanyan, A. P.; Tatikolov, A. S., Singlet oxygen quenching by stable nitroxyl radicals. *Journal of Photochemistry* **1986**, *32*, 157-163.
172. Vidoczy, T.; Baranyai, P., Quenching of Porphyrin Triplet and Singlet Oxygen by Stable Nitroxide Radicals: Importance of Steric Hindrance. *Helvetica Chimica Acta* **2001**, *84*, 2640-2652.
173. Likhtenshtein, G. I., *Nitroxides: Brief History, Fundamentals, and Recent Developments*. Springer International Publishing: 2020; p 316.
174. Noda, M.; Ma, Y.; Yoshikawa, Y.; Imanaka, T.; Mori, T.; Furuta, M.; Tsuruyama, T.; Yoshikawa, K., A single-molecule assessment of the protective effect of DMSO against DNA double-strand breaks induced by photo-and gamma-ray-irradiation, and freezing. *Scientific Reports* **2017**, *7* (1), 8557.
175. Tułodziecki, M.; Tarascon, J. M.; Taberna, P. L.; Guéry, C., Catalytic reduction of TFSI-containing ionic liquid in the presence of lithium cations. *Electrochemistry Communications* **2017**, *77*, 128-132.
176. Chen, Y.; Freunberger, S. A.; Peng, Z.; Fontaine, O.; Bruce, P. G., Charging a Li-O₂ battery using a redox mediator. *Nature Chemistry* **2013**, *5* (6), 489-494.
177. Chen, Y.; Gao, X.; Johnson, L. R.; Bruce, P. G., Kinetics of lithium peroxide oxidation by redox mediators and consequences for the lithium-oxygen cell. *Nature Communications* **2018**, *9* (1), 767.
178. Balaish, M.; Gao, X.; Bruce, P. G.; Ein-Eli, Y., Enhanced Li-O₂ Battery Performance in a Binary "Liquid Teflon" and Dual Redox Mediators. *Advanced Materials Technologies* **2019**, *4* (4), 1800645.
179. Yang, C.; Wang, S.; Zhang, X.; Zhang, Q.; Ma, W.; Yu, S.; Sun, G., Substituent Effect of Imidazolium Ionic Liquid: A Potential Strategy for High Coulombic Efficiency Al Battery. *The Journal of Physical Chemistry C* **2019**, *123* (18), 11522-11528.
180. Zhang, W.; Qiu, L.; Chen, X.; Yan, F., Imidazolium Functionalized Bis-2,2,6,6-Tetramethylpiperidine-1-oxyl (TEMPO) Bi-redox Couples for Highly Efficient Dye-Sensitized Solar Cells. *Electrochimica Acta* **2014**, *117*, 48-54.
181. Tamura, T.; Yoshida, K.; Hachida, T.; Tsuchiya, M.; Nakamura, M.; Kazue, Y.; Tachikawa, N.; Dokko, K.; Watanabe, M., Physicochemical Properties of Glyme-Li Salt Complexes as a New Family of Room-temperature Ionic Liquids. *Chemistry Letters* **2010**, *39* (7), 753-755.
182. Rocha, M. A.; Neves, C. M.; Freire, M. G.; Russina, O.; Triolo, A.; Coutinho, J. A.; Santos, L. M., Alkylimidazolium based ionic liquids: impact of cation symmetry on their nanoscale structural organization. *Journal of Physical Chemistry B* **2013**, *117* (37), 10889-10897.
183. Canongia Lopes, J. N.; Padua, A. A., Nanostructural organization in ionic liquids. *The Journal of Physical Chemistry B* **2006**, *110* (7), 3330-3335.
184. Tokuda, H.; Hayamizu, K.; Ishii, K.; Susan, M. A.; Watanabe, M., Physicochemical properties and structures of room temperature ionic liquids. 2. Variation of alkyl chain length in imidazolium cation. *The Journal of Physical Chemistry B* **2005**, *109* (13), 6103-6110.
185. Augustin, M.; Vullum, P. E.; Vullum-Bruer, F.; Svensson, A. M., Inside the electrode: Looking at cycling products in Li/O₂ batteries. *Journal of Power Sources* **2019**, *414*, 130-140.
186. Torriero, A. A. J.; Howlett, P. C., Ionic liquid effects on the redox potential of ferrocene. *Electrochemistry Communications* **2012**, *16* (1), 84-87.
187. Noviandri, I.; Brown, K. N.; Fleming, D. S.; Gulyas, P. T.; Lay, P. A.; Masters, A. F.; Phillips, L., The Decamethylferrocenium/Decamethylferrocene Redox Couple: A Superior Redox Standard to

the Ferrocenium/Ferrocene Redox Couple for Studying Solvent Effects on the Thermodynamics of Electron Transfer. *The Journal of Physical Chemistry B* **1999**, *103*, 6713-6722.

188. Wang, X.-G.; Wang, C.; Xie, Z.; Zhang, X.; Chen, Y.; Wu, D.; Zhou, Z., Improving Electrochemical Performances of Rechargeable Li-CO₂ Batteries with an Electrolyte Redox Mediator. *ChemElectroChem* **2017**, *4* (9), 2145-2149.

189. Nutting, J. E.; Rafiee, M.; Stahl, S. S., Tetramethylpiperidine N-Oxyl (TEMPO), Phthalimide N-Oxyl (PINO), and Related N-Oxyl Species: Electrochemical Properties and Their Use in Electrocatalytic Reactions. *Chemical Reviews* **2018**, *118* (9), 4834-4885.

190. Kato, Y.; Shimizu, Y.; Yijing, L.; Unoura, K.; Utsumi, H.; Ogata, T., Reversible half-wave potentials of reduction processes on nitroxide radicals. *Electrochimica Acta* **1995**, *40* (17), 2799-2802.

191. Likhtenshtein, G. I., *Nitroxides: Brief History, Fundamentals, and Recent Developments*. Springer Nature: 2020.

192. Neale, A. R.; Li, P.; Jacquemin, J.; Goodrich, P.; Ball, S. C.; Compton, R. G.; Hardacre, C., Effect of cation structure on the oxygen solubility and diffusivity in a range of bis{(trifluoromethyl)sulfonyl}imide anion based ionic liquids for lithium-air battery electrolytes. *Physical Chemistry Chemical Physics* **2016**, *18*, 11251-11262.

193. Xiangyi Luo; Amine, R.; Lau, K. C.; Lu, J.; Zhan, C.; Curtiss, L. A.; Hallaj, S. A.; Chaplin, B. P.; Amine, K., Mass and charge transport relevant to the formation of toroidal lithium peroxide nanoparticles in aprotic lithium-oxygen battery: an experimental and theoretical modelling study. *Green Energy and Environment* **2017**, *2* (3), 186-203.

194. Song, M.; Zhu, D.; Zhang, L.; Wang, X.; Mi, R.; Liu, H.; Mei, J.; Lau, L. W. M.; Chen, Y., Temperature characteristics of nonaqueous Li-O₂ batteries. *Journal of Solid State Electrochemistry* **2013**, *18* (3), 739-745.

195. Grübl, D.; Bergner, B.; Schröder, D.; Janek, J.; Bessler, W. G., Multistep Reaction Mechanisms in Nonaqueous Lithium-Oxygen Batteries with Redox Mediator: A Model-Based Study. *The Journal of Physical Chemistry C* **2016**, *120* (43), 24623-24636.

196. Mahne, N.; Renfrew, S. E.; McCloskey, B. D.; Freunberger, S. A., Electrochemical Oxidation of Lithium Carbonate Generates Singlet Oxygen. *Angewandte Chemie International Edition* **2018**, *57* (19), 5529-5533.

197. Schafzahl, L.; Mahne, N.; Schafzahl, B.; Wilkening, M.; Slugovc, C.; Borisov, S. M.; Freunberger, S. A., Singlet Oxygen during Cycling of the Aprotic Sodium-O₂ Battery. *Angewandte Chemie International Edition* **2017**, *56* (49), 15728-15732.

198. Mahne, N.; Schafzahl, B.; Leypold, C.; Leypold, M.; Grumm, S.; Leitgeb, A.; Strohmeier, G. A.; Wilkening, M.; Fontaine, O.; Kramer, D.; Slugovc, C.; Borisov, S. M.; Freunberger, S. A., Singlet Oxygen Generation as a Major Cause for Parasitic Reactions during Cycling of Aprotic Lithium-Oxygen Batteries. *Nature Energy* **2017**, *2* (5), 17036.

199. Schmitz, P.; Jakelski, R.; Pyschik, M.; Jalkanen, K.; Nowak, S.; Winter, M.; Bieker, P., Decomposition of Imidazolium-Based Ionic Liquids in Contact with Lithium Metal. *ChemSusChem* **2017**, *10* (5), 876-883.

200. Qiao, Y.; He, Y.; Wu, S.; Jiang, K.; Li, X.; Guo, S.; He, P.; Zhou, H., MOF-Based Separator in an Li-O₂ Battery: An Effective Strategy to Restrain the Shuttling of Dual Redox Mediators. *ACS Energy Letters* **2018**, *3* (2), 463-468.

201. Gao, X.; Chen, Y.; Johnson, L.; Bruce, P. G., Promoting solution phase discharge in Li-O₂ batteries containing weakly solvating electrolyte solutions. *Nature Materials* **2016**, *15*, 882-888.

202. Zhang, T.; Liao, K.; He, P.; Zhou, H., A self-defense redox mediator for efficient lithium-O₂ batteries. *Energy & Environmental Science* **2016**, *9* (3), 1024-1030.

203. Duan, W.; Vemuri, R. S.; Milshtein, J. D.; Laramie, S.; Dmello, R. D.; Huang, J.; Zhang, L.; Hu, D.; Vijayakumar, M.; Wang, W.; Liu, J.; Darling, R. M.; Thompson, L.; Smith, K.; Moore, J. S.; Brushett, F. R.; Wei, X., A symmetric organic-based nonaqueous redox flow battery and its state of charge diagnostics by FTIR. *Journal of Materials Chemistry A* **2016**, *4*, 5448-5456.
204. Voufack, A. B.; Claiser, N.; Lecomte, C.; Pillet, S.; Pontillon, Y.; Gillon, B.; Yan, Z.; Gillet, J. M.; Marazzi, M.; Genoni, A.; Souhassou, M., When combined X-ray and polarized neutron diffraction data challenge high-level calculations: spin-resolved electron density of an organic radical. *Acta Crystallographica Section B: Structural Science, Crystal Engineering and Materials* **2017**, *73* (Pt 4), 544-549.
205. Romanov, V.; Bagryanskaya, I.; Gritsan, N.; Gorbunov, D.; Vlasenko, Y.; Yusubov, M.; Zaytseva, E.; Luneau, D.; Tretyakov, E., Assembly of Imidazolyl-Substituted Nitronyl Nitroxides into Ferromagnetically Coupled Chains. *Crystals* **2019**, *9* (4), 219.
206. Zheludev, A.; Barone, V.; Bonnet, M.; DeUey, B.; Grand, A.; Ressouche, E.; Rey, P.; Subra, R.; Schweizer, J., Spin Density in a Nitronyl Nitroxide Free Radical. Polarized Neutron Diffraction Investigation and ab Initio Calculations. *Journal of the American Chemical Society* **1994**, *116* (5), 2019-2027.
207. Suga, T.; Sugita, S.; Ohshiro, H.; Oyaizu, K.; Nishide, H., p- and n-Type bipolar redox-active radical polymer: Toward totally organic polymer-based rechargeable devices with variable configuration. *Advanced Materials* **2011**, *23* (6), 751-754.
208. Lee, J.; Lee, E.; Kim, S.; Bang, G. S.; Shultz, D. A.; Schmidt, R. D.; Forbes, M. D.; Lee, H., Nitronyl nitroxide radicals as organic memory elements with both n- and p-type properties. *Angewandte Chemie International Edition* **2011**, *50* (19), 4414-4418.
209. Volodarsky, L. B.; Reznikov, V. A.; Ovcharenko, V. I., *Synthetic Chemistry of Stable Nitroxides*. CRC press: 2017.
210. Dooley, B. M. The Role of Charge-Transfer Interactions and Delocalization in Annelated Nitronyl Nitroxides. PhD, Okanagan University College, 2005.
211. Borozdina, Y. B. Aminoxyl Radicals – Pure Organic Materials with Tunable Magnetic and Sensing Properties. PhD dissertation, Johannes Gutenberg-Universität Mainz, Germany, 2012.
212. Budnikova, Y. G.; Gryaznova, T. V.; Kadirov, M. K.; Tret'yakov, E. V.; Kholin, K. V.; Ovcharenko, V. I.; Sagdeev, R. Z.; Sinyashin, O. G., Electrochemistry of nitronyl and imino nitroxides. *Russian Journal of Physical Chemistry A* **2009**, *83* (11), 1976-1980.
213. Suga, T.; Nishide, H., Redox-Active Radical Polymers for a Totally Organic Rechargeable Battery. In *Polymers for Energy Storage and Delivery: Polyelectrolytes for Batteries and Fuel Cells*, 2012; pp 45-53.
214. Kurata, T.; Koshika, K.; Kato, F.; Kido, J.; Nishide, H., Triarylamine-combined nitronyl nitroxide and its hole-transporting property. *Polyhedron* **2007**, *26*, 1776–1780.
215. Sukegawa, T.; Kai, A.; Oyaizu, K.; Nishide, H., Synthesis of Pendant Nitronyl Nitroxide Radical-Containing Poly(norbornene)s as Ambipolar Electrode-Active Materials. *Macromolecules* **2013**, *46* (4), 1361-1367.
216. Coronado, E.; Giménez-Saiz, C.; Nicolas, M.; Romero, F. M.; Rusanov, E.; Stoeckli-Evans, H., Synthesis, crystal structures and electronic properties of imidazoline nitroxide radicals bearing active groups in electropolymerisation. *New Journal of Chemistry* **2003**, *27* (3), 490-497.
217. Hagemann, T.; Winsberg, J.; Häupler, B.; Janoschka, T.; Gruber, J. J.; Wild, A.; Schubert, U. S., A bipolar nitronyl nitroxide small molecule for an all-organic symmetric redox-flow battery. *NPG Asia Materials* **2017**, *9* (1), e340.

218. Tretyakov, E.; Okada, K.; Suzuki, S.; Baumgarten, M.; Romanenko, G.; Bogomyakov, A.; Ovcharenko, V., Synthesis, structure and properties of nitronyl nitroxide diradicals with fused-thiophene couplers. *Journal of Physical Organic Chemistry* **2016**, 29 (12), 725-734.
219. Ziessel, R.; Ulrich, G.; Lawson, R. C.; Echegoyen, L., Oligopyridine bis(nitronyl nitroxides): synthesis, structures, electrochemical, magnetic and electronic properties. *Journal of Materials Chemistry* **1999**, 9, 1435–1448.
220. Ullman, E. F.; Osiecki, J. H.; Boocock, D. G. B.; Darcy, R., Studies of Stable Free Radicals. X. Nitronyl Nitroxide Monoradicals and Biradicals as Possible Small Molecule Spin Labels. *Journal of the American Chemical Society* **1972**, 94 (20), 7049-7059.
221. Caneschi, A.; Gatteschi, D.; Rey, P., The Chemistry and Magnetic Properties of Metal Nitronyl Nitroxide Complexes. John Wiley & Sons, Inc.: 1991; pp 331-429.
222. Bard, A. J.; Faulkner, L. R., *Electrochemical methods: fundamentals and applications*. 2nd ed.; Wiley: New York, 2001.
223. Elgrishi, N.; Rountree, K. J.; McCarthy, B. D.; Rountree, E. S.; Eisenhart, T. T.; Dempsey, J. L., A Practical Beginner's Guide to Cyclic Voltammetry. *Journal of Chemical Education* **2017**, 95 (2), 197-206.
224. Edwin F. Ullman. Jeanne H. Osiecki, D. G. B. B., and R. Darcy, Studies of Stable Free Radicals. X.1 Nitronyl Nitroxide Monoradicals and Biradicals as Possible Small Molecule Spin Labels. *Journal of the American Chemical Society* **1972**, 94 (20), 7049-7059.
225. Nakahara, K.; Iwasa, S.; Iriyama, J.; Morioka, Y.; Suguro, M.; Satoh, M.; Cairns, E. J., Electrochemical and spectroscopic measurements for stable nitroxyl radicals. *Electrochimica Acta* **2006**, 52 (3), 921-927.
226. Bashkin, J. K.; Kinlen, P. J., Oxygen-Stable Ferrocene Reference Electrodes. *Inorganic Chemistry* **1990**, 29, 4507-4509.
227. Kojima, H.; Takahashi, S.; Hagihar, N., An Oxygen Adduct of Cobaltocene. *Journal of the Chemical Society, Chemical Communications* **1973**, 230-231.
228. Simonova, A.; Magrina, I.; Sykorova, V.; Pohl, R.; Ortiz, M.; Havran, L.; Fojta, M.; O'Sullivan, C. K.; Hock, M., Tuning of Oxidation Potential of Ferrocene for Ratiometric Redox Labeling and Coding of Nucleotides and DNA. *Chemistry* **2020**, 26 (6), 1286-1291.
229. Meini, S.; Elazari, R.; Rosenman, A.; Garsuch, A.; Aurbach, D., The Use of Redox Mediators for Enhancing Utilization of Li₂S Cathodes for Advanced Li-S Battery Systems. *The Journal of Physical Chemistry Letters* **2014**, 5 (5), 915-918.